Geochemical and Mineralogical characterisation of Vaalputs palaeosols: Inference of paleoclimates

by

Thando Olwethu Majodina

Thesis presented in fulfilment of the requirements for the degree of Master of Science in the faculty of Science at Stellenbosch University.

Stellenbosch University

Supervisor: Dr. Catherine Clarke

Co-supervisor: Dr. Daniel Mikeš

March 2013

Declaration

By submitting this thesis electronically, I declare that the entirety of the work contained therein is my own, original work, that I am sole author thereof, that production and publication by Stellenbosch University will not infringe any third party rights and that I have not previously in its entirety or in part submitted it for obtaining any qualification.

Date: March 2013

Abstract

Vaalputs radioactive waste disposal facility is situated in an arid region of Bushmanland currently with evapotranspiration potential that far exceeds precipitation. Dominant soil features in Vaalputs are palimpsests of climates under which they formed. Particle sizes vary drastically between horizons which suggest different modes of sediment transport. Petrographic analyses revealed euhedral habits of primary mineral feldspar within the soils of Vaalputs. This suggests a proximal source of sediments and minimal primary mineral weathering under an arid climate where euhedral grains of feldspar are maintained.

The surface horizon of the soils is covered by an equigranular coarse sand of residual aeolian origin. The transition from the surface horizon to the subsurface horizons is widely marked by a pebble sized stone-line. The pebble sized material of the stone-line suggests residual accumulation during the weathering of a previously surface exposed horizon.

Since deposition of subsurface sediments (15 Ma) pedogenic alteration has been active in Vaalputs. This has resulted to a complex soil system which displays varied forms of thick dorbank horizons including massive polygonal peds and platy horizons. The polygonal peds are defined by desiccation cracks where vertical and horizontal laminations are hosted. Slaking tests as well as bulk chemistry confirmed that the laminations are composed largely of secondary calcite, however elemental mapping revealed numerous illite bands alternating with calcite layers. It is proposed that calcite layers represent solution features rather than cutanic features.

Signs of hydromorphy are commonly observed within the dorbank horizons, since an arid climate currently prevails in Vaalputs such hydromorphic features may indicate formation under past climates. The occurrences of palygorskite, sepiolite and dorbank horizons in Vaalputs require high soil pH (generated by high concentrations of Na) for their formation. Vaalputs soils, however, measured circumneutral pH and relatively low Na concentrations which suggests that palygorskite, sepiolite and dorbank horizons are relic features.

Salt casts of lenticular texture occur between polygonal peds of massive dorbank horizons and their enveloping vertical and horizontal laminations. Scanning Electron Microscope analyses indicate high concentrations of Mg, Al, Si and O which suggests sepiolite and palygorskite accumulation through a replacement of gypsum.

Elemental maps in conjunction with x-ray tomography and bulk chemical analyses revealed that high concentrations of secondary barite occur along the contact surfaces between dorbank horizons and the laminations. The solution chemistry of all horizons show supersaturation with respect to barite suggesting that the Ba accumulation adjacent to the laminations is likely to have taken place at lower sulphate conditions than those present in the soils today.

Evidence shows that Vaalputs soils have experienced at least one climate shift. The preserved soil mottles are indicative of soil environments that remain wet for an extended period. A fine textured platy dorbank horizon is an extensive feature in Vaalputs. The presence of this horizon indicates that the sediments were deposited from a low energy fluvial system. The large polygonal ped units in the lower dorbank units as well as the barite enrichments in pore spaces suggests a climate shift from wet to dry began after the sediments were deposited.

Uittreksel

Vaalputs radioaktiewe afval fasiliteit is geleë in 'n ariede streek van Namakwaland met evapotranspirasie potensiaal wat neerslag tans ver oorskry. Dominante grond funksies in Vaalputs sluit in ‘palimpsests’ klimaat kondisies waaronder dit gevorm het. Deeltjies groottes wissel drasties tussen horisonne wat op verskillende vorme van sediment vervoer dui. Die oppervlak in Vaalputs word gedek deur 'n gelyke korrelagtige growwe sand van residuele eoliese oorsprong. Die oorgang vanaf die oppervlak horison na die ondergrondse horisonne word algemeen gekenmerk deur 'n spoelsteen grootte kliplyn. Die spoelsteen grootte materiaal van die kliplyn dui op residuele opbou gedurende die verwering van 'n voormalige oppervlak blootgestelde horison.

Sedert afsetting van die ondergrondse sedimente (15 Mj) is pedogenetiese veranderinge reeds aktief in Vaalputs. Dit het gelei tot 'n komplekse grond stelsel wat verskillende vorme van dik dorbank horisonne insluitend massiewe veelhoekige pedons en plaatagtige horisonne vertoon. Die veelhoekige pedons word gedefinieer deur uitgedroogde krake waar die vertikale en horisontale lamellering aangetref word. Ontbindingstoetse sowel as heelrots chemiese analiese bevestig dat die lamellering grootliks bestaan uit 'n sekondêre kalsiet. Elementele kartering het egter talle illiet bande afgewissel met kalsiet lae openbaar. Daar word voorgestel dat kalsiet lae verteenwoordigend van oplossingskenmerke is eerder as kuntanise kenmerke.

Tekens van hidromorfie word algemeen binne die dorbank horisonne waargeneem, aangesien droë klimaat tans in Vaalputs heers kan sulke hidromorfiese kenmerke dui op die vorming onder vorige klimate. Die groot voorkomste van paligorskiet, sepioliet en dorbank horisonne in Vaalputs vereis hoë grond pH (wat gegenereer word deur hoë konsentrasies van Na) vir hul vorming. Vaalputs grond het egter relatief neutrale pH gemeet en relatief lae Na konsentrasies wat daarop dui dat paligorskiet, sepioliet en dorbank horisonne oorblyfsel kenmerke is.

Sout gietforme met lentikulare texture kom voor tussen veelhoekige pedons van massieve dorbank horisonne en hul omhullende vertikale en horisontale lamellerings. SEM analiese toon hoe konsentrasies Mg, Al, Si en O aan wat opbou van sepioliet en paligorskiet deur verplasing van gips voorstel.

Petrografiese analiese het euhedraal geaardheid van primere veldspaat mineraal getoon binne die grond van Vaalputs. Dit stel ‘n bron van sediment voor en minimale pedogenese in dorre klimaat waar euhedraal korrels veldspate bewaar bly.

Elementele kartering tesame met x-straal tomografie en heelrots chemiese analiese het getoon dat hoe konsetrasies sekondere bariet langs die kontak oppervlakke tussen dorbank horisonne en lamellerings voorkom. Die oplossingschemie van alle horisonne toon superversadiging met betrekking tot bariet wat voorstel dat die opbou van Ba langs die lamellerings waarskynlik plaasgevind het by laer sulfaat kondisies eerder as die kondisies wat heedendaags in grond voorkom.

Bewyse toon dat Vaalputs grond ten minste een klimaatsverandering ondergaan het. Die gepreserveerde grond vlekke is kenmerkend aan grond omgewings wat vogtig gebly het vir ‘n geruime tyd. ‘n Fyn getekstuurde plaatagtige dorbank horison is ‘n uitgebreide verskynsel in Vaalputs. Die teenwoordiheid van hierdie dorbank toon aan dat sedimente vanuit ‘n lae energie fluviale sisteem afgeset het. Die groot veelhoekige pedon eenhede in die laer dorbank eenhede sowel as die bariet verryking in porie spasies stel voor dat ‘n klimaatsverandering vanaf vogtig na droog begin het nadat die sediment afgeset het.

Acknowledgements

I would like to thank the Earth Science department at the University of Stellenbosch for giving me an opportunity to be enrolled for a Masters' degree. Inkaba yeAfrica for funding this research project. Special thanks to my Supervisor, Dr. Cathy Clarke for every support she provided throughout as well as my co-supervisor Dr. Daniel Mikeš. I thank NECSA staff including Dr. Marco Andreoli and Andrew Logue for their support and input as well as the x-ray tomography lab for the analyses they performed. iThemba LABS staff, most importantly Dr. Wojciech Przybylowicz for the PIXE analyses and his further input as well as Dr. Remy Butcher for the XRD analyses. A thanks is also owed to Dr. Cornie van Huysteen for his insight in the field. I also thank family, friends and fellow students for their ideas and support.

Table Contents

List of Figures

List of tables

1. Chapter 1: Introduction

1.1. Overview

South Africa planned its first nuclear power station in the mid-1970s. There was therefore a need to develop a plan for the disposal of the waste to be generated. A search for a suitable waste disposal site began in the early 1980s while following strict criteria. This criteria included; low rainfall and extremely high evaporation, deep water-table, stable seismic conditions, stable surface and groundwater conditions, minimal impact on surrounding nature reserve or ecologically sensitive systems, the site must have thick clay-rich soils and sediments of low hydraulic conductivities, low agricultural, mining and economic growth potential, distance from international borders, low population density. The search for a suitable waste disposal site ended in the mid-1980s with the identification of the Vaalputs area. The first low and intermediate radioactive waste load was scheduled for delivery in the late 1986. Currently Vaalputs is managed by the Nuclear Energy Cooperation of South Africa (NECSA) which hosts low and intermediate level waste. The low level waste is disposed in metal drums whereas the intermediate level waste is disposed in concrete drums and buried in trenches excavated to depths of no more than 8 m. The excavation of trenches and a large number of boreholes have revealed a complex system of fluvial sediments which have been pedologically altered since deposition in the Neogene period. Several studies conducted within the area of Vaalputs (Andreoli *et al*., 2006; Brandt, 1998; Brandt *et al*., 2003; Brandt *et al*., 2005; Majodina, 2010; McCarthy, *et al* 1985) suggest a need to understand a long-term behaviour of pedogenic and sedimentary features in order to fully assess the Vaalputs site.

Gaining knowledge about the physico-chemical conditions from which the anomalous soils features formed provides an understanding of geochemical processes that have occurred or are occurring in the soil. These anomalous pedogenic and sedimentary features hosted within the Vaalputs soils include (i) aeolian sand, (ii) stone-line below aeolian sand, (iii) a thick package of dorbank (duricrust) horizons, (iv) vertically and horizontally orientated laminated structures which dissect dorbank horizons, (v) barite ($BaSO_4$) accumulation along orientated laminated structures. The presence of mineral barite associated with vertically and horizontally orientated laminations documented by Majodina, (2010) suggest complex near-surface geochemical and possibly groundwater activities previously

unrecognised, yet potentially important to the as sealing material to the waste filled trenches. Therefore the importance of understanding the genesis and evolution of Vaalputs soils also provides input data for modelling to further reaffirm the stability of geochemical activities. The understanding of formation of these anomalous soil features provides an opportunity to gain insights into the past climates that have shaped the palaeosols at Vaalputs.

1.2. Aims and Objectives

The overall aim of this study is to characterise the morphological, geochemical as well as mineralogical composition and distribution within selected Vaalputs palaeosols. This is to complement the postulation of physico-chemical conditions under which the formation of the observed features including (i) aeolian sand, (ii) extensive stone-line observed on profile of several trenches, (iii) large occurrences of surface exposed and buried dorbank (duricrust) horizons, (iv) vertically and horizontally (box-shaped) laminated structures and often associated with barite accumulations occurred. In doing so, tentative deductions may be made on the palaeoclimatic conditions that have influenced the formation of these soils.

In order to achieve this aim the following objectives will be met:

- Determine morphological features that provide evidence about physical conditions such as climate, sediment source and deposition mechanisms that were active during the accumulation of sediments in Vaalputs.

- Determine elemental associations and distribution on both a macro and micro scale in order to explain the accumulation mechanisms of the sediments as well as the formation of the morphological and chemical features observed in the profiles.

- Determine the composition and distribution of clay mineralogy and assess their conditions of formation and evaluate their stability under current climate conditions.

- Using chemical equilibrium modelling of the soil solution, to determine the inherited vs. contemporary nature of the secondary mineral suite.

- Finally using all the morphological, chemical and mineralogical information acquired an attempt will be made to put tentative constraints of palaeoclimates in the region.

1.3. Site description

Vaalputs is located in an arid region with an average annual rainfall of 74 mm within Bushmanland along the eastern edge of Namaqualand. This area falls within the coordinates of 30°08' south and 18°53' east at approximately 1000m above mean sea level (Brandt *et al.*, 2005). Vaalputs lies approximately 100km south east of Springbok town in the Northern Cape Province, South Africa. The site is covered by an undulating sheet of NNE-SSW trending linear sand dunes of low amplitudes (McCarthy *et al.*, 1985; Brandt, 1998 and Brandt *et al.*, 2005). To the west of the Vaalputs site lies the great escarpment (approximately 1200 to 1700 metres above mean sea level) that runs parallel, north-south, to the west coast of South Africa giving rise to a landward gently sloping surface (Brandt *et al.*, 2005 and Andreoli *et al.*, 2006). To the east of the Vaalputs site, the surface is relatively flat and the dominating surface geology is of sedimentary origin such as sand cover and duricrusts .

At trench scale highly heterogeneous geochemical and pedogenic environments are observed. and sedimentary features are revealed. Features observed on one trench may not be represented on the wall of the adjacent trench.

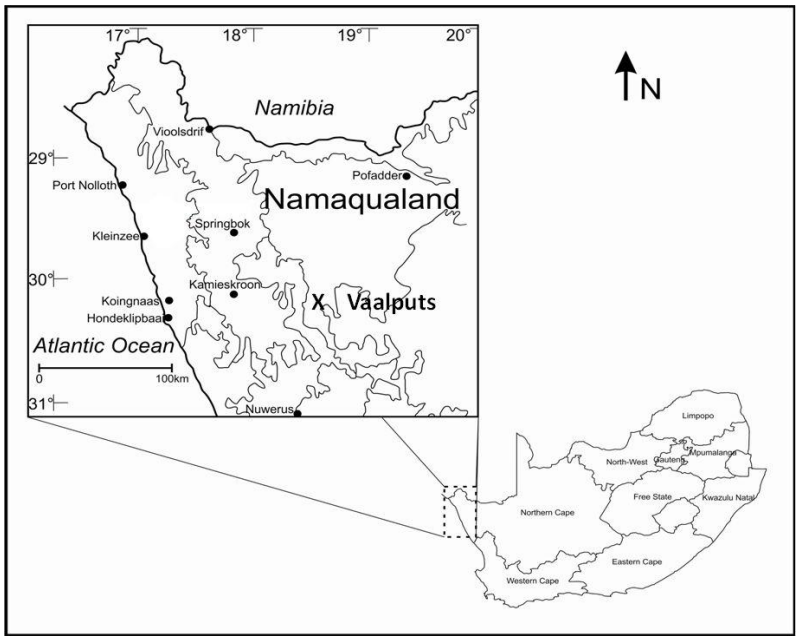

Figure 1.1: Map indicating roughly the location of Vaalputs in the Northern Cape Province

1.4. Regional Geology and Soils

1.4.1. Geology

The basement lithology is dominated by the Namaqualand metamorphic complex which is subdivided into numerous formations such as Augen gneiss of Little Namaqualand Suite (~1200 Ma), various granitiods of Southern Megacrystic Suite dated at ~1060 Ma, the charnokites of Kliprand Charnokitic Suite of ~1060 to 1030 Ma and finally the diorites, norites, hypersthernites and Enderbites of Koperberg Suite dated at ~1030 Ma (Pretorius, 2012). Conradie & Schoch (1986) and Duchesne *et al.*, (2007) reported up to 10wt% of calcite within the diorites and norites of the Koperberg Suite near Okiep. Duchesne *et al.*, (2007) further reported up to 4800ppm Ba concentrations on the diorite series. The basement granitic rock formation in Vaalputs is unconformably overlain by an unconsolidated sedimentary package that may reach depths of approximately 15 metres below surface (Brandt, 1998; Brandt *et al.*, 2005). The lower zones of the transition from the underlying basement granite-gneiss to the sedimentary units is marked by palaeo-weathered (kaolinised) basement which may grade over two metres. The upper zone of the transition from the basement to the above lying sediments is usually silicified and abrupt, occurring within half a metre (Brandt *et al.*, 2005). The lower most sediments of the Dasdap Formation (not yet accepted by SACS) mainly consist of conglomerates and immature cross-bedded arkosic grits. Overlying the Dasdap Formation is the Vaalputs Formation that is largely composed of grits and pebbles on clay rich sediments. The lower zone of the Vaalputs Formation has been interpreted as being deposited from unchannelised floodouts whereas the upper zone is thought to indicate fluvial origin under much wet conditions. Overlying the Vaalputs sediments are highly indurated dorbank horizons (silica cemented) and occasionally calcareous materials which are usually over metre thick. The top most unit is an unconsolidated undulating red sand of Gordonia Formation which was interpreted by Brandt (1998) as reworked sediments by aeolian activities.

1.4.2. Soils

In this study, the Vaalputs radioactive waste disposal site is loosely divided into two sections by R355 road. The two sections are referred as Vaalputs East and Vaalputs West. Vaalputs West falls within the Namaqualand region and the large portion of the Vaalputs site (Vaalputs East) falls within the Bushmanland plains. The Bushmanland region is

characterised by summer rains (Cowling *et al.*, 1999) with an average annual precipitation of 130mm and evapotranspiration potential of 2450 mm. The site temperature ranges from a minimum of -5°C to a maximum of 36°C (Pretorius, 2012). Soils of the Bushmanland plain are largely covered by red soil derived from reworking of fluvial deposits. The soils along the Namaqualand-Bushmanland boundary may be slightly enriched with clay material. Dorbank and calcrete horizons are also common in this region (Desmet, 2007).

The soils of Namaqualand region, which Vaalputs West is part of, are more studied (Francis, 2008; Francis *et al.*, 2007; Desmet, 2007; Ellis & Schloms, 1982). The Namaqualand region is dominated by winter rainfalls (Cowling *et al.*, 1999; Francis, 2008) with an average annual precipitation of 160mm. Francis (2008) conducted a detailed study of soils along the Namaqualand coastal plain and demonstrated that marine component has a significant influence on soil chemistry which in turn has a result on the mineralogical make-up of the soils. This verified the mineralogical study by Singer *et al.*, (1995) that concluded that coastal soils in Namaqualand contain the fibrous mineral sepiolite ($Mg_4Si_6O_{15}(OH)_2 \cdot 6(H_2O)$), while soils further inland contain the more Al-rich species palygorskite ($(Mg,Al)_2Si_4O_{10}(OH) \cdot 4(H_2O)$). Other information on the soils of the region is limited to the Land Type Survey (Land Type Survey Staff, 1987), the PhD thesis of Ellis (1988) and a number of unpublished irrigation reports.

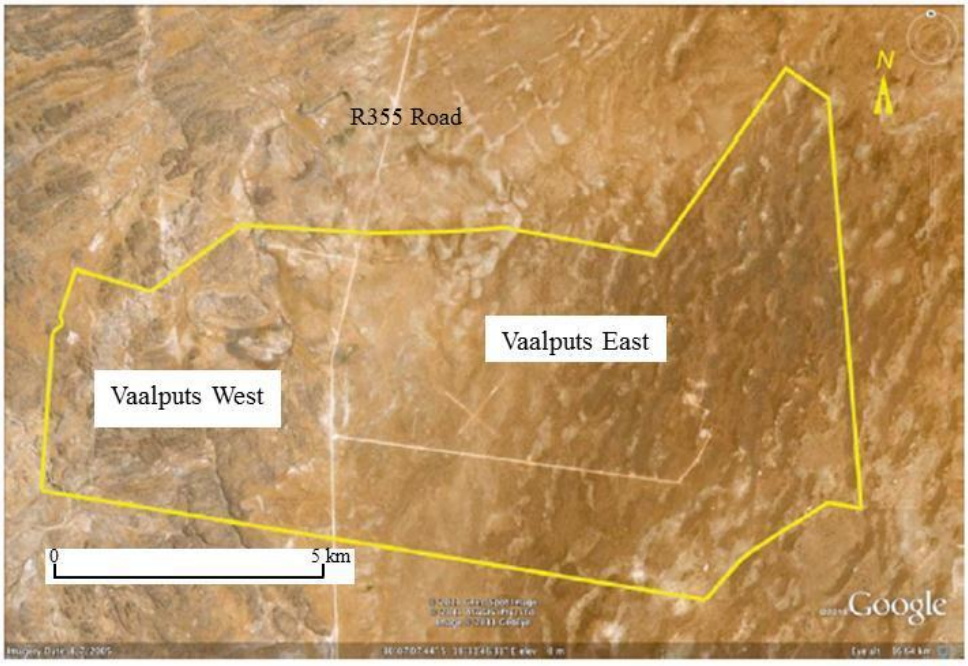

Figure 1.2: An aerial photo showing the extent of the Vaalputs radioactive waste disposal site. The R355 road cutting through the site is used in this study as the boundary between the Namaqualand (Vaalputs West) and Bushmanland (Vaalputs East) plains (modified from Desmet, 2007).

1.4.3. Palaeo-environment

Several palaeo-environmental studies have been conducted within the Northern Cape Province (Kent & Gribnitz, 1985; Pickford *et al.*, 1999). Vaalputs sediments have received much attention as they host South Africa's radioactive waste. McCarthy *et al.* (1985) conducted a study and observed poorly sorted sediments in Vaalputs. These sediments were interpreted as an alluvial fan deposit. Later, Brandt *et al.* (2003) and Brandt *et al.* (2005) produced stratigraphic interpretations of the Vaalputs sediments. Both these studies concluded that, apart from the lowermost sediments of the weathering basement (locally know as white clay) and the surface sediments (locally known as Gordonia Formation), the Vaalputs sediments are largely alluvial in origin. According to Brandt *et al.* (2005), Vaalputs sediments were generated during the mid-Tertiary. This timing coincides the Post-African cycle I of Partridge & Maud (1987) which peaked during early mid-Miocene to late Pliocene time. During this period, wet conditions prevailed in the Namaqualand region and large volumes of sediments were generated and deposited on proximate basins. Pickford *et al.* (1999) later studied the age of calcrete (indicative of dry environments) in from Areb (approximately 50km north east of Vaalputs) Namaqualand using biochronology. Findings from latter study suggest that the Areb calcretes date to the Pliocene-Pleistocene boundary. Thus dry climates prevailed after the deposition of Vaalputs sediments. The study of Kent & Gribnitz (1985) (conducted on a pan in Swartkolkvloer, approximately 150km south east of Vaalputs) indicated that the climate during the late Pleistocene (~17500 Ka) was cold and relatively dry and later the precipitation drastically increased around 15000 Ka. Subsequently, the climate became drier and warmer around 11000 Ka.

1.5. Brief chapter overviews

This study presents geochemical, mineralogical as well as macro and micro-morphological features observed in Vaalputs and attempts to infer climatic conditions related to their formation and distribution.

Chapter 1 is an introductory section in which general information about this research project including the location of Vaalputs, the history of the area as well as the surrounding geology and soils.

Chapter 2 investigates structural features to gain knowledge about its conditions of formation in order to infer palaeoclimates and soil environments that may have been active during formation of each feature. These observations are made on field relations, hand sample and thin sections.

Chapter 3 presents geochemical characteristics and relationships within Vaalputs palaeosols. Elemental distributions are investigated while interpreting their associations.

Chapter 4 presents dominant clay (<2µm) mineralogy and the chemical equilibria within the soils in order to determine the inherited vs. contemporary nature of the secondary mineral suite.

Chapter5 is an overall discussion of the work presented through this document and communicates elemental, mineral and morphological relationships which are all tied together in order to infer palaeoclimates.

Chapter 6 concludes the overall research and recommends further work.

1.6. Previous work

An honours research project was conducted by Majodina, (2010) with an aim of characterising the chemical and mineralogical compositions of the Vaalputs palaeosols. The main deductions made from this study suggested that the subsurface soils were largely composed and cemented by silica and fairly high calcite concentrations thus classifying as calcareous dorbank horizons. High Ba concentrations were also detected in this study however very little was done to determine the mineralogy of Ba and spatial distribution. Some of the data used in the current study is taken from a preliminary study on the Vaalputs palaeosols by the author of this thesis (Majodina, 2010: Appendix 1). Where data is used from the study of Majodina, 2010 it is fully referenced in the current study. All interpretations made on the samples collected for this study and for the study of Majodina, 2010 are new and reflect new insights gained in the analysis of further samples.

2. Chapter 2: Geomorphological Characterisation of Vaalputs palaeosols and sediments

2.1. Introduction

Vaalputs radioactive waste disposal facility is located in an arid region of Bushmanland characterised by soil morphologies indicative of such arid environments. Numerous geological studies have been conducted within the Bushmanland terrain however very little is known about the soil and sedimentary cover in the region. Several sporadic soil and sedimentary studies have been conducted within Namaqualand region (Ellis and Schloms, 1982; Francis *et al.*, 2007; Francis, 2008; Fey, 2010; Le Roux et al., 2010) and even less within Vaalputs (McCarthy et al., 1985; Brandt, 1998; Brandt, *et al.*, 2003; Brandt *et al.*, 2005). Although (Partridge & Maud, 1987; Partridge *et al.*, 1996) presented regional soil morphologies throughout Southern Africa, no soil morphological study has been conducted at soil horizon scale within Vaalputs area.

Palaeoclimate interpretations deduced from relic soil features has been used by numerous authors (e.g. Retallack, 2001).

The aim of this chapter is to investigate each structural feature to gain knowledge about its conditions of formation. This will further present an opportunity to infer palaeoclimates that were active during formation of each feature. Morphological features have been widely used in soil environments as palaeoclimate indicators however due to complexities presented by the soils in Vaalputs, inference of palaeo-environmental conditions must be viewed as a starting point upon which further studies can be based. Accurate palaeoclimate interpretations in and around Vaalputs will require numerous studies within which dates of sediment depositions are constrained.

2.2. Materials and Methods

Two trench profiles at the Vaalputs radioactive waste disposal facility in the Northern Cape were sampled over the period of 2009 to 2010. Field classification of horizons was partly based on the degree of induration, stratigraphic appearance as well as in accordance to the South African Soil Classification system (RSA Soil Classification Working Group, 1991). The collected samples have been labelled using conventional master horizon

abbreviations (A,B,C etc.), however due to the complex nature of the soil profile these demarcations may not strictly comply with master horizon definitions. The samples were carefully obtained in dry state from two profiles of trenches B(1,1) (Figure 2.2a and b) and C(1,5) (Figure 2.3a and b).

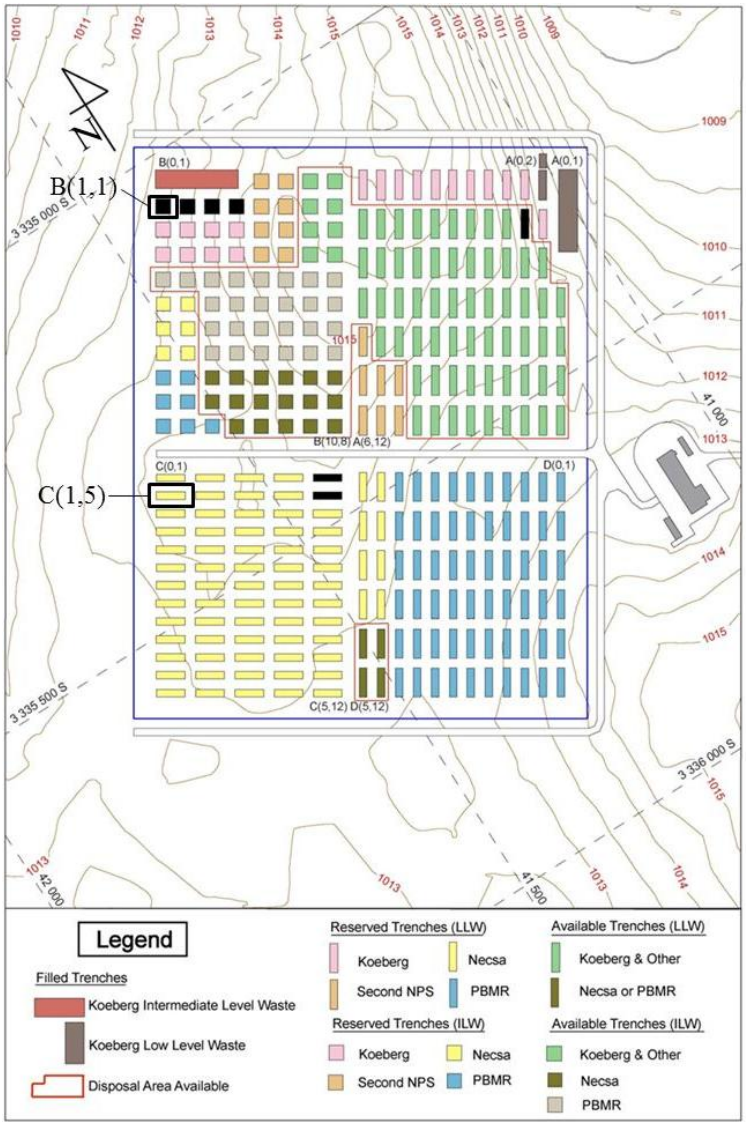

Figure 2.1: The distribution of radioactive waste disposal trenches at Vaalputs. Trenches B(1,1) and C(1,5) were selected as representative trenches to be used in this study. The relative location of the sampled trenches is indicated on the map.

The soils in Vaalputs are highly heterogeneous and show a large spatial variability in morphology features as well as mineralogical and chemical composition. The process of selecting a trench with a representative soil profile was complicated and led to the identification of B(1,1) and C(1,5) trench profiles (Figure 2.1). This decision was largely influenced by the typical system of laminae around dorbank horizons which these profiles displayed. Both profiles were classified according to the South African Soil Classification

system (RSA Soil Classification Working Group, 1991) (Table 2.1 and Table 2.2). After classification, samples were collected from loose to highly indurated soil horizons.

Figure 2.2b and Figure 2.3b are simplified diagrams of the sampled trench profiles with their respective horizons. All samples obtained from horizons of trench B(1,1) were labelled from top to bottom as A, B1, B2, H-L, B3 (B3E and B3W), V-L, B4 and C. Samples H-L and V-L were collected from the typical horizontal and vertical system of laminated materials enveloping the lower dorbank horizons, respectively. H-L (horizontal laminations) is a material that lies horizontally between the B2 from the B3 horizons. The V-L (vertical laminations) is a material which occurs on the outer most surfaces of the polygonal ped units of B3 horizon. Two adjacent ped units separated by V-L were sampled from the dorbank B3 horizon. These peds are sampled east (B3E) and west (B3W) of the laminated zone. B2L is vertical streak of laminated material that begins from the B2 horizon at the top and ends by joining the V-L material near the bottom of V-L. Trench C(1,5) exhibited a similar soil profile as trench B(1,1) only with the absence of horizon B2.

Although the trenches are excavated to a maximum depth of 8 metres below soil surface, only the top 3 metres were accessible for sampling. The collection of samples from each horizon was achieved using a geological hammer and a spade. The samples were stored in sampling bags for safe transporting.

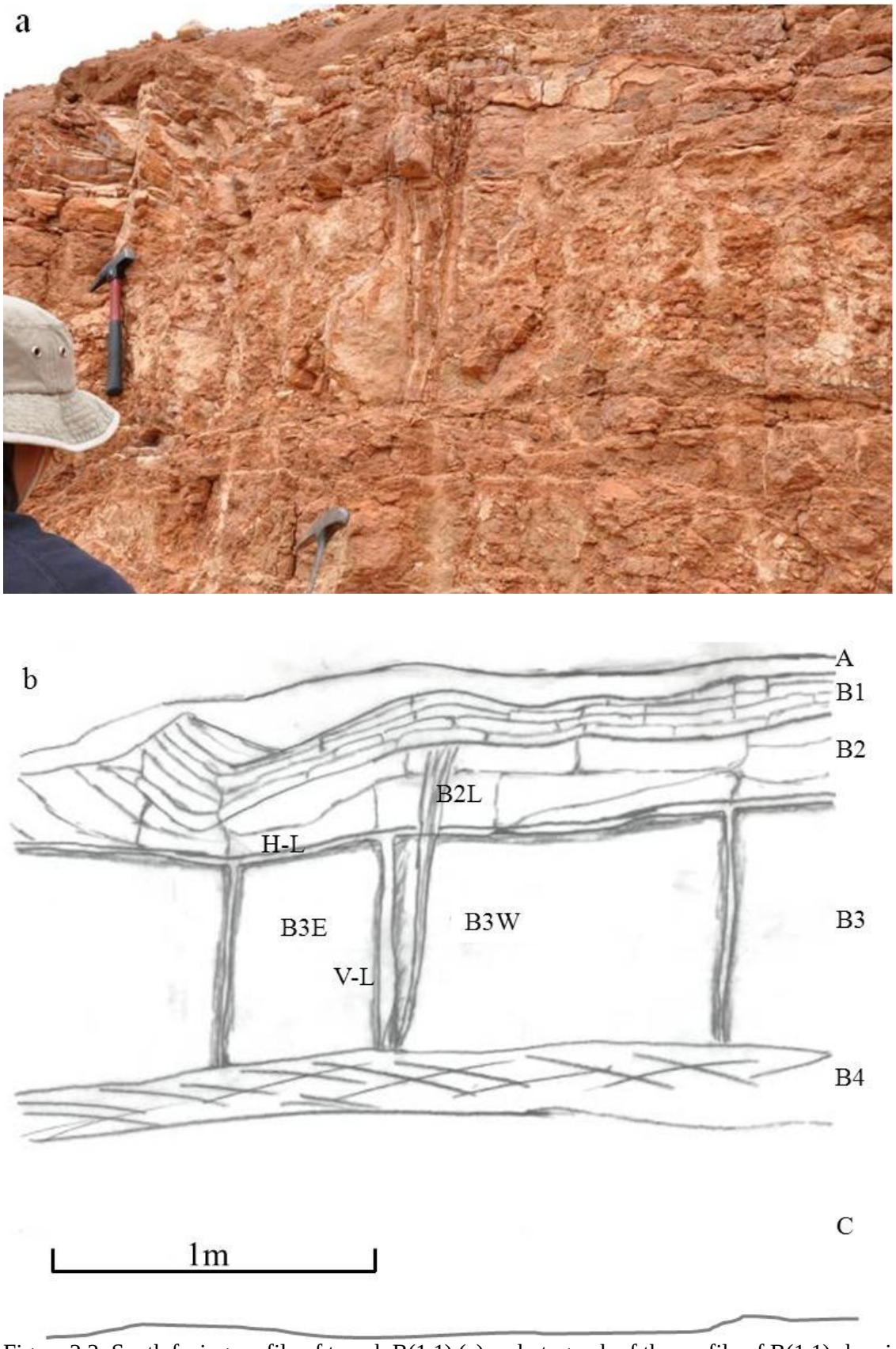

Figure 2.2: South facing profile of trench B(1,1) (a) a photograph of the profile of B(1,1) showing a typical arrangement of horizons in Vaalputs (b) a schematic diagram of trench B(1,1) which includes horizons from which samples were collected.

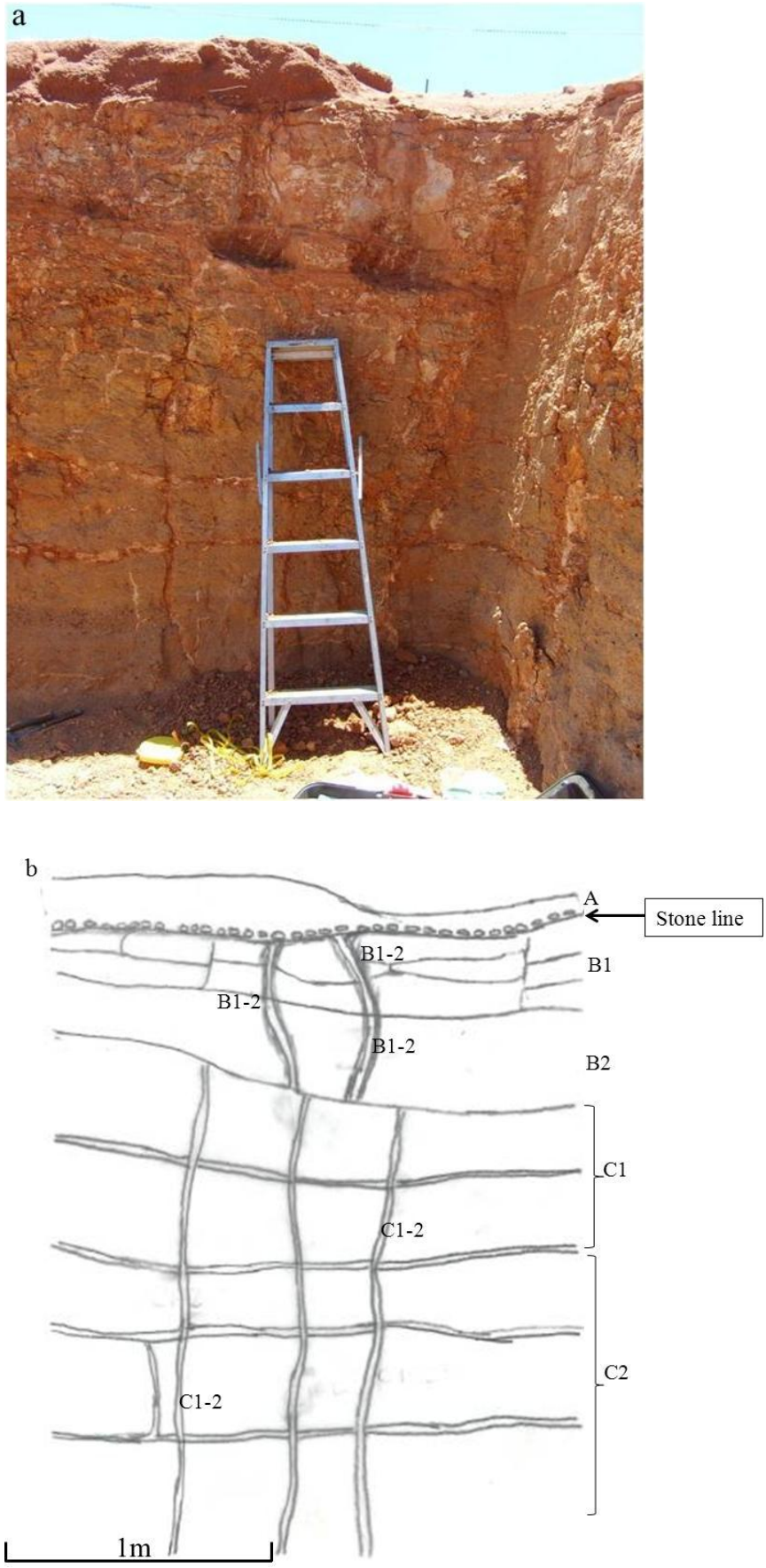

Figure 2.3: A north facing profile of trench C(1,5) (a) a photograph of the profile of C(1,5) showing a typical arrangement of horizons as well as the a stone-line between A and B1 horizons (b) a schematic diagram of thrench B(1,1) which includes horizons from which samples were collected.

Subsequent analyses were executed on all samples collected for each horizon and laminated materials of both trench profiles.

Thin section preparations were carried out on consolidated soil materials using epoxy resin. Since not all horizons were composed of consolidated soil materials, only B1, B2, B2L, H-L, V-L, B3E and B3W materials from trench B(1,1) as well as B1-2 laminated material from trench C(1,5) were selected for petrography. The resulting polished thin sections were studied under a petrographic light microscope and Scanning Electron Microscope (Chapter 3). All thin section photomicrographs were taken under plane polarised light (ppl) and cross polarised light (xpl) at 40 times magnification.

Particle size analyses were carried out on samples from all horizons of trench B(1,1) following the method of Gee and Bauder (1986). The aim of this analysis was to determine the mechanism through which Vaalputs sediments were deposited.

2.3. Results

2.3.1. Macro-morphology

Both profiles were classified as the Garies soil form which consists of an Orthic A horizon on a red apedal B horizon on dorbank. A detailed description of profiles B(1,1) and C(1,5) are provided in Table 2.1 and Table 2.2, respectively.

Table 2.1: Trench B(1,1) sample description and Soil profile classification according to the RSA Soil Classification Working Group (1991).

Depth (cm)	Description	Sample name	
0-20	Dry, reddish yellow (7.5YR 5/6), sandy loam, massive structure, loose to slightly hard consistency, few rounded coarse fragments abrupt transition to	A	
20-28	Dry, pink ped interior (2.5YR 4/8) and reddish-yellow (7.5YR 8/4) cutans, coarse platy structure, very hard consistency, strong HCl reaction, moderate HCl reaction on clay cutans, abrupt transition to	B1	
28-50	Dry, red (5YR 5/8), coarse platy structure, highly indurated, very hard consistency, few Mn mottles and cutans around peds, no HCl reaction, abrupt transition to horizontal (H)-laminations	B2	
50-52	Horizontal dense whitish (10YR 8/2) and brown (7.5YR 8/4) laminated material, both white region and brown regions have a fine texture, moderate HCl reaction, showing clay accumulation on outer ped face, abrupt transition to	H-L	
52-90	Dry, red (5YR 5/6) with 40% reddish-yellow mottles (5YR 8/3), primary structure very large (40-47cm) prismatic structure, secondary structure massive, very hard consistency slight HCl reaction, abrupt transition to B4	B3E and B3W	B3 horizon
52-90	Vertical laminations, as for H-L.	V-L	
90-104	Dry, red (5YR 5/8), coarse platy structure, brittle consistency, fine horizontal lamination network system with moderate HCl reaction, abrupt transition to	B4	
104-240	Dry, yellowish (10YR 6/8), slightly hard, dissected by diagonally intersecting fractures at low angles (<25°), many white (5Y 8/2) sepiolite and/or palygorskite flakes (-ve HCl reaction, positive methyl orange test) at 160 cm depth.	C	

Table 2.2: Trench C(1,5) Soil profile classification according to the RSA Soil Classification Working Group (1991).

Depth (cm)	Description	Horizon	Laminated samples
0-30	Slightly moist, strong brown (7.5YR 5/6), sandy loam, apedal structure, loose consistency; few roots, no HCl reaction, abrupt transition through a stone-line to	A	
30-60	Dry, mottled pink (5YR 5/6) and cream (10YR 8/3), highly indurated dorbank, very coarse platy structure, macro peds with few cracks, very hard and brittle (Petroduric), many hard and fine grained vertical and horizontal pinkish red (7.5YR 8/4) and whitish (10YR 8/2) laminated materials (no HCl reaction) between peds; MnO_2 oxide lenses at 40 cm, abrupt transition, through the laminations to	B1	
60 -90	Dry, mottled pale red, red and reddish yellow (7.5YR 5/6), very coarse laminated structure, very large macro peds (40-50 cm) with few cracks, very hard (slightly less hard than B1) substantially more $CaCO_3$ mottles than above horizon many vertical and horizontal cream laminated materials between peds, most of the lamination material does not react with HCl, but some $CaCO_3$ was present between laminations, abrupt transition across the lamination to	B2	B1-2
90-140	Dry, yellowish (10YR 6/6) with abundant red mottles and few white mottles, massive structure, hard (less than B2), -ve HCl reaction, white horizontal and vertical laminations (+ve HCl reaction), many coarse fairly rounded gravel fragments, few MnO_2 mottles	C1	
140- 290	Dry, yellowish (10YR 6/6) with abundant red mottles and few white mottles, sandy loam, massive structure, slightly hard (less than C1), (-ve HCl reaction), white horizontal and vertical laminations (+ve HCl reaction) spaced further apart than above B2, many coarse fragments in beds, many white (5Y 8/2) sepiolite and/or palygorskite flakes (-ve HCl reaction, positive methyl orange test)	C2	C1-2

Profiles B(1,1) and C(1,5) are very similar with the exception that the fine platy B1 horizon of B(1,1) is not present in C(1,5). Generalised descriptions of the horizon materials are given below.

The A horizon is the topmost horizon of trench profiles in Vaalputs (Figure 2.3, Figure 2.4, and Figure 2.5). It is composed of uniform red loose to moderately indurated material which has a sandy loam texture. The transition from the loose A horizon to the underlying indurated B1 horizon is marked by a distinct stone-line (Figure 2.3b) which is observed in a similar position in other trenches within the site. The upper dorbank horizon (B1) has a fine platy structure (Figure 2.3, Figure 2.4, and Figure 2.5). Within the peds a finely laminated substructure is evident. The exterior of the peds have a light brown colour (7.5YR 8/4) while the ped interiors are reddish brown (2.5YR 4/8) thus the horizon has a distinct cutanic nature. Both the ped interiors and the cutans (defined below) do not react with a dilute HCl acid. The texture of the B1 horizon is substantially finer than that of the above A horizon. The transition between the B1 and underlying B2 horizon is abrupt (Figure 2.5).

Figure 2.4: The loose uniform red A horizon on top underlain by the platy B1 horizon. The transition between the two horizons is abrupt (indicated with a white line) from A to B1 horizon.

The B2 is slightly less indurated and has a coarser platy structure than the overlying B1 horizon. Horizontal cracks within the peds of B2 horizon are prevalent and create an appearance of a fine platy substructure (Figure 2.5). Between cracks there is evidence of clay mobilisation which gives the peds a cutanic appearance. Generally the texture is significantly coarser than the overlying B1, however there are substantial variations in texture within layered zones of the peds. The matrix material hosts numerous large (up to 1mm in diameter) pore spaces. Disseminated Mn oxide mottles are prevalent in all dorbank horizons (B1, B2 and B3), in addition the B2 horizon shows a distinct 3-5 cm Mn oxide band which occurs continuously along the length of the trench (Figure 2.6). The B2 horizon shows no reaction with a dilute HCl acid.

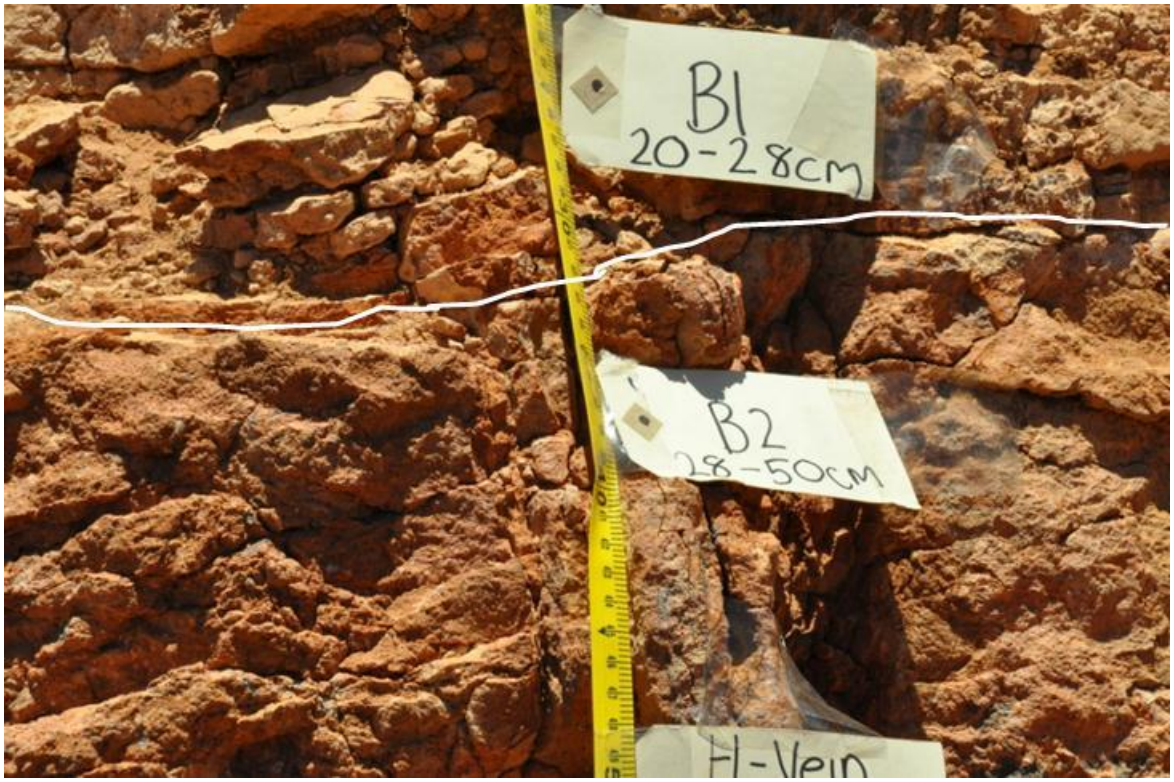

Figure 2.5: Abrupt transition (indicated by a white line) from the fine grained platy dorbank (B1) to a substantially coarse grained dorbank (B2) horizon with a massive structure.

Underlying B2 (of trench B(1,1)) is the B3 horizon comprised of large polygonal features (macro peds 40-50 cm wide) that are enveloped by a series of fine white laminations (Figure 2.2, Figure 2.3 and Figure 2.7). The macro peds are separated into discrete units by relatively large gaps of approximately 2 mm wide (Figure 2.7: white arrows). The substructure within the macro peds (B3E and B3W) is best described as massive to weak coarse blocky.

Figure 2.6: 5cm wide Mn band running through the length of B2 horizon

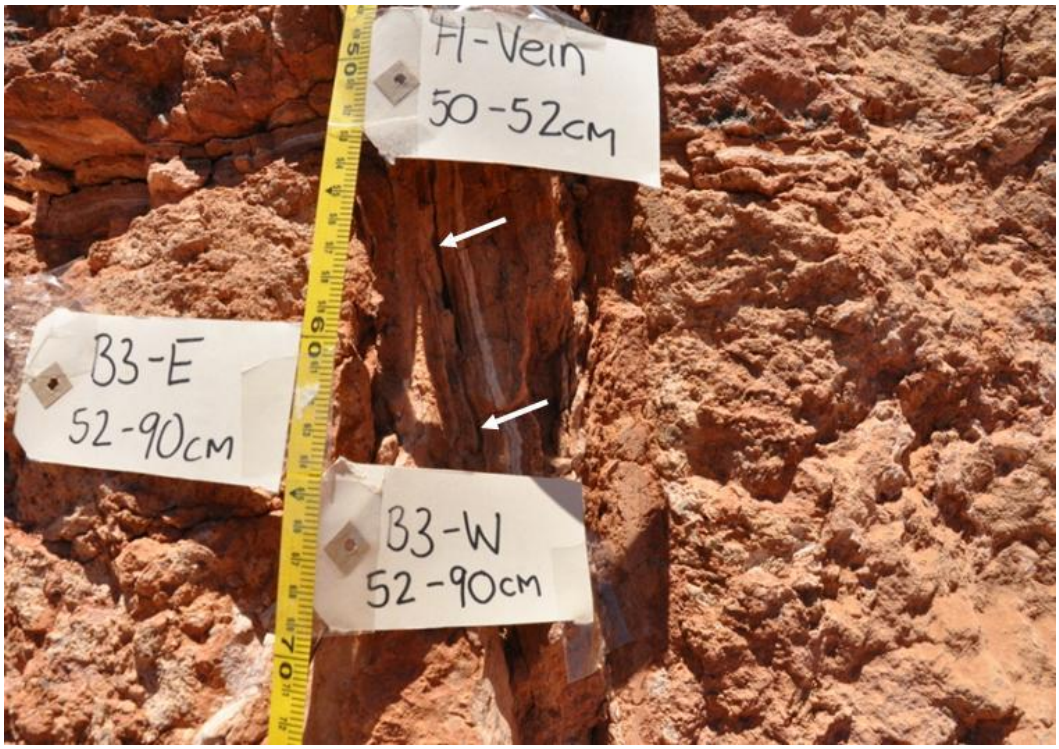

Figure 2.7: B3E and B3W with H-V material on the edges of each ped unit. The peds are separated into discrete units by a 2mm wide crack (white arrows).

Macro ped units (Figure 2.7) are coated with light coloured (7.5YR 8/4) cutans. These cutans often appear to be composed of numerous layers. The general white bands (H-L and V-L), which envelope the macro peds, vary in distance from the outer cutans (Figure 2.8a). In some instances the band of laminations lies directly adjacent to the cutanic layers and in

other areas it occurs at 10-15 mm from the edge of the ped. At higher magnification (40X) the white bands of laminations appear wavy and consist of white layers interlayered with fine brown layers (Figure 2.8b). In some instances the laminated material extends 3 to 4 cm into the ped. The zone of laminations is distinctly finer textured that the matrix material of the ped.

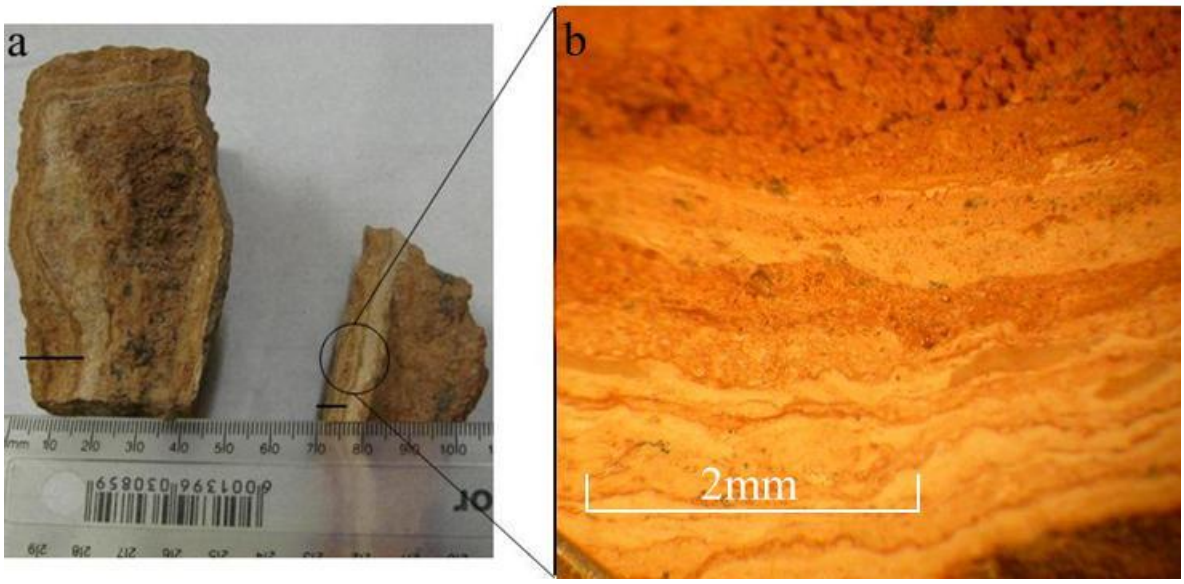

Figure 2.8: Samples showing laminated zones along the edges of ped surfaces (a) two hand samples showing varying distances (indicated by black lines) from white region to the outermost ped coating cutans (b) a magnified (50X) micrograph showing wavy white calcitic material alternating with a brown clayey material which together envelop the dorbank ped units.

Adjacent to the laminated zone within the B3 dorbank matrix, fine lenticular salt casts are observed (Figure 2.9a - c). Although it is difficult to determine the origin of these casts, the spatial density and shape suggests that they are most probably salt casts rather than root casts.

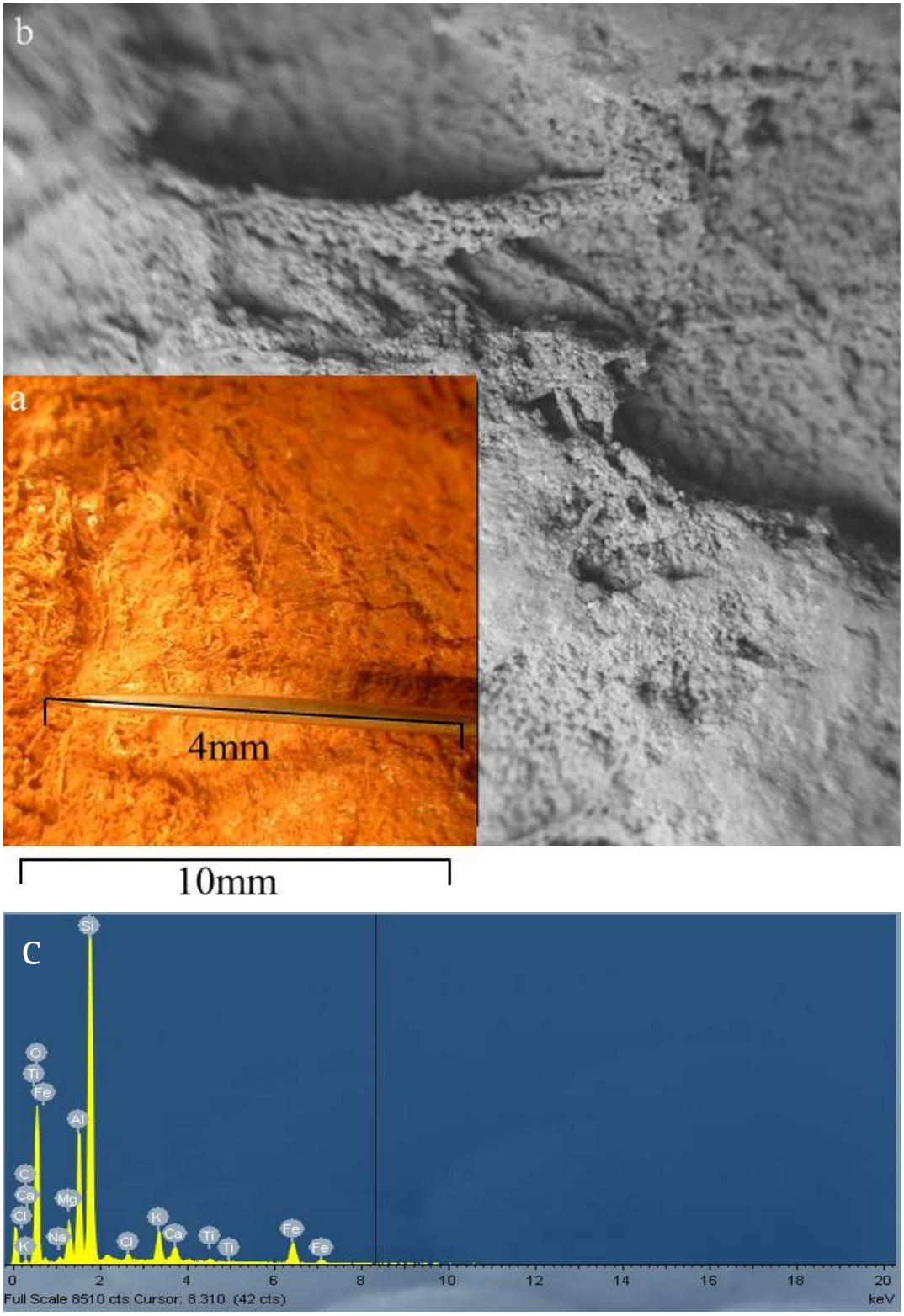

Figure 2.9: A contact surface of the B3 horizon and the laminated (H-L and V-L) material showing salt casts of lenticular texture (a) micrograph of hand sample (b) backscatter image rendered using SEM and (c) EDS graph showing high Si, Al, Mg and O thus indicating palygorskite (and sepiolite).

The transition from the B3 horizon to the underlying B4 horizon is abrupt. A fine grained and thin (~3mm wide) cutanic material of pink colour (7.5YR8/4) is commonly observed

between B3 and B4 horizons. The B4 horizon (Figure 2.2b and Figure 2.10) has a fine platy to blocky structure and is significantly less indurated than the B3 horizon. Clay cutans are present on fine ped units. The texture of the matrix is slightly finer than the overlying B3 horizon. Numerous sub-horizontal veins which cross cut at low angles occur throughout the B4 horizon. These veins are fine grained and have the same colour as the cutanic materials.

Figure 2.10: An abrupt transition from the overlying massive and coarse dorbank horizon to a slightly loose and fine grained B4 horizon which dominated by fractures cross-cutting at low angles (<20°).

The B4 horizon grades gradually into the yellowish green C horizon which has a brittle consistency and is significantly less indurated than the above horizons. The C horizon marks the boundary of the upper pedogenically altered material and the lower fluvial sediments.

One of the dominant morphological soil features in Vaalputs is the mottling (large bleached zones within a red matrix) that occurs within the dorbank horizons (B1, B2 and B3). In the case of trench B(1,1) and C(1,5), the mottles are largely dominant across the B1 and B2 horizons of trench C1,5 and within the B3 horizon of trench B1,1.

2.3.2. Micromorphology

Micromorphological studies of Vaalputs soil horizons from B(1,1) and C(1,5) trench profiles have been conducted on thin sections using petrographic microscopes and scanning electron microscopes. All thin sections used for this purpose were also mapped for elemental distribution using proton induced x-ray emission (PIXE) technique (Chapter 3). As a result thin sections were made with an average thickness of 70µm, therefore true petrographic colours maybe obscured. In order to make plausible deductions about the origin of the sediments in Vaalputs, properties of residual primary minerals are investigated. The dominant primary minerals are quartz (SiO_2) and feldspar ($KAlSi_3O_8$); quartz grains being the most dominant followed by feldspar grains.

Petrographic properties of B1 horizon (Figure 2.11) are largely composed of fine grained deep red matrix (m) which hosts randomly distributed quartz (qt) (no more than 0.2mm in diameter) and feldspar (fs) grains (no more than 0.4mm in diameter). Quartz grains are generally smaller than those of feldspar and are largely angularly shaped whereas the feldspar grains maintain euhedral to sub-euhedral shapes. Wavy clay cutans (cc) are evident throughout the B1 horizon. Although several quartz grains are randomly distributed, some present accumulation along these cutanic features. Occasionally, randomly distributed and orientated micro-fractures are observed. Under cross polarised light (Figure 2.11b and d), quartz and feldspar grains show low birefringence colours and the matrix material becomes darker and maintains the same deep red colour when stage is rotated over 360° angle.

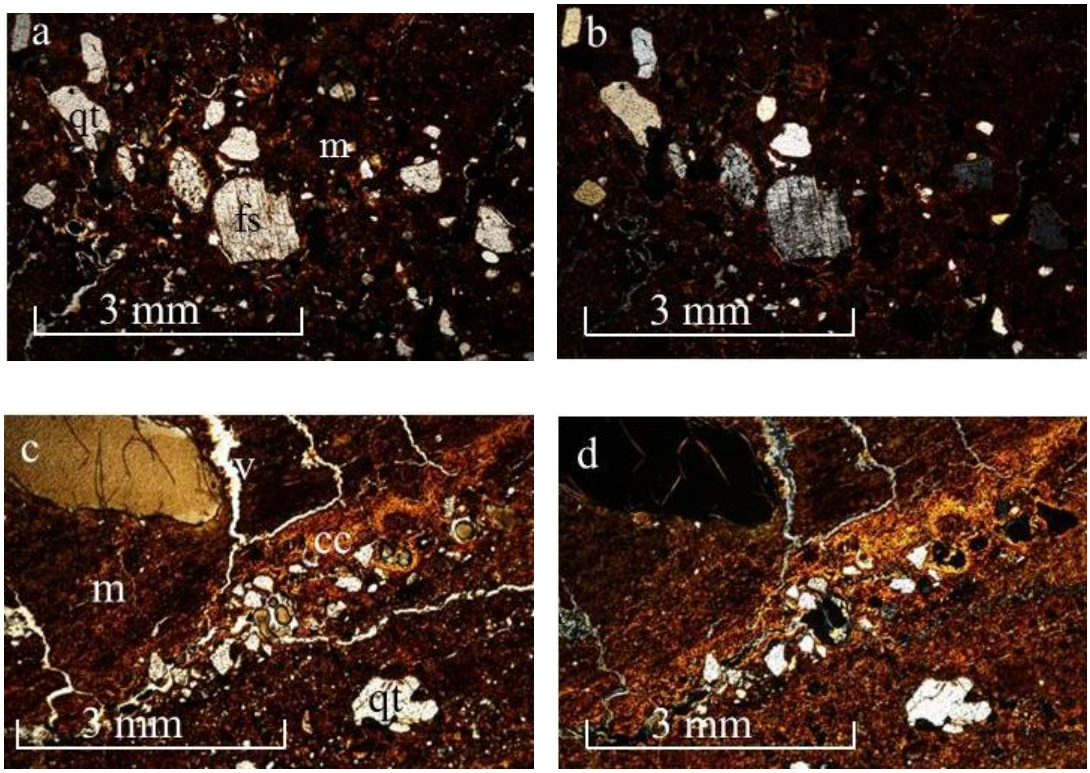

Figure 2.11: Micrographs of the weakly indurated B1 horizon of trench B(1,1) under ppl (a and c) and xpl (b and d) showing euhedral grains of feldspar (fs), deep red matrix material (m), clay accumulation (cc), void spaces (v) and quartz grains (qt) along clay cutans.

Micromorphological features of B2 horizon are displayed on Figure 2.12. Quartz and feldspar are the dominant primary minerals. Grains of both minerals are slightly larger than those observed from the above B1 horizon. Quartz grains have angular shapes whereas feldspar shows euhedral to sub-euhedral grains. All grains are supported by a deep red and fine grained matrix. Under cross polarised light (Figure 2.12b) microcline twinning is observed on feldspar grains. Quartz grains account for approximately 20% of mineral abundance, feldspar accounts for 10% whereas 45% is occupied by the matrix material and the rest (25%) are void spaces.

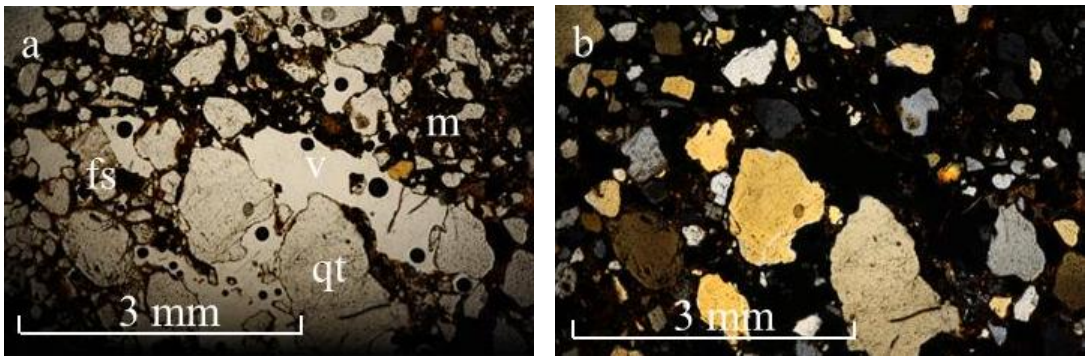

Figure 2.12: Micrographs of B2 sample taken from two different positions under ppl (a and c) and under xpl (b and d) showing large void spaces (v), reddish-brown matrix (m) euhedral feldspar grains and angular quartz grains (qt).

The dorbank hosted laminated material (H-L and V-L) (Figure 2.13) is composed largely of grey calcic material which is interlayered with much thinner reddish brown clay cutans. The regions directly adjacent but outside the ped enveloping laminations are observed to have increased quartz grains whereas the regions adjacent and inside the lamination maintain reduced grain sizes which increase with increasing distance into the ped. The quartz grains outside the lamination have angular shapes and are embedded on a fine grained matrix with reddish brown colour. Under cross polarised light, the reddish brown clay cutans (and matrix around lamination) and grey calcic layers of the laminations do not show any birefringence colours or become extinct at any rotational angle probably because the thin sections were made to be 50µm and thicker to accommodate PIXE analytical requirements.

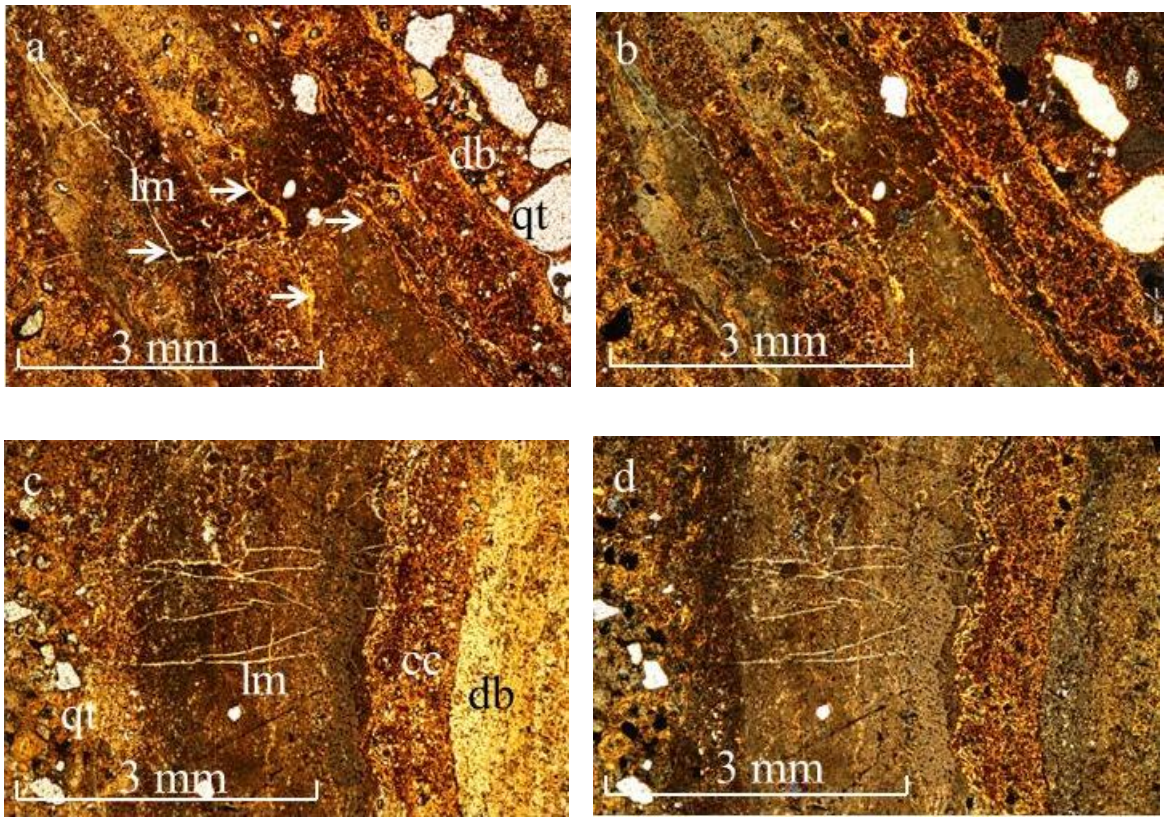

Figure 2.13: Micrographs of H-L (a and b) and V-L (c and d) materials showing the grey coloured zones interlayered with thin brown layers (indicated by white arrows) laminated material (lm), deep brown clayey material (cm) and light brown zones of dorbank material (db) under ppl and xpl, respectively.

The microstructure of B3 horizon (Figure 2.14) is defined by fine grained matrix (m), void spaces (v), quartz grains (qt) and feldspar grains (fs). Quartz grains are randomly distributed and occur in variable sizes with angular shapes. Feldspar grains are also randomly distributed and orientated however these grains have euhedral shapes. Similar to

the rest of the soils in Vaalputs, mineral phases on the B3 horizon are matrix supported. Under cross polarised light, grains of both minerals show low birefringence colours (Figure 2.14b and d). Up to 45% thin section volume is composed of matrix material and up to 35% volume of the sample is occupied by quartz followed by feldspar at 10%. The pore spaces make up the rest of 20% volume (Figure 2.14a).

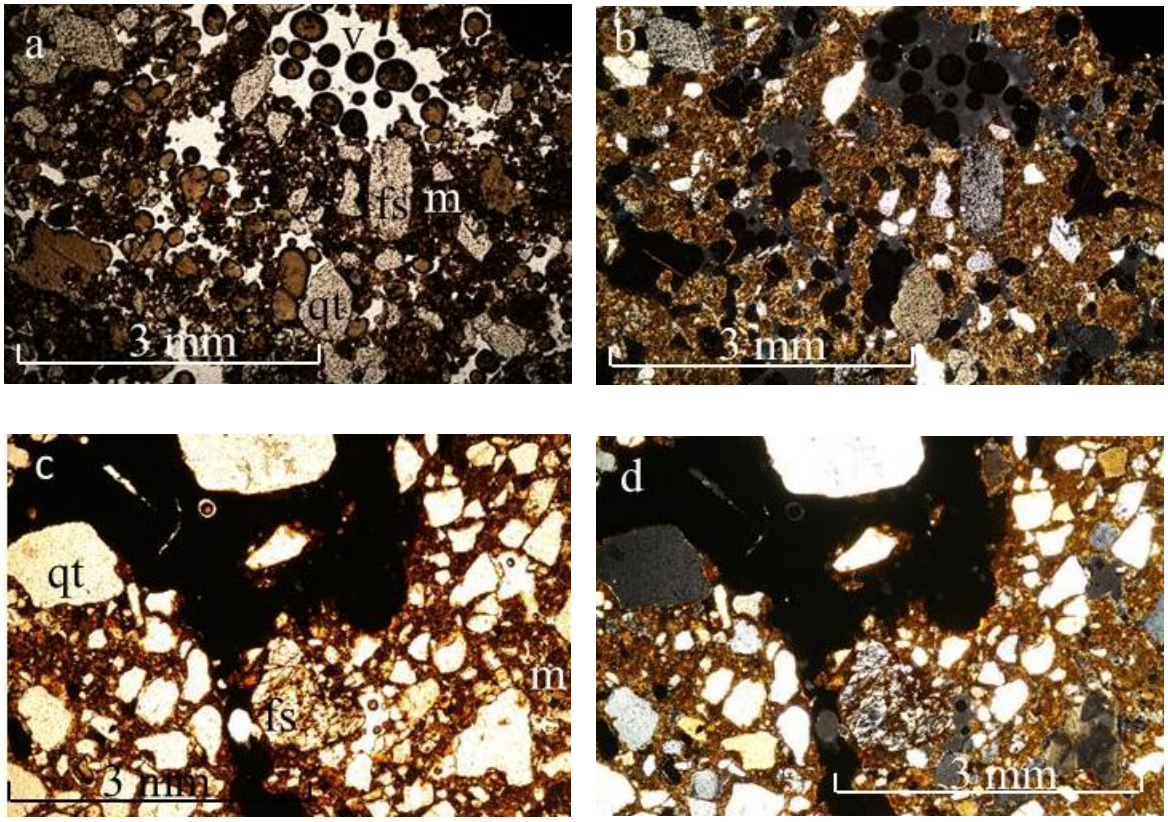

Figure 2.14: Thin section images of B3-W (a and b under ppl and xpl, respectively) and B3-E (c and d under ppl and xpl, respectively) from trench B(1,1). These sections show relatively large void spaces, angular quartz and euhedral feldspar grains and are matrix supported.

Particle size analyses were carried out on samples of trench B(1,1) and the results are displayed in Table 2.3. All soil horizons of Vaalputs are almost entirely composed of sand size materials. The silt and clay contents for all horizons fall within a narrow range of 0.12 - 1.41% with an exception of B1 and B2L which measured 2.79% and 2.50%, respectively. Due to low portions silt and clay could not be determined separately. A, B2, B3E, B3W and C horizons show similar grain size distribution trends where coarse fraction dominates their soil materials whereas B1, B2L, H-L, V-L and B4 are composed of considerably finer materials.

Table 2.3: Particle size analysis in weight percentage (wt%) for all soil materials occurring within trench B(1,1)

	Sand				Silt+Clay
Sample	Coarse	Medium	Fine	Very fine	<50µm
A	56.91	25.13	15.02	2.82	0.12
B1	5.57	31.05	35.03	25.56	2.79
B2	37.29	36.14	21.53	4.88	0.15
B2L	11.67	23.33	40.00	22.50	2.50
HL	14.08	34.21	28.17	22.13	1.41
B3E	43.76	28.26	20.97	6.84	0.18
VL	16.94	34.64	25.40	22.09	0.92
B3W	45.01	29.02	19.97	5.71	0.29
B4	30.69	33.86	25.94	9.31	0.20
C	42.91	35.28	16.98	4.71	0.12

Coarse sand: 2 – 0.5mm
Medium sand: 0.5 – 0.25mm
Fine sand: 0.25 – 0.106
Very fine sand: 0.106 – 0.05mm
Silt and Clay: <0.05mm

2.4. Discussion

The application of soil macro- and micro-morphology in palaeoclimate studies has received much attention since the early 1990s (Shankar & Achyuthan, 2007; Achyuthan, 2003; Bronger *et al.*, 1993; Sullivan, 1993). The morphology of a soil profile can be a useful tool to indicate possible soil forming processes that have been active in the past as well as climates under which these processes occurred (McCarthy *et al.*, 1998). When a climate shifts from humid to arid, many of the morphological traits of the wetter climate may be retained in the profile as aridity slows down geochemical processes within soil profiles. However, a great deal of care is needed in identifying which traits are relics and which traits represent active soil processes. One of the central objectives in this study is to attempt to establish the processes that may have produced current soil characteristics and in turn infer palaeoclimate(s) under which the Vaalputs sediments have been deposited and pedological altered. However, due to the age and great complexity of these soils deductions about palaeoclimates must be viewed as tentative at best. The employment of morphological observations and descriptions of each horizon from both trench profiles (B(1,1) and C(1,5)) and those of the entire profiles (Table 2.1 and Table 2.2) are being used to try and reconstruct palaeoenvironmental conditions. Although profiles of trenches B(1,1) and C(1,5) are similar and have been selected as ‘representative profiles’, the great

spatial variability of the soils means that identifying a representative profile is problematic and interpretation of soil morphology of these profiles can only serve as a starting point for understanding the complex Vaalputs soil system.

2.4.1. Macromorphology

The topmost horizon of Gordonia Formation has an undulating surface which was described by McCarthy *et al.*, (1985) and Brandt (1998) as residual aeolian dunes of low amplitude. The relative positioning of the A horizon suggests the youngest age of deposition. In localised areas, this horizon is slightly to moderately indurated (difficult to break with hands but can be scratched with a nail: Mohs scale of 2 – 2.5) suggesting recent and possibly on-going cementing processes. This further suggests extended periods of non-deposition under arid climate. As a result of the persisting arid climate in Vaalputs, the A horizon is mottle free and maintains a uniform red colour.

The sharp transition of the A horizon to the B1 horizon is marked by the presence of a stone-line (Figure 2.3b). This stone-line is observed in the same position in other excavated trenches across the Vaalputs site.

Stone-lines are common in soil environments and have been encountered by numerous authors (Ruhe, 1956; Ruhe, 1959; Johnson, 1989; Johnson & Balek, 1991). Such features have been interpreted as indicators of palaeo-surfaces (Johnson, 1989; Johnson & Balek, 1991; Brown *et al.,* 2004; Morrás *et al.,* 2005). A stone-line is defined by Johnson (1989) as a three dimensional entity on a soil profile, which from a trench or excavation view appears as a linear feature. Although stone-lines have been discussed almost to exhaustion, their origin seems controversial such that no single hypothesis is accepted to date. Extensive reviews relating to the origin of stone-lines are presented by Johnson (1989); Johnson & Balek (1991); Braucher *et al.,* (2004); Brown *et al.,* (2004); Glaser & Zech (2005). Currently there are two main hypotheses about their formation. One hypothesis suggests formation from fluvial (allochthonic) erosion of lighter and less dense materials followed by the deposition and concentration of residual sediments (Brown *et al.,* 2004). The second hypothesis involves bioturbation (autochthonic faunal turbation) and sorting of sediments (Johnson and Balek, 1991; Brown *et al.,* 2004; Morrás *et al.,* 2005). Over the years, authors (Ruhe, 1959; Johnson, 1989) have presented compelling evidence for both

theories relating to the genesis of stone-lines. From trench excavations on the Vaalputs soils, the stone-line appears to be extensive between the top A and underlying B1 horizon. The fact that the stone-line in the Vaalputs soils underlies an aeolian deposit would suggest that the stone-line is most likely to represent a former soil surface (thus coarse fragments are not expected in a windblown deposit). The semi-rounded stones within the stone-line would also suggest they are of fluvial origin which would relate to the older fluvial Vaalputs sediments. It is unclear whether the B1 horizon represents former topsoil or whether the former topsoil was removed by erosion prior to the deposition of the aeolian deposit. A certain amount of erosion is necessary to ensure a substantial removal of lighter particles while concentrating the larger sediment fraction at the top of the newly exposed B1 horizon surface, thus a degree of erosion of the former surface is expected. This stone-line therefore suggests a lithological discontinuity between the top A and the underlying B1 horizon. The presence of the stone-line indicates that, strictly speaking, the B1 horizon marks the surface of a buried palaeosol as defied by Retallack (2001). The material overlying the stone layer is an unconsolidated A horizon of aeolian origin with little evidence of bioturbation. The A horizon lying above the stone-line further shows no grading in grain size, in fact the A horizon is almost equigranular (Table 2.3). This further affirms that the stone-line could not have resulted from sediment redistribution of the A horizon during bioturbation. Thus two deductions can be made regarding the stone-line (i) the stone-line is derived from a once surface exposed horizon which was much thicker than it appears today and (ii) because the stone-line is composed of material much coarser than any grain from the B1 horizon, it is unlikely that the stone-line material is related to the underlying fine grained platy B1 horizon. This again suggests that the sediments from which the stone-line is derived have been completely eroded leaving only the heavier material to concentrate as a residual stone-line above the B1 horizon.

The B1 horizon along with the underlying B2 of B(1,1) and C(1,5) trench profiles as well as the B3 horizons would classify locally as dorbank and internationally as petroduric horizons. The occurrences of dorbank soils have been well documented in South Africa (Ellis & Schloms, 1982; Francis, 2008; Fey, 2010) yet relatively little is known about these soil horizons. Dorbank horizons have been reported to occur either with a platy or a massive structure (Francis, 2008; Fey, 2010). The platy dorbank horizons form from an accumulation of layered sediments coupled with the downward movement of silica rich

infiltrating waters (Fey, 2010). The massive dorbank horizons form over extended periods of chemical weathering under arid climates where mobilisation and redeposition of amorphous silica from upper units to the low lying horizon is essential (Fey, 2010). Both platy and massive varieties of dorbank occur in Vaalputs with the upper B1 horizon having a well-defined platy structure and the lower B3 horizon comprising of large polygonal peds with a massive substructure. It is possible that the two different structures represent two different phases of sediment deposition. The platy structure of the B1 horizons (Figure 2.2, Figure 2.3 and Figure 2.4) is strongly reminiscent of sedimentation layering of fine materials. The fact that the sedimentation layering can still be observed in the B1 indicates that pedogenic alteration of the sediments was in its infancy when the more arid conditions set in.

The occurrences of petroduric horizons are largely reported from arid climates (Bettenay & Churchward, 1974; Chadwick *et al.*, 1987a; Chadwick *et al.*, 1987b; Chartres & Fitzgerald, 1990; Blank & Fosberg, 1991; Francis *et al.*, 2007; Francis, 2008; Fey, 2010) suggesting that accumulation and development occurs over thousands or even millions of years. The pertinent question that arises with regards to the Vaalputs dorbank, is whether the dorbank is a relic feature or whether it is in phase with current soil forming processes. Fey (2010) used the positive relationship between the permeability of the horizon above the dorbank layer and the depth of the dorbank horizon as proof that dorbank formation is in phase with current day pedogenic processes. He notes however, that within the Garies soil form (Orthic A-Red Apedal B –Dorbank), the lithological discontinuity between the underlying dorbank and the overlying aeolian material suggest the dorbank is likely to be relic. Such a lithological discontinuity (stone-line) exists between the A and the B1 horizon of the Vaalputs soils thus it is plausible that the dorbank is likely to be a palaeo-feature. However, there are zones of highly indurated aeolian material which would most certainly indicate that silica cementation is currently an active pedogenic process in the surface soils. While the cementation appears to be an active process within the surface A horizon, large parts of this horizon remain unconsolidated. The subsurface dorbank horizons on the other hand are highly indurated.

The indurated B3 horizon occurs as large polygonal peds which are generally detached from other adjacent ped units. The large vertical cracks observed within the indurated B3 horizon define the boundaries of each ped unit. These polygonal units can clearly be

observed from the soil surface in areas where the A, B1 and B2 horizons are absent. This surface exposed polygonal dorbank material of the B horizon (Figure 2.15) is highly indurated and has a coarse texture. The surface of these large ped units are covered with red clay cutans. Various authors including Bettenay & Churchward (1974) and Chartres (1985) have described vertical partings on petroduric horizons and interpreted them as cracks resulting from desiccation during volume loss. The shrinkage cracks developed from all directions resulting in vertically orientated polygonal shaped structures. The presence of these polygonal units within the B3 horizon may suggest that the onset of aridity may have been fairly sudden. The coarse platy B2 dorbank horizon that occurs above the polygonal units of B3 horizon is likely to represent a different depositional unit. The contact surfaces of the discrete polygonal ped units (B3 horizon) are coated with clay cutans followed by a series of white laminations further interlayered with brown clay cutans towards exterior ped surfaces.

Figure 2.15: Surface exposed indurated subsoil horizon showing desiccation cracks forming polygonal pedal shapes seen from above. Clay cutans coat ped surfaces and exist between desiccation cracks of macro ped units.

Cross sections through the surface of the macro ped units in the B3 horizon show that the cutans lie adjacent to laminated zones that can be 3 to 4 cm thick. The inner laminated zone grades into the distinct white band that can be observed around the rim of the polygonal units (Figure 2.2a and Figure 2.7). In some instances these white laminations

occur near the surface of the ped and in other regions they occur 1-1.5cm from the edge of the ped (Figure 2.8). Thus their origin as either solution features or cutanic features is in question.

Under correct conditions, clay materials move in suspension (Pal *et al.,* 2003) and have potential of forming argillans (also known as clay cutans) after deposition. Such are common soil features expressed on surfaces of vertical cracks within the Vaalputs palaeosols. Soil cutans are defined as "the modification of the texture, structure, or fabric at natural surface in soil materials due to concentration of particular soil constituents or in situ modification of the plasma" (Retallack, 2001 and references therein). The movement of fine clay particles occurs when clay is in suspension under wet soil conditions (Pal *et al.,* 2003 and references therein). When ped materials begin to dry out, the water is absorbed into ped interiors, the ped faces or void walls act as filters leaving deposited clay materials as argillans around ped exterior surfaces. The deposited argillans are oriented parallel to the surface of deposition giving rise to clay illuviation texture. Several studies (e.g. (Retallack, 2001)) suggest that argillans are useful palaeoclimate indicators. For that reason, this topic of argillic horizons has received great attention over the decades (Goss *et al.,* 1973; Reheis, 1987; Ransom & Bidwell, 1990) especially in the recent years (Kleber, 2000; Konstantin, 2002; Khormali *et al.,* 2003; Pal *et al.,* 2003; Gunal & Ransom, 2006; Bai Haifeng *et al.,* 2011). A comprehensive review on soil cutans and their origin and implication on palaeosols was composed by Retallack (2001). Three general processes resulting in the formation of soil cutans were identified and these include; 1) illuviation cutans formed by clay migration from heights into open cracks, 2) diffusion cutans formed by progressive ped alteration as well as, 3) stress cutans which form from differential forces within the soil. Retallack (2001) further reported that of all three mechanisms of formation, cutans formed through illuviation are the most diagnostic of palaeosols. Schaetzl (2005) later suggested the use of cutans in palaeoclimate interpretations and described them as palaeoenvironmental palimpsests. In this review, two environmental extremes were of significance; dry as well as humid climate where it is suggested that the most cutans indicative of dry and wet climates are calcans (cutans composed of carbonate materials) and argillans, respectively.

Processes involved in clay illuviation under calcic soils have been described by several authors who suggest different conditions of formation. Although this topic has been discussed to almost exhaustion, there seems to be no single explanation that is widely accepted. There are contradicting theories with regards to the mobilisation of clay materials in calcareous soils; the widely accepted include the 1) clay illuviation prior carbonate accumulation or post complete carbonate removal, 2) the translocation of clay material unaffected by the presence of Ca^{2+} ions and 3) the deposition of argillans simultaneously with the carbonated accumulation. Kleber (2000) and Ransom & Bidwell (1990) present conditions where clay illuviation occurring prior the deposition of carbonate materials suggesting that climates can only be recorded from wet to dry conditions (Pal *et al.,* 2003 and references therein). The opposite of this has also been reported, although with less frequency. An experiment conducted by Goss *et al.,* (1973) demonstrated that clay can move through calcareous materials. This was later supported by Reheis (1987) who claimed that despite the tendency of clay to flocculate in the presence of Ca^{2+} ions in soil solution, clay materials can be translocated through calcareous material. This suggests that argillan and calcans can be used as climate indicators from wet to dry and from dry to wet conditions. In other cases, argillans have been documented to deposit simultaneously with the carbonate formation (Pal *et al.,* 2003; Bai Haifeng *et al.,* 2011). The repetitive nature of argillans alternating with calcans forming a highly banded argillic-calcic horizon within the soils of Vaalputs shows no evidence for simultaneous formation. It is possible that the deposition of B2 and B1 horizons brought along the development of clay cutans as infill along the vertical partings of the lower horizons. The accumulation of calcic material along these vertical partings of B3 and B2 horizons may have occurred during the onset of arid climates in Vaalputs. The associated clay materials are likely to have been brought in during the continuous drying of sediment. It is also possible that the clay material associated with carbonates was brought into the system during sporadic rains prior to the burial of hosting horizons (B3 and B2). Therefore the alternating argillic-calcic features observed in Vaalputs are likely to indicate a wet to dry climate change.

The subsoil horizons of both the B(1,1) and C(1,5) trench profiles show abundant mottling with white, bleached zones occurring throughout the reddish brown matrix. This mottling is interpreted as being a hydromorphic feature which suggests that the soils have been temporarily waterlogged for a period of time. Such signs of hydromorphy are not limited in

B(1,1) and C(1,5) trenches, mottling is a common feature in all exposed trenches. Soil mottles provide information related to the water regime of the soils. The sizes, contrast, abundance and distributions of soil mottles across a soil horizon contain potentially useful information about the water saturation status of the soils at some point in their history. The subsurface soils of Vaalputs show zones of mottling throughout the entire depth of the profile (down to 4m), especially in the B2 horizons. On certain dorbank soil horizons near the soil surface, redoxymorphic features are extensively marked on roots and dendritic root channels (Figure 2.16).

Determining whether the redoxymorphic features in the soils are relic or forming under current day climate at Vaalputs is difficult. The hydromorphy observed in the deep (>4 m) parts of the profile of trench C(1,5) are likely to be relic as the iron mottles follow zones probably representative of depositional layers (Figure 2.17). This suggests that the environment was significantly more humid and that water was involved in sediment deposition. Hydromorphic features in the upper 2 m of the profile are more difficult to interpret. Evidence that reduction is occurring under current day conditions is clearly visible in the gleyed zone surrounding active root zones (Figure 2.16a). Root growth is restricted to cracks within the dorbank due to the impermeability of the dorbank to water (Fey, 2010). Thus any current day redox changes would be expected to only occur on the surface of peds where roots (and water) can penetrate. This would suggest that the redoxymorphic features occurring within the large polygonal dorbank peds may represent a much earlier phase of pedogenesis prior to cementation when water and organic matter could penetrate the ped units. The Mn oxide staining that commonly occurs within a horizontal band along the dorbank horizons (Figure 2.6) is likely to represent current day processes, where redox conditions fall sufficiently to allow Mn redistribution but not Fe reduction. The redistribution of Mn around root zones is clearly evident in Figure 2.16b. Thus it would appear that the redoxymorphic features observed within the sediments and soils represent both palaeo and current day pedogenesis.

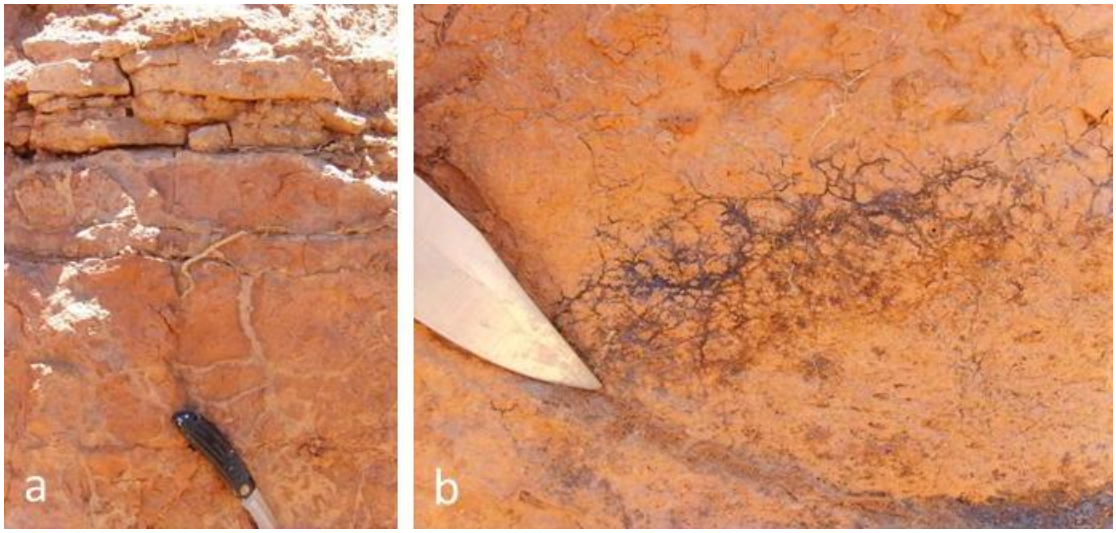

Figure 2.16: Redoxymorphic features marked along roots and root channels, (a) shows root channels on a ped face where Fe in depleted and (b) shows an accumulation of Mn and possibly Fe along root channels.

Figure 2.17: Bleached regions along possible deposition plains at a depth of 5m within C02 trench indicating possibly hydromorphic feature that are largely observed within the B horizons of both trenches.

2.4.2. Micromorphology

Micromorphological studies have been wildly conducted in soils. The use of soil micromorphology presents an opportunity to gain knowledge about past soil processes and even past climates under which these processes occurred (McCarthy *et al.,* 1998) and references therein). Some of the early works conducted on soil micromorphologies were carried out by Gile *et al.,* (1966) who looked at soil genesis from carbonate morphologies in dessert soils. Norton (1993) and Sullivan (1993) independently studied the micromorphology of silica cementation in soils. Bronger *et al.,* (1993) further made palaeoclimate deductions based on micromorphology of palaeosols. More recently Brock & Buck (2005) studied formation processes of calcic pendants from micromorphologies. Brewer (1972) reviewed and outlined possible interpretations micromorphological features in soils.

Arid climates are prevalent today in Vaalputs. Under such conditions mineral precipitates including those of salts may be common as major soil constituents. One of the most abundant salt mineral in Vaalputs, visible to the eye above and on some trench walls, is that of gypsum ($CaSO_4.2H_2O$). The contact surface between the ped and the laminated material in trench B(1,1) is largely defined by fine randomly orientated and distributed salt casts of lenticular texture. These salt features are extensively marked and densely packed along the contact surfaces of the peds and laminated materials. The observed salt casts are defined by a fine texture of woven fibres under a light microscope (Figure 2.9a and b). Due to small sizes of each fibrous strands and the difficulty that lies in separating the material from ped surfaces, the mineralogical composition of salt casts could only be analysed using scanning electron microscope (SEM) methods on a small piece of gold coated hand sample (1.5X1.5cm). The matrix material of the soil is dominated by quartz, amorphous silica and secondary calcite ($CaCO_3$). Spot analyses of the salt casts Figure 2.9 indicate palygorskite and possibly sepiolite occur within salt casts. This suggests that these salt casts are fossil salts. Calcite pseudomorphs after gypsum have been largely reported (Daley, 1967; Drees & Wilding, 1987; Sullivan & Koppi, 1993). In Vaalputs, it is evident that palygorskite in association with sepiolite are forming gypsum pseudomorphs. Daley (1967) identified fossil salt features where calcic clasts were found as pseudomorphs of mineral gypsum on indurated and thinly laminated bands of clays and calcareous siltstone. Depending on the

distribution and form relative to other grains, (Daley, 1967) divided the observed residual materials (pseudomorphs) of gypsum into four types. A review of these divisions include: (i) Simple lenticular crystals, (ii) Intergrowths of two or more crystals in a regular manner, (iii) Clusters of more numerous crystals which form small knobs protruding outwards and (iv) Irregular patches or lines of crystals, in some cases consisting of anastomosed rosettes. Although the existence of type (i) and (iii) is not witnessed in Vaalputs sediments, the observations made by Daley (1967) regarding the location of the salt casts is highly comparable to those observed in Vaalputs today. Thus it is possible that the observed salt casts are palygorskite-sepiolite pseudomorphs after gypsum.

Micromorphological studies in soils have so far been focused solely on pedogenic processes with very little consideration of sediment source. In Vaalputs, soils do not only exhibit pedogenic features but primary minerals remain as soil constituents. Observations of micromorphologies within the Vaalputs palaeosols show soil properties that remain constant throughout the trench profiles of C(1,5) and B(1,1). The most dominant micro features in these trench profiles include randomly orientated and distributed quartz and feldspar grains. The majority of quartz crystals are largely angularly shaped whereas feldspar grains have euhedral shapes (Figure 2.11, Figure 2.12 and Figure 2.14). In every appearance, primary minerals are supported by a reddish brown matrix which may sometimes show clay accumulations (Figure 2.11c).

The source of sediments from which Vaalputs soils are derived is suggested as being the basement granite-gneiss (Partridge & Maud 1987). Quartz and feldspar grains as soil constituents in Vaalputs support these findings. The appearance of angularly shaped quartz grains suggests minimum transportation of sediments from a nearby sediment source. Although feldspar is less dominant, its euhedral grains in Vaalputs soils further support a relatively close sediment source. The euhedral feldspar grains further suggest that the onset of arid climates was sudden enough to prevent significant weathering of euhedral feldspar grains. The clay laminations observed from the host reddish brown matrix material suggest clay movements under wet conditions. Such a process is likely to be responsible for the deposition of clay along developing calcic materials within the desiccation cracks of B3 horizon. Clay illuviation is not restricted only on these horizons, it is a common feature throughout the soils of Vaalputs.

2.5. Conclusions

Vaalputs palaeosols are extremely complex features that contain valuable palimpsests of by-gone climates. These palaeosols are covered by an equigranular sand that may be interpreted as a residual aeolian accumulation. This sand is underlain by a distinct remnant stone-line which marks a non-existing horizon that was once at surface. The stone-line separates the overlying aeolian deposits of Gordonia Formation from the underlying dorbank horizons. The highly varied particle sizes of the underlying subsurface horizons suggest fluvial origin.

The subsurface materials are highly indurated dorbank horizons which occur as platy and massive varieties in Vaalputs. The massive variety is further defined in two horizons; one is a uniform massive structured dorbank horizon and the other is composed massive polygonal ped units along which argillic-calcic laminations occur.

The occurrence of laminations is attributed to a late stage calcic precipitation within a region previously dominated by argillans. The age of the laminations is unknown however the accumulation of calcic material is likely to have been occurring since arid climate along the west coast set in. It is therefore likely that calcite continues to precipitate under persisting arid climate today.

The indurated subsurface dorbank horizons of Vaalputs are likely to be palaeo-features. The horizon exposed at surface in Vaalputs is however moderately indurated in sporadic areas. This indicates that silica cementation is currently an active pedogenic process in Vaalputs. The combination of surface and subsurface silicified horizons suggests that climates conducive of dorbank formation have been active and continuous ever since the first dorbank formed.

Lenticular textured salt casts observed in Vaalputs are mineralogical pseudomorphs composed of sepiolite and/or palygorskite after mineral gypsum.

Signs of hydromorphy observed in the deep (>4 m) (Figure 2.17) are Fe mottles representative of depositional layers. These features are likely to be relic thus suggesting that their depositional environment was significantly more humid and that water was involved in the sediment deposition. The gleyed zones around active roots bring forth

evidence that reduction is occurring under current day conditions. The dorbank horizons are impermeable to water thus the redoxymorphic features within the massive dorbank horizons may represent a much earlier (prior to cementation) phase of pedogenesis. Thus the redoxymorphic features observed within the sediments and soils are likely to represent both palaeo and current day pedogenesis.

Particle size analyses reveal wide grain size variation hosted within horizons this indicates fluvial deposition from relatively high energy systems.

3. Chapter 3: Geochemical characterisation of Vaalputs palaeosols

3.1. Introduction

Geochemical reactions and environmental condition continuously dictate mineral composition in soils. Vaalputs is located in an arid region of Bushmanland therefore the soils have been geochemically inert for an extended period. Several pedogenic features are observed in Vaalputs and these include (1) subsurface dorbank (petroduric) horizons, (2) calcareous horizon, (3) laminated materials composed of horizontally and vertically layered calcic and argillic bands within dorbank horizons and (4) barite accumulation within dorbank horizons. Dorbank and calcareous horizons have been described by several authors throughout the world and they are largely interpreted as forming under opposing environmental pH conditions. Therefore the occurrences of both features in Vaalputs have implications about environmental conditions of formation.

Barite in soils has also been described across the world however its geochemistry is not very well understood. Several authors have looked at its origins, geochemical conditions of formation and behaviour in soils. The occurrences of barite in various parts of the world implicate diversity in environments of formation. Lynn *et al.,* (1971) described authigenic barite in extremely acidic and base saturated soils in the USA. Stoops & Zavaleta (1978) later described authigenic barite associated with saline groundwater under hydromorphic conditions in Peru. Pedogenic barite has also been described under arid to semi-arid climates of central Australia by Sullivan & Koppi (1993) and Sullivan & Koppi (1995). Around the same time Podwojewski (1995) also described pedogenic barite in Vertisols of New Caledonia. Most recently pedogenic barite has been described in petrocalcic horizons in Nevada, USA by Brock-Hon *et al.,* (2012). Barium is highly immobile under normal soil conditions (Alberta *et al.,* 2009) therefore the understanding of Ba mobilisation and accumulation in Vaalputs can be used to constrain environmental conditions at the time.

The aim of this chapter is to geochemically characterise Vaalputs palaeosol while mapping the distribution of mineral barite and associated elements and minerals at micro-scale

within the dorbank horizons. This will provide an opportunity to gain insights into the past climates that have shaped the palaeosols at Vaalputs.

3.2. Materials and Methods

Samples described in Chapter 2 from trench B(1,1) were sent for chemical analyses. Samples from the C(1,5) trench profile were analysed as part of an earlier study (Majodina, 2010: Appendix 1). Samples of trench B(1,1) were analysed following the same protocol and those of C(1,5) trench profile.

Major cation and trace metals of samples were determined using a PANalytical Axios x-ray fluorescence (XRF) instrument with a 2.4kWatt Rh X-ray tube. The trace element analyses were completed on pressed samples after being milled to pass through a 65 µm sieve, while the major element analyses were performed on fused beads. It was relatively easy to subsample the materials for analyses, however, the laminated zones (H-L and V-L) posed difficulty. The separation of the clayey material residing between the polygonal ped unit (Figure 2.15) and its enveloping white material of H-L and V-L (Figure 3.1) was complicated due to its very small widths and high induration. Therefore the red-brown clay material between the dorbank and the laminations of H-L and V-L could not be analysed as a separate entity. Instead, composite material of H-L and V-L including the fine clay cutans most adjacent to the laminations were analysed for trace metals (labelled as B3L, Table 3.5). The laminated material of B1-2 from trench C(1,5) was also analysed in a similar manner as B3L. To quantify analytical results of the laminated zones, H-L and V-L were analysed again as a separate interties (free of clayey materials) where only the white-brown alternating layers were analysed (Figure 3.1).

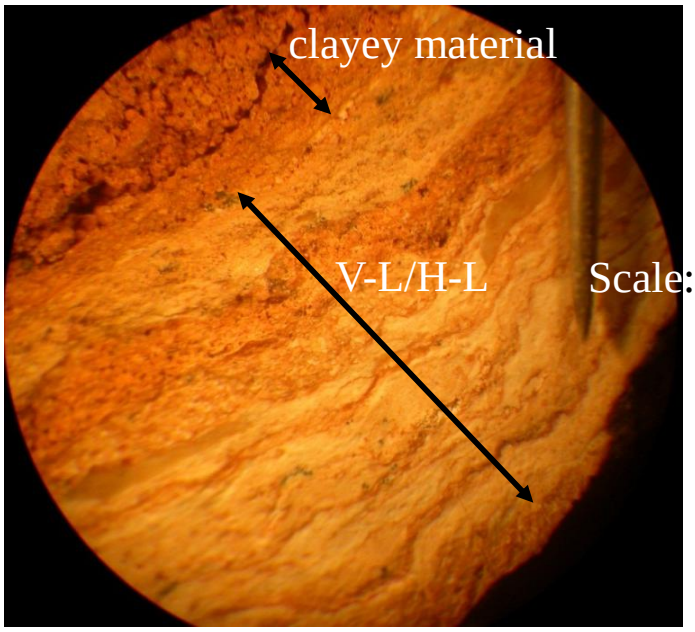

Figure 3.1: A photomicrograph illustrating different regions of the laminated zones. The large double arrow shows typical H-L and V-L materials where calcareous and argillic materials are interlayered. The small double arrow indicates a fine grained (clayey) zone most adjacent to the H-L and V-L. A sewing need tip indicates scale.

Microanalyses were performed using the nuclear microprobe at the Materials Research Department, iThemba LABS, South Africa. The detailed description of the facility can be found elsewhere (Prozesky *et al.*, 1995; Przybylowicz *et al.*, 1999). A proton beam of 3 MeV energy, provided by the 6 MV single-ended Van de Graaff accelerator, was focused to a 3 x 3 μm^2 spot and raster scanned over the areas of interest, using square and rectangular scan patterns with a variable number of pixels (up to 128 x 128). Particle-induced X-ray emission (PIXE) spectra were registered with a Si (Li) detector (30 mm^2 active area and 8.5 μm Be window). Additional external absorber was also used – either 125 μm thick Be layer or 170 μm thick Kapton layer. The effective energy resolution of the PIXE system (for the Mn Kα line) was 170-180 eV, measured for individual spectra. The detector was positioned at a take-off angle of 135^o and a working distance of 25 mm. The X-ray energy range was set between 1 and 42 keV. The normalization of results was done using the integrated beam charge, collected from the insulated specimen holder. The total accumulated charge per scan varied from 1.5 to 10.7 μC.

Quantitative results were obtained by standardless method using GeoPIXE II software package (Ryan, 2000). The error estimates are extracted from the error matrix generated in the fit, and the minimum detection limits (MDL) are calculated using the Currie equation (Currie, 1968). The detailed calibration of detector efficiency, the thicknesses of selectable

X-ray attenuating filters and studies on the accuracy and precision have been reported elsewhere (van Achterbergh *et al.,* 1995). The calibration of the analytical system was tested by measurements on standards - pure elements and synthetic glasses with known quantities of selected minor elements (internal standards), the X-ray peaks which cover practically the entire measurable energy range. Quantitative elemental mapping was performed using *Dynamic Analysis* method (Ryan and Jamieson, 1993; Ryan *et al.,* 1995; Ryan, 2000). Maps were complemented by data extracted from arbitrarily selected micro-areas PIXE spectra were employed to obtain average concentrations from these micro-areas using a full nonlinear deconvolution procedure to fit PIXE spectra (Ryan *et al.,* 1990a; Ryan *et al.,* 1990b).

The following elements were detected: Al, Si, S, K, Ca, Mn, Fe, Cu, Sr, Ba. Barium was measured using K and L X-ray lines.

Imaging of the samples and analysis of the phase compositions was accomplished using a Zeiss EVO® MA15 Scanning Electron Microscope (SEM) at the Stellenbosch University. Samples were identified with backscattered electron (BSE) and phase compositions were quantified by EDX analysis using an Oxford Instruments® X-Max 20mm2 detector and Oxford INCA software. Beam conditions during the quantitative analyses were 20 KV, with a working distance of 8.5 mm and approximately beam current of – 20nA. The counting time was 10 seconds live-time. Internal Astimex Scientific mineral standards were used for standardization and verification of the analyses. To correct for detector drift pure Co was used periodically.

Energy dispersive spectroscopy is only suitable for determining major elements of minerals at concentrations over 0.1 wt% for heavy elements, and over 0.01 wt% for light elements. Elements including Na, Mg, Al, Si, S, K, Ca, Mn, Fe, Cu, Sr and Ba were selectively quantified via WDS analysis using an Oxford Instrument ® Wave Dispersive X-ray Spectrometer and Oxford INCA software.

The x-ray tomography (XRT) measurements were done using a Nikon XTH 225 ST micro-focus X-ray tomography system described elsewhere (Hoffman and De Beer, 2012). These analyses were done at the Micro-focus X-ray Radiography and Tomography facility (MIXRAD) supported by the South African National Centre for Radiography and Tomography (SANCRAT), housed at NECSA. Using micro-focus x-ray computed

tomography ensures rendering of high quality micron-level information of the interior as well as composition of samples non-invasively and non-destructively. The results are computed using an advanced volume rendering software, VGStudio MAX 2.1. All samples were scanned using 160kV and 11 µA of beam current.

To determine the chemical nature of the material cementing the indurated samples in Vaalputs slaking tests were conducted. This was achieved by submerging a fragment of cemented materials of no more than 10 ml in strong acid and alkali solutions. B1, B1-2, B2 and C1-2 were samples used from the C(1,5) trench for this test meanwhile, from trench B(1,1), samples B1, B2, B2L, H-L, B3E, V-L, B3W, B4 and C were used. One sample from each cemented horizon was placed in a 5M HCl solution and another fragment of the same material and similar size was placed in a warm (40 °C) 6M NaOH solution. Samples were left to equilibrate simultaneously for 7 days. For samples that did not slake, alternate HCl and NaOH treatments were applied.

Saturated paste extracts of samples from B(1,1) and C(1,5) samples were prepared by equilibrating deionised water with milled soil material for 24 hours prior to extracting soil solution under vacuum. Extracts were analysed for major anions and metals, using a Metrohm 761 compact ion chromatography (IC) and a Varian Agilent 7700 ICP-MS instruments, respectively. Dissolved inorganic silica was measured, using a modified molybdated-blue spectrophotometry (Mortlock and Froelich, 1989) using a Thermo Scientific Genesys 10uv scannint instrument. Alkalinity was determined by potentiometric method using 0.001M HCl acid solution. The pH and electrical conductivity (EC) were measured directly from the soil-water pastes after 24 hour of equilibration period, just before solution extracts were collected.

3.3. Results

3.3.1. Bulk Chemistry

Major elemental composition for samples collected from B(1,1) (Table 3.1) and C(1,5) (Table 3.2) trench profiles were measured using XRF and are displayed in weight percentage (wt%). Significantly elevated CaO contents are observed throughout the profile of trench B(1,1) with an exception to A horizon. The highest CaO concentrations were measured within the H-L (15.77wt%) and V-L (26.08wt%) materials. High concentration

of CaO was also measured within the B3 horizon (where B3E and B3W measured 15.93wt% and 8.99wt%, respectively). The A horizon measured the lowest CaO concentrations (0.29wt%). Elevated MgO concentrations were also measured from the H-L and V-L (7.9wt% and 5.70wt%, respectively). Similarly to the CaO, the lowest MgO concentrations are measured from the A horizon. The SiO_2 content shows an opposite trend to CaO concentrations (Figure 3.9 and Figure 3.10). The highest SiO_2 concentrations are measured within A horizon (86.22wt%) and the lowest are measured from the laminated zones of H-L (39.08wt%) and V-L (28.57wt%). The B3E and B3W matrices measured 50.38wt% and 59.51wt% of SiO_2, respectively. The LOI in general is directly proportional to the CaO concentrations. The Fe_2O_3 concentration shows a direct correlation to the Al_2O_3 content throughout the B(1,1) and C(1,5) profiles and K_2O concentrations also correlate to Al_2O_3. Numerous elemental concentrations are uniform throughout the depths of B(1,1) and C(1,5) trench profiles however the A horizon shows a significant depletion of MgO with respect to the underlying horizons (Table 3.1 and Table 3.2).

Table 3.1: XRF data of major ions bulk composition generated from horizons of Trench B(1,1).

Sample	Al_2O_3	CaO	Cr_2O_3	Fe_2O_3	K_2O	MgO	MnO	Na_2O	P_2O_5	SiO_2	TiO_2	LOI	H_2O	Sum
	wt %													
A	5.14	0.29	<0.01	2.48	1.52	0.54	0.05	0.25	0.05	86.22	0.46	2.58	0.44	99.58
B1	15.81	1.98	0.01	7.15	2.93	3.01	0.05	0.27	0.10	54.19	0.50	14.22	5.48	100.22
B2	8.00	0.44	<0.01	3.38	2.14	2.13	0.04	0.37	0.04	75.54	0.47	7.40	3.25	99.95
B2L	15.07	0.82	0.01	6.15	2.23	2.90	0.04	0.44	0.06	55.62	0.37	16.14	7.83	99.85
H-L	6.20	15.77	<0.01	2.75	1.14	7.97	0.04	0.32	0.22	39.08	0.19	26.54	7.78	100.22
B3E	6.84	15.93	0.01	2.56	1.51	2.53	0.03	0.21	0.05	50.38	0.29	19.75	2.90	100.09
V-L	4.85	26.08	<0.01	2.14	0.88	5.70	0.02	0.33	0.28	28.57	0.15	30.80	4.90	99.80
B3W	7.59	8.99	<0.01	3.12	1.72	2.95	0.04	0.30	0.06	59.51	0.37	15.44	3.91	100.09
B4	12.02	3.17	0.01	5.34	2.34	2.60	0.06	0.54	0.10	61.14	0.49	12.46	4.03	100.27
C	10.44	2.17	0.01	3.86	2.03	1.75	0.04	0.32	0.05	68.55	0.39	9.36	2.79	98.97

Similar to trench B(1,1), the highest CaO and MgO concentrations in trench C(1,5) are measured from the laminated zones that lie on the ped exteriors whereas their lowest concentrations are measured from the A horizon.

Table 3.2: XRF data of major ions bulk composition generated from horizons of Trench C(1,5) (As presented in Mortlock and Froelich (1989).

Sample	Al_2O_3	CaO	Cr_2O_3	Fe_2O_3	K_2O	MgO	MnO	Na_2O	P_2O_5	SiO_2	TiO_2	LOI	H_2O	sum
	wt%													
A	4.92	0.14	<0.01	2.48	1.48	0.17	0.04	0.29	0.04	85.48	0.57	1.95	0.73	98.27
B1	6.88	0.27	<0.01	2.73	1.81	1.58	0.02	0.33	0.03	74.49	0.39	6.97	3.57	99.08
B1-2	6.39	18.46	<0.01	2.52	1.14	5.16	0.02	0.28	0.07	38.42	0.15	23.00	4.39	100.00
B2	7.39	6.59	<0.01	2.93	1.65	1.79	0.02	0.18	0.04	62.52	0.38	12.60	3.54	99.64
C1	10.61	0.32	<0.01	3.68	2.79	1.33	0.03	0.43	0.05	64.50	0.46	15.37	2.94	102.50
C1-2	7.90	12.23	<0.01	2.89	2.12	1.65	0.02	0.29	0.05	60.02	0.34	8.47	4.00	100.00
C2	6.53	0.40	<0.01	3.75	2.20	0.49	0.03	0.32	0.04	76.26	0.43	4.80	2.39	97.65

To compare major elemental enrichment and depletion levels within each laminated zone, enrichment ratios (ER) are calculated between all laminated materials (H-L and V-L from trench B(1,1) as well as B1-2 from trench C(1,5)) against their associated matrices. The ERs are calculated according to equation (eqn) 1 and the results are given in Table 3.3 and Table 3.4.

ER = [component in lamination]/[component in matrix] eqn.1

Enrichment ratio values for materials of trench B(1,1) are calculated as H-L against B2 and B3E whereas V-L is calculated against B3E and B3W. The B1-2 materials from trench C(1,5) is calculated against the concentrations of B1 and B2 matrices of trench C(1,5).

The results obtained from ER calculations of major elements of trench B(1,1) are shown in Table 3.3 and Table 3.4. The H-L material is extremely enriched in CaO content (35.84) with respect to the overlying B2 horizon and equal concentration (0.99) relative to the underlying B3E horizon. H-L further shows slight enrichments in MgO, MnO and P_2O_5 and slight depletion in the rest of the major elements relative to both B2 and B3E horizons. The V-L material shows similar enrichment patterns to those of H-L, although with respect to the B3E horizon, the V-L material is slightly enriched in CaO (1.64). The B1-2 laminated material of trench C(1,5) profile is depleted in some of the major components with the exceptions of Na_2O, CaO, MgO, MnO and P_2O_5. Within the B1-2 laminated material, the CaO content is 68.89 times that of the upper B1 and only 2.80 times more than in lower B2 horizon.

Table 3.3: Enrichment Ratios of XRF data of major ions of Trench B(1,1).

Sample	Al_2O_3	CaO	Cr_2O_3	Fe_2O_3	K_2O	MgO	MnO	Na_2O	P_2O_5	SiO_2	TiO_2
H-L/B2	0.78	35.84	<0.00	0.81	0.53	3.74	1.00	0.86	5.50	0.52	0.40
H-L/B3E	0.91	0.99	<0.00	1.07	0.75	3.15	1.33	1.52	4.40	0.78	0.66
V-L/B3E	0.71	1.64	<0.00	0.84	0.58	2.25	0.67	1.57	5.60	0.57	0.52
V-L/B3W	0.64	2.90	<0.00	0.69	0.51	1.93	0.50	1.10	4.67	0.48	0.41

Table 3.4: Enrichment Ratios of XRF data of major ions of Trench C(1,5). Taken from Majodina (2010).

Sample	Al_2O_3	CaO	Cr_2O_3	Fe_2O_3	K_2O	MgO	MnO	Na_2O	P_2O_5	SiO_2	TiO_2
B1-2/B1	0.93	68.89	0.58	0.92	0.63	3.26	1.16	0.86	2.16	0.52	0.38
B1-2/B2	0.86	2.80	1.02	0.86	0.69	2.88	0.95	1.55	1.78	0.61	0.39

Trace elemental composition of all soil horizons from both trench profiles (B(1,1) and C(1,5)) are given in Table 3.5 and Table 3.6.

For comparison regional trace elemental concentrations are also provided in Table 3.5. Copper (Cu) concentrations are elevated throughout the B(1,1) trench profile. The highest Cu content (20.82 mmol/kg) is measured from V-L material. Barium measured the highest Ba concentration (33.18mmol/kg) from the C horizon followed by the B2L material which measured 22.37mmol/kg. During the analyses of H-L and V-L materials only the alternating white-brown bands of the laminations (Figure 3.1) were considered as representatives. Therefore the results provided relating to H-L and V-L do not represent the clay cutans most adjacent to these laminations. B3L on the other hand is a composite material of the laminated band (H-L and V-L) and the clay cutans most adjacent to the lamination. The banded H-L and V-L materials measured the lowest Ba concentrations of 1.30 and 1.19 mmol/kg, respectively. Within the clayey B3L material 17.62mmol/kg of Ba concentration were measured. The samples from C(1,5) trench measured relatively low Cu concentrations throughout the profile. The highest Ba composition is measured from the B1-2 (60.56mmol/kg) and the lowest Ba concentrations (1.15mmol/kg) were measured from the topmost A horizon.

Table 3.5: XRF data of trace element composition generated from horizons of Trench B(1,1) accompanied by regional trace metal data. Taken from Hansen (unpublished data).

Sample	V	Cr	Co	Ni	Cu	Zn	Ga	Rb	Sr	Y	Zr	Nb	Ba	La	Ce	Nd	Pb	Th	U
	mmol.Kg^{-1}																		
A	1.03	0.93	0.95	0.20	10.15	0.56	0.13	0.85	0.47	0.24	2.57	0.12	1.45	0.16	0.28	0.08	0.06	0.09	0.02
B1	1.68	2.00	0.65	0.62	17.88	1.60	0.33	1.76	1.10	0.27	1.29	0.13	1.65	0.22	0.35	0.10	0.15	0.07	0.04
B2	1.20	1.26	0.79	0.53	11.82	0.53	0.17	1.24	1.13	0.42	2.28	0.13	6.62	0.29	0.70	0.21	0.11	0.08	0.03
B2L	1.67	1.70	0.40	0.70	15.26	1.10	0.28	1.50	2.83	0.42	0.92	0.10	21.37	0.29	0.66	0.20	0.13	0.07	0.03
H-L	0.58	0.88	0.20	0.61	15.76	0.77	0.15	0.69	3.15	0.87	0.49	0.06	1.30	0.20	0.30	0.09	0.09	0.04	0.01
B3E	0.84	0.89	0.34	0.35	17.77	0.44	0.14	0.93	2.06	0.37	1.54	0.10	10.30	0.17	0.41	0.12	0.10	0.06	0.01
V-L	0.45	0.80	0.13	0.44	20.82	0.62	0.13	0.53	5.08	0.37	0.35	0.05	1.19	0.06	0.27	0.08	0.07	0.03	<0.00
B3W	0.96	1.47	0.73	0.50	16.05	0.50	0.16	1.06	1.60	0.53	2.13	0.11	6.83	0.26	0.64	0.19	0.20	0.06	0.02
B3L	0.53	0.49	0.77	0.41	0.81	0.58	0.08	0.52	5.32	0.13	0.60	0.06	17.62	0.08	0.46	0.15	0.14	0.02	0.01
B4	1.42	1.45	0.76	0.59	12.49	1.17	0.24	1.41	1.25	0.32	1.67	0.12	1.58	0.15	0.33	0.10	0.15	0.08	0.03
C	1.73	1.11	0.70	0.36	12.98	0.63	0.20	1.30	1.46	0.34	2.75	0.12	33.18	0.25	0.99	0.29	0.15	0.08	0.02
----------Regional concentrations----------																			
Percentile 25	1.30	1.17	0.15	0.31	0.38	0.93	-	1.65	1.61	0.55	7.63	0.19	3.52	-	-	-	0.11	0.10	0.00
Percentile 75	1.94	2.00	0.24	0.44	0.77	1.39	-	2.36	2.20	1.03	16.66	0.26	4.97	-	-	-	0.16	0.34	0.01
Mean	1.77	1.84	0.20	0.41	0.96	1.22	-	2.06	2.06	0.93	14.38	0.24	4.52	-	-	-	0.15	0.34	0.02

Table 3.6: XRF data of trace element composition generated from horizons of Trench C(1,5). Taken from Majodina (2010)

Sample	V	Cr	Co	Ni	Cu	Zn	Ga	Rb	Sr	Y	Zr	Nb	Ba	La	Ce	Nd	Pb	Th	U
	mmol.kg^{-1}																		
A	1.21	0.66	1.86	0.17	0.08	0.37	0.10	0.88	0.61	0.25	3.19	0.17	1.51	0.16	0.37	0.15	0.11	0.12	0.02
B1	0.87	1.11	1.07	1.15	0.08	0.40	0.14	1.17	0.96	0.38	2.00	0.11	5.85	0.23	0.59	0.23	0.13	0.08	0.01
B1-2	1.16	0.65	1.17	0.79	0.70	0.58	0.09	0.68	5.02	0.87	0.84	0.06	60.56	0.50	1.50	0.53	0.11	0.04	0.02
B2	0.87	0.81	0.92	0.31	0.31	0.46	0.15	1.06	1.16	0.34	1.83	0.11	2.58	0.32	0.56	0.22	0.13	0.08	0.01
C1	1.34	0.80	1.17	0.41	0.26	0.70	0.24	1.93	0.92	0.74	2.31	0.15	2.30	0.56	0.99	0.40	0.18	0.11	0.02
C1-2	0.73	0.52	0.75	0.20	0.41	0.46	0.15	1.26	1.59	0.39	1.56	0.11	1.66	0.39	0.54	0.21	0.14	0.08	0.01
C2	1.14	0.69	1.56	0.22	0.23	0.37	0.16	1.44	0.77	0.31	2.42	0.16	2.58	0.34	0.65	0.25	0.16	0.13	0.03

To determine enrichment and/or depletion levels within each laminated zone, ERs are also presented for trace elements between all laminated materials (H-L and V-L from trench B(1,1) as well as B1-2 and from trench C(1,5)) against their matrices. The ERs are calculated according to equation (eqn) 1 and the results are given in (Table 3.7 and Table 3.8).

The results obtained from ER calculations of trench B(1,1) show that with respect to the surrounding matrices, both H-L and V-L (predominantly white banded zones) laminations show extreme Ba depletions. The B1-2 laminated material of trench C(1,5) however shows Ba ER values of 10 and 23 times the surrounding B1 and B2 matrices, respectively. The B1-2 further shows a substantial accumulation of Cu and Sr represented by values of 8.6 and 5.2 times the concentration within the host B1 horizon, respectively. Generally the composite material of the laminated zones (cutans and white laminations) of B1-2 from trench C(1,5) and B3L from trench B(1,1) indicate higher trace metal concentrations than their surrounding matrices. The laminated white materials on the other hand (H-L and V-L) are depleted in most trace metals.

Table 3.7: Enrichment Factors of XRF data of trace metals of Trench B(1,1).

Sample	V	Cr	Co	Ni	Cu	Zn	Ga	Rb	Sr	Y	Zr	Nb	Ba	La	Ce	Nd	Pb	Th	U
H-L/B2	0.48	0.70	0.26	1.13	1.33	1.45	0.92	0.56	2.80	2.07	0.22	0.49	0.20	0.70	0.42	0.42	0.79	0.43	0.24
H-L/B3E	0.69	0.98	0.59	1.71	0.89	1.76	1.07	0.74	1.53	2.39	0.32	0.67	0.13	1.19	0.73	0.73	0.86	0.57	0.54
V-L/B3E	0.54	0.89	0.38	1.25	1.17	1.41	0.90	0.57	2.46	1.02	0.23	0.56	0.12	0.38	0.65	0.65	0.64	0.48	0.00
V-L/B3W	0.46	0.54	0.18	0.89	1.30	1.25	0.79	0.50	3.18	0.70	0.17	0.50	0.17	0.25	0.41	0.41	0.33	0.53	0.00
B3L/B2	0.44	0.39	0.97	0.77	0.07	1.08	0.50	0.42	4.72	0.32	0.26	0.47	2.66	0.27	0.66	0.73	1.28	0.30	0.51
B3L/B3E	0.63	0.55	2.24	1.16	0.05	1.31	0.59	0.56	2.58	0.37	0.39	0.65	1.71	0.46	1.14	1.27	1.40	0.39	1.14
B3L/B3W	0.55	0.33	1.05	0.83	0.05	1.17	0.52	0.50	3.33	0.25	0.28	0.59	2.58	0.30	0.72	0.80	0.73	0.43	0.74

Table 3.8: Trench C(1,5) XRF trace element ER. Taken from Majodina (2010).

Sample	V	Cr	Co	Ni	Cu	Zn	Ga	Rb	Sr	Y	Zr	Nb	Ba	La	Ce	Nd	Pb	Th	U
B1-2/B1	1.33	0.58	1.09	0.68	8.60	1.46	0.60	0.58	5.23	2.27	0.42	0.57	10.35	2.17	2.52	2.34	0.84	0.51	1.40
B1-2/B2	1.33	0.80	1.28	2.52	2.26	1.26	0.56	0.64	4.33	2.55	0.46	0.58	23.49	1.59	2.65	2.46	0.84	0.54	1.48

3.3.2. Elemental mapping

Understanding spatial distributions and associations of major and trace metals within the trench samples is essential when delineating and interpreting geochemical processes. Proton Induced X-ray Emissions and SEM analytical techniques are applied to provide comprehensive chemical details of the matrices and laminated zones of H-L, V-L and B1-2.

Elemental mapping of selected areas along laminated zones of H-L (Figure 3.2) and V-L (Figure 3.3) indicate associations of major elements and their distribution in relation to each other. The elemental maps displayed in Figure 3.2 and Figure 3.3 show similar elemental associations: Al, K and Fe are strongly associated with each other and show a negative relationship with Ca (Figure 3.2b-e and Figure 3.3a-d). The relationship of Si and Ca is less easy to establish but in most regions there appears to be a negative association between the two elements, in certain zones, however, there is an overlap of distribution (Figure 3.2a and b).

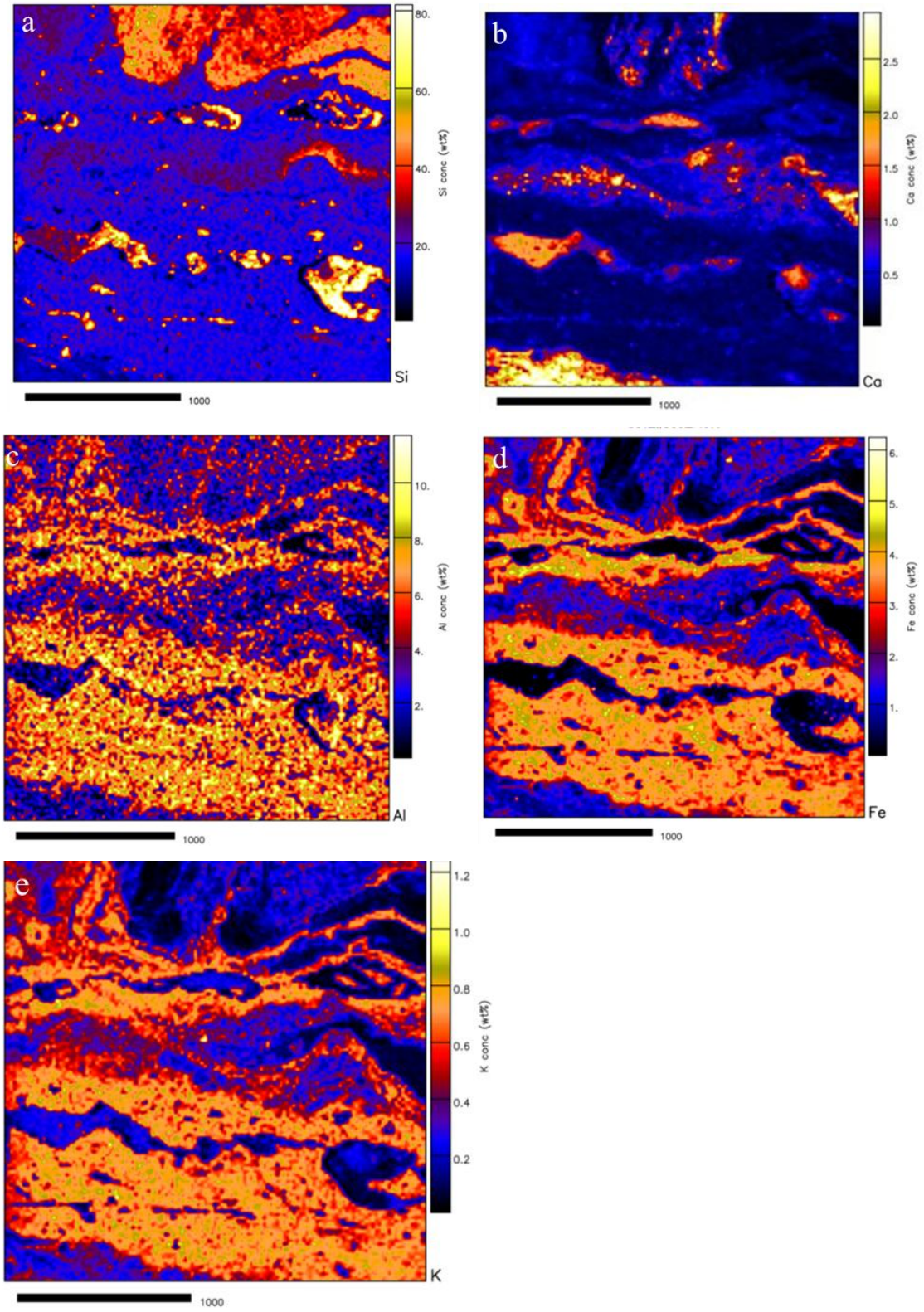

Figure 3.2: Elemental maps of the same region along the transition zone of the laminations to the dorbank (V-L to the adjacent B3) expressing chemical distributions of (a) Si, (b) Ca, (c) Al (d) Fe and (e) K. The maps are produced using PIXE measurements and the given scale bar is 1000 µm.

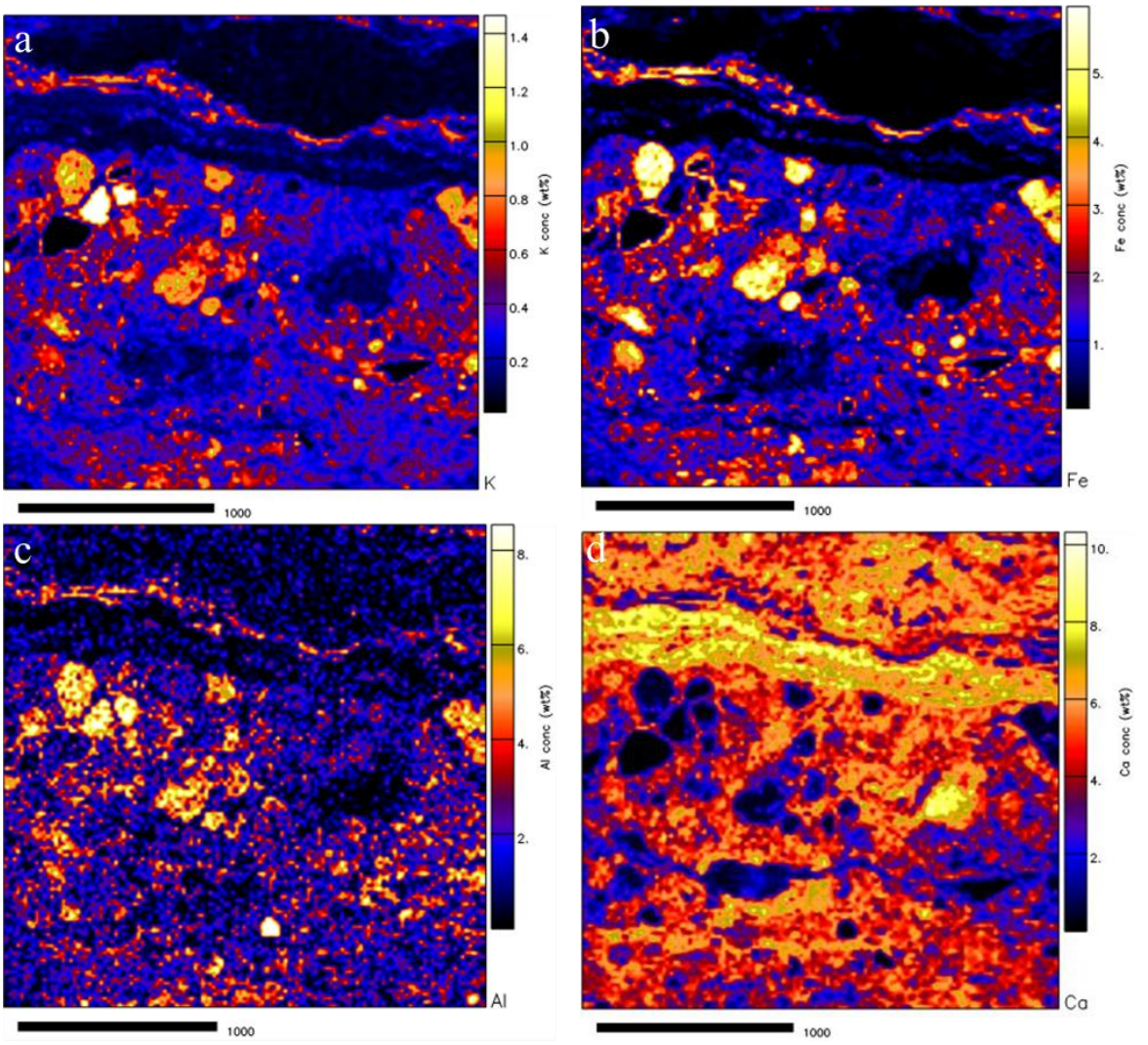

Figure 3.3: Elemental maps of the same region along the transition zone of the laminations to the dorbank (H-L to the underlying B3) showing the distributions of (a) K, (b) Fe, (c) Al with respect to (d) calcium. The maps were produced using Proton Induced X-ray Emissions method. The given scale bar is 1000 µm.

Trace element accumulations occur largely along the contact surfaces of the laminated materials (within the vertical partings of B3 horizon) and the polygonal dorbank ped units. Trace elements are especially enriched in micro-voids along the most exterior surfaces of the polygonal B3 dorbank horizon as well as within void spaces that occur along the contact surfaces of B3 horizon and the laminated material. Trace element distribution maps of two regions (surrounding a void) are shown in Figure 3.4 and Figure 3.5. Barium, strontium, copper and manganese show a strong association with the rim of the void. Although the analyses are only semiquantitative, Ba concentrations measured as high as 3 wt% in these regions.

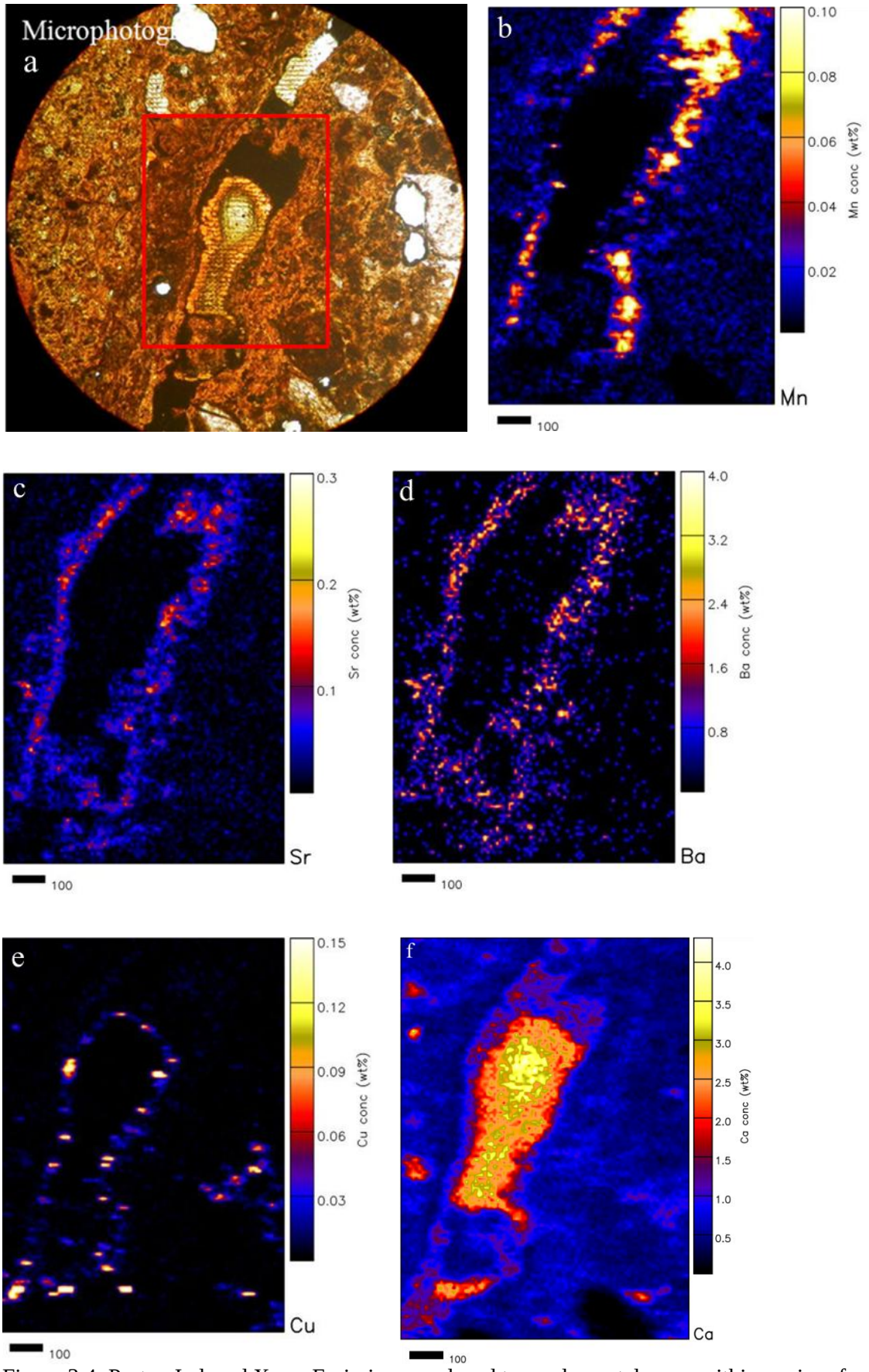

Figure 3.4: Proton Induced X-ray Emissions produced trace elemental maps within a micro fracture adjacent to the lamination zone (microphotograph) showing the distributions of (b) Mn, (c) Sr, (d) Ba (e) Cu and (f) Ca. The given scale bar is 100 µm.

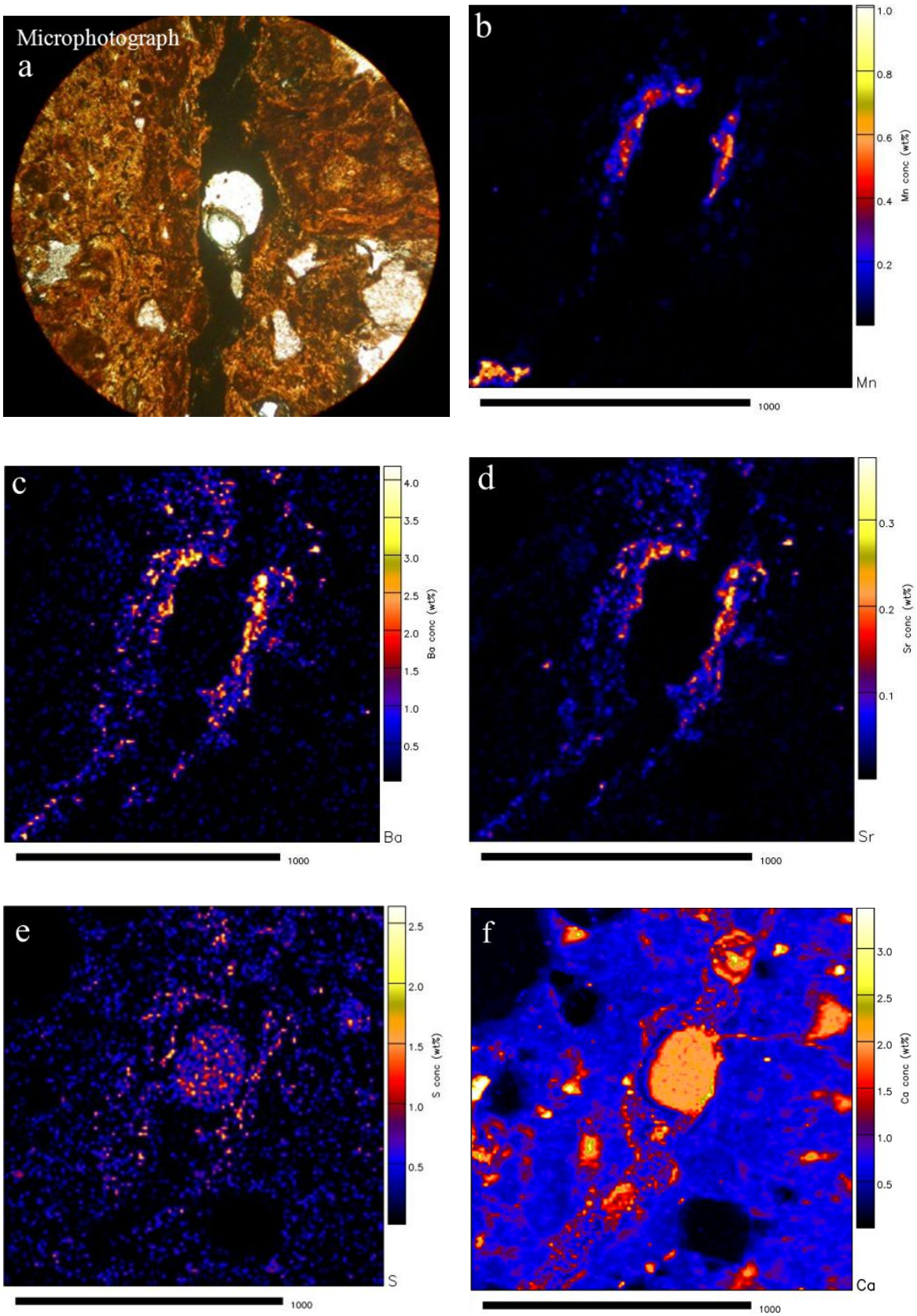

Figure 3.5: Proton Induced X-ray Emissions produced trace elemental maps within a micro fracture adjacent to the lamination zone showing (a) a microphotograph of an area analysed for the distributions of (b) Mn, (c) Ba, (d) Sr, (e) S and (f) Ca. The given scale bar is 1000 µm.

In order to analyse for lighter elements (<Al), SEM mapping (of similar regions to those mapped with PIXE) was conducted (Figure 3.7 and Figure 3.8). Results obtained using

SEM and PIXE are consistent with respect to the distribution of Al, Fe and K as well as trace metals. The Mg maps from the SEM data indicate even distribution throughout the analysed samples (Figure 3.8). Barium distribution is associated with high sulphur concentration (Figure 3.5 and Figure 3.6a). Large Ba accumulation occurs within the clay cutans between the dorbank and the laminated zones of H-L and V-L. Commonly Ba accumulation appears as linear features (Figure 3.4a, Figure 3.5c, Figure 3.7a and f and Figure 3.8f and) parallel to the laminations but occasionally the latter element is observed as semi rounded sporadic features.

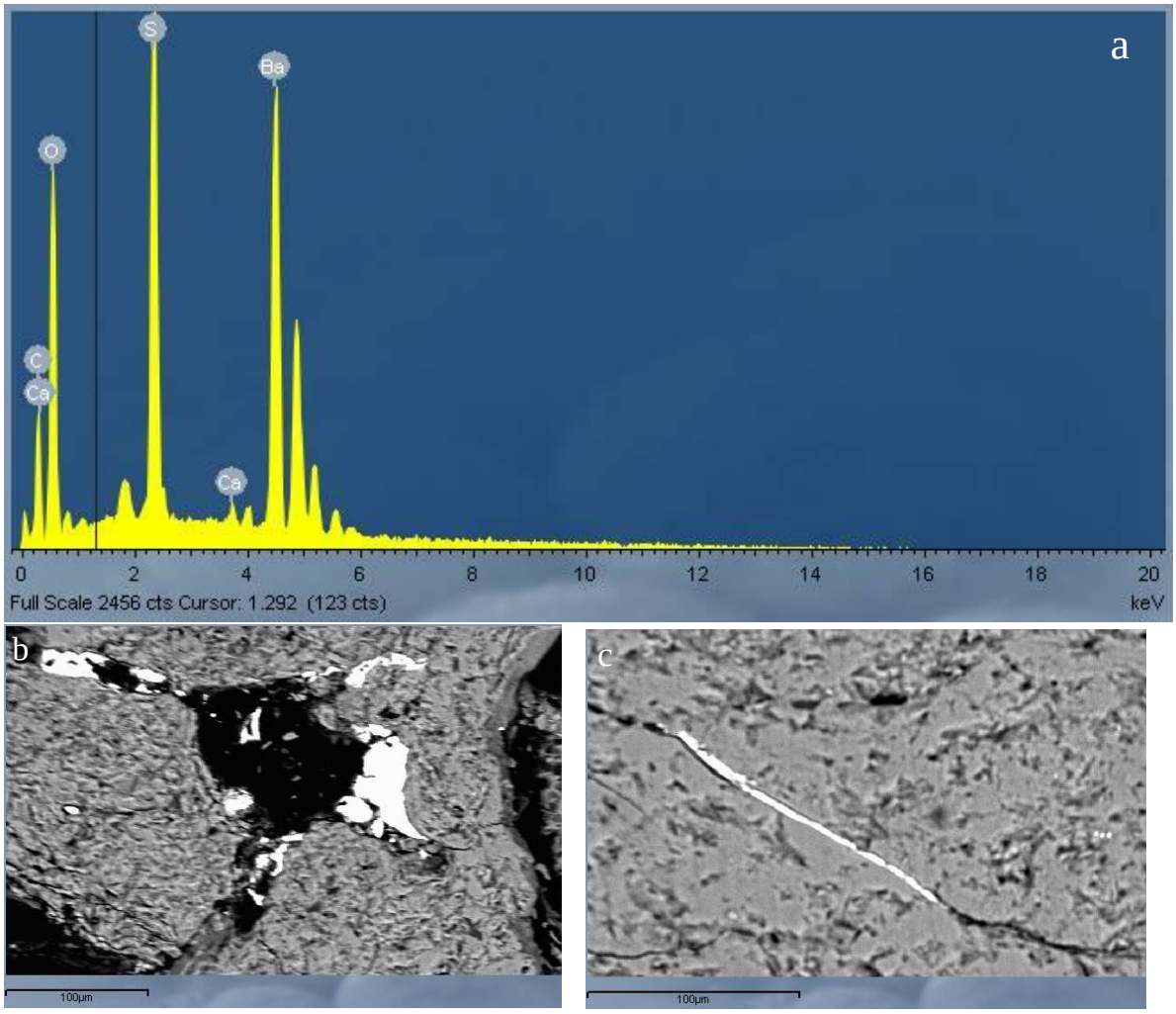

Figure 3.6: SEM images showing common barite distribution patterns within Vaalputs palaeosols (a) EDS graph showing elemental peaks indicative of mineral barite (b) typical occurrence of barite as a coating material along the inner surfaces of micro-veins (c) linear void hosting mineral barite. The scale bar on both images is 100 µm

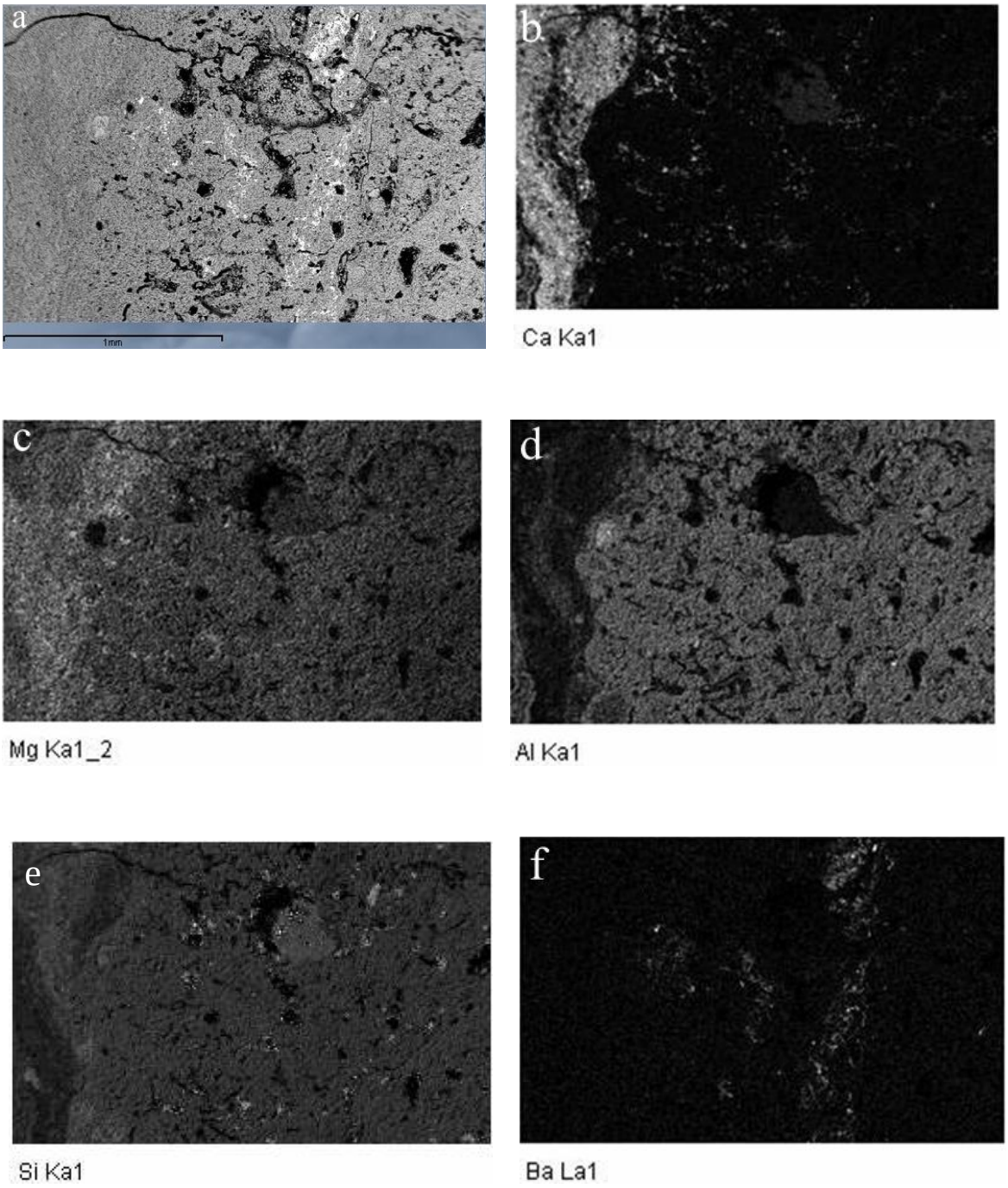

Figure 3.7: Elemental maps showing an (a) EDS image where the bright spots indicate barite accumulation and the distribution of (b) Ca, (c) Mg, (d) Al, (e) Si and (f) Ba. The maps are produced using scanning electron microscope method. The scale bar on the EDS image is 1 mm.

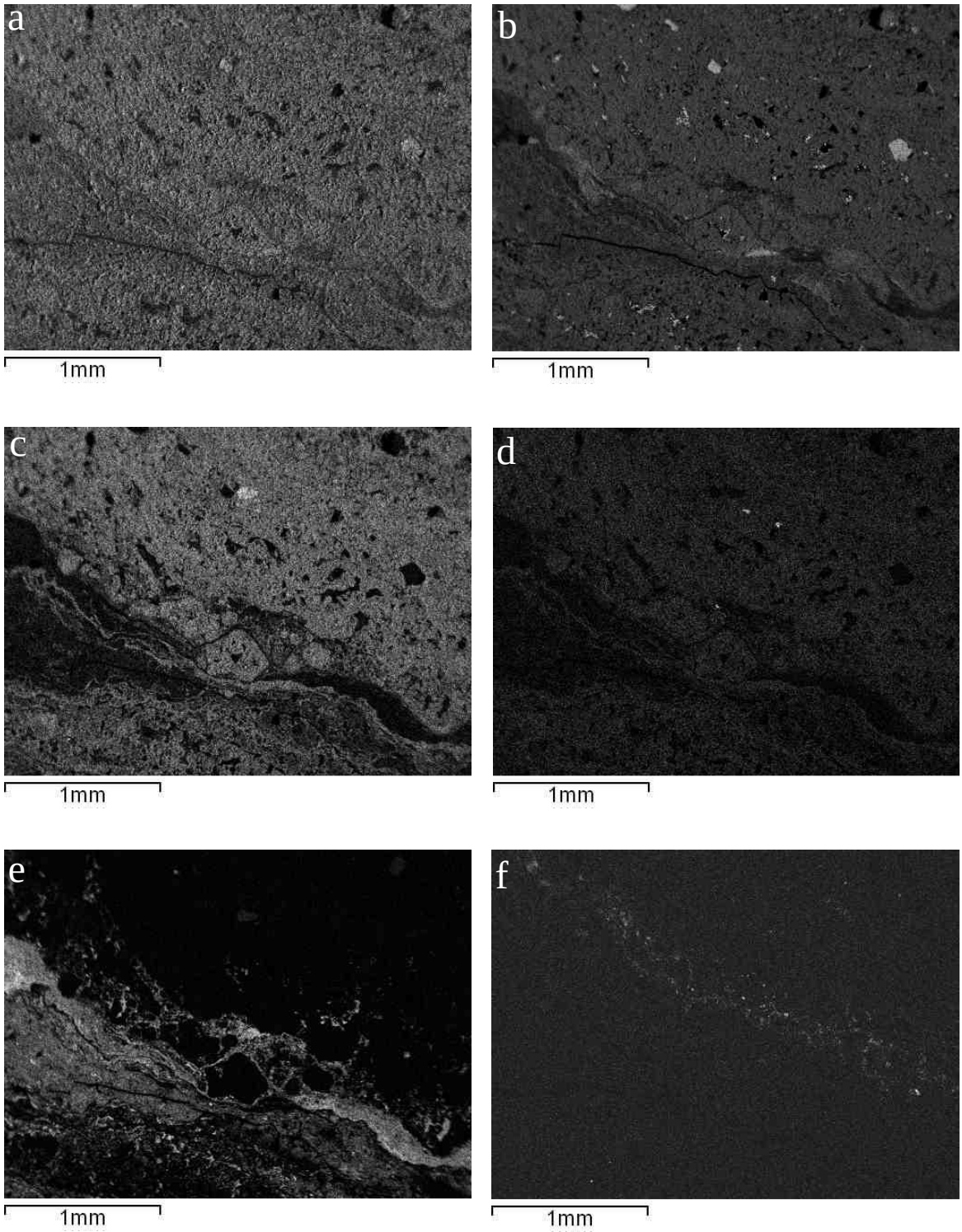

Figure 3.8: Elemental maps of the same region showing the distribution of (a) Mg (b) Si (c) Al, (d) K, (e) Ca and (f) Ba. The maps are produced using scanning electron microscope method.

3.3.3. Slaking tests

Slaking tests are designed to determine the nature of the material cementing the indurated horizons in Vaalputs. Table 3.9, Table 3.10 and Table 3.11 display the observations made when the samples are placed in strong acid and base solutions as well as the results taken every seventh day of equilibration. A scale of 0 - 5 is used indicating the intensity of

reaction when samples are placed in HCl and/or NaOH and the degree of slaking at the end of equilibration period. When samples are inserted in HCl and NaOH, the level "0" indicates no reaction occurred at all and "5" indicates most vigorous (Insert 1, 2 and 3 in Table 3.9, Table 3.10 and Table 3.11) meanwhile after seven days the level "0" indicates no slaking at all and "5" indicates complete slaking (Results 1, 2 and 3 in Table 3.9, Table 3.10 and Table 3.11).

The slaking results from profile C(1,5) are described in (Majodina, 2010). The data of the C(1,5) profile is provided in Table 3.9 to Table 3.11 for convenience. In the B(1,1) profile the B3 horizon samples (B3E and B3W) display vigorous effervescence when placed in strong HCl solution. The laminated materials (H-L and V-L) also exhibited substantial reaction in HCl solution along the clay cutan-lamination contacts (Table 3.9: Insert 1). In NaOH, samples of B1, B2L and B4 displayed complete slaking within the first seven days since the commencing of the tests. The clay cutans along the H-L and V-L also displayed complete slaking leaving only the white bands of the laminations completely intact. Samples of horizons B1 and B4 showed small amounts of fragments at the bottom of testing beaker. B3E and B3W did not slake at all in NaOH (Table 3.9: Results 1). For samples that did not slake (or incompletely slaked) in HCl and NaOH alternating acid/alkali treatments were applied. When samples were alternated (samples originally placed in HCl were then placed in NaOH solution and vice versa) B3E and B3W still showed most effervescence in HCl solution. V-L and C samples on the other hand showed slightly more reactivity after being originally treated with NaOH meanwhile H-L showed no reactivity at all. At the end of the second slaking interval samples B2, H-L and C completely slaked while samples B3E, V-L and B3W showed no signs of slaking. The remaining samples were alternated back to their original solutions (as in Table 3.9). B3E and B3W continued to display effervescence however none of the three samples slaked.

Table 3.9: Slaking tests results of samples from profile B(1,1) and C(1,5) (as presented in (Majodina, 2010)).The beginning of slaking tests (Insert 1) and the results observed after the first seven days (Results 1).

B11

	Insert 1		Results 1	
Sample	5M HCl	6M NaOH	5M HCl	6M NaOH
B1	1	0	1	5
B2	0	0	0	2
B2L	0	0	0	5
H-L	3	0	0	3
B3E	5	0	0	1
V-L	3	0	0	3
B3W	5	0	0	0
B4	1	0	0	5
C	0	0	0	2

C02

B1	0	0	0	5
B1-2	0	0	0	1
B2	0	0	0	5
C1-2	5	0	1	0

Table 3.10: Slaking tests results of samples from profile B(1,1) and C(1,5) (as presented in(Majodina, 2010)). First alternation of samples from acid to base and from base to acid solutions (Insert 2) and the results observed just before the samples were alternated every seven days.

B11

	Insert 2		Results 2	
Sample	5M HCl	6M NaOH	5M HCl	6M NaOH
B1	-	-	-	-
B2	1	0	2	5
B2L	-	-	-	-
H-L	0	0	4	5
B3E	5	0	2	0
V-L	4	0	0	0
B3W	5	0	1	0
B4	-	-	-	-
C	2	0	0	5

C02

B1	-	-	-	-
B1-2	4	0	3	4
B2	-	-	-	-
C1-2	5	0	0	0

Table 3.11: Slaking tests results of samples from profile B(1,1) and C(1,5) (as presented in (Majodina, 2010). Samples originally placed in acid (Table 3.9) were placed back into acid and those originally placed in base solution were also placed back in base.

B11

	Insert 3		Results 3	
Sample	5M HCl	6M NaOH	5M HCl	6M NaOH
B1	-	-	-	-
B2	-	-	-	-
B2L	-	-	-	-
H-L	-	-	-	-
B3E	2	0	0	0
V-L	0	0	0	0
B3W	2	0	0	0
B4	-	-	-	-
C	-	-	-	-

C02

B1	-	-	-	-
B1-2	-	-	-	-
B2	-	-	-	-
C1-2	0	0	0	0

3.3.4. Equilibrated soil solution - water pastes

Chemical data obtained from soil-water saturated paste extract solutions of B(1,1) trench profile is provided in Table 3.12. This chemical data only serves as a proxy for the soil solution therefore true equilibrium between minerals and water may not have been reached due to kinetic constraints. The chemistry of all soil solutions from trench B(1,1) show general trends of cations as $Na^{+}>Ca^{2+}=Mg^{2+}>K^{+}$ and anions as $Cl^{-}>SO_4^{2-}>>NO_3^{-}=F^{-}>PO_4^{3-}$. The pH levels of the soils fall within the neutral to moderately alkaline (7.69 – 9.16) range. The soil solution chemistry of all horizons does not differ substantially. The measured dissolved salts using electrical conductivity method fall within the 2.1-6.9 mS/cm range. The exception to this range are values measured from the A horizon having lowest dissolved salts (EC = 0.54 mS/cm) and B3L material measuring highest EC (23.1 mS/cm). The A horizon measured the highest levels of alkalinity (4.9 mM) and dissolved Ba (35.5 µM). Apart from the high Ba concentration within the A horizon and the low concentrations within the C horizon (3.0 µM) and B3L material (3.2 µM), the dissolved Ba for the rest of the horizons falls within a narrow range of 5.2-8.1 µM. The Ba levels are slightly higher within the H-L and V-L materials (7.01 and 8.12 µM, respectively) than enveloped dorbank material.

Table 3.12: pH, EC and major anions, cations and dissolved silica measured in the saturated paste extracts. Alkalinity is calculated as HCO_3^- and Si represents dissolved silica measure calorimetrically from trenchC(1,5) in Majodina (2010) and B(1,1).

Sample	pH	EC (µS/cm)	Alkalinity	F^-	Cl^-	NO_3^-	P_2O_5	SO_4^{2-}	Si	Ca	Mg	Na	K	Ba
			mM											µM
B11														
A	7.69	545.5	4.90	0.12	6.82	0.04	<0.00	2.31	0.44	1.51	1.74	7.68	1.62	35.48
B1	9.16	2795.0	2.20	0.03	<0.00	0.12	<0.00	3.84	0.90	1.09	0.55	3.38	1.83	7.14
B2	8.24	2123.0	1.70	0.14	57.81	0.00	<0.00	3.77	0.85	8.42	7.06	41.67	1.71	6.44
B2L	7.61	4317.0	1.53	0.08	108.38	0.00	<0.00	6.46	0.69	15.28	12.15	77.68	3.70	5.81
H-L	7.72	4025.0	1.86	0.09	<0.00	0.50	<0.00	8.62	1.04	3.13	2.17	10.51	3.59	7.01
B3E	8.09	3364.0	1.85	0.06	<0.00	0.31	0.02	8.91	1.06	3.05	2.10	10.07	3.86	6.40
V-L	7.85	4212.0	1.80	0.11	92.59	0.25	<0.00	3.20	0.86	9.44	7.36	61.48	2.01	8.12
B3W	7.91	5214.0	1.55	0.10	150.83	0.24	<0.00	3.94	0.84	19.82	16.31	80.72	3.20	5.68
B3L	7.10	23120.0	1.65	<0.00	282.68	0.00	<0.00	8.21	0.71	32.04	36.77	131.46	5.02	3.16
B4	7.84	6869.0	2.10	<0.00	180.51	0.17	<0.00	7.50	0.79	24.44	19.83	106.98	3.42	5.17
C	7.77	4794.0	1.75	0.16	88.91	0.33	<0.00	5.69	0.59	8.40	9.11	64.91	2.28	2.98
C02														
A	6.70	419.0	1.05	<0.00	1.41	0.08	<0.00	0.55	0.32	0.31	0.25	1.50	1.13	0.22
B1	7.10	8138.0	1.20	0.11	86.28	0.40	<0.00	7.54	0.59	8.53	17.24	40.87	2.40	0.87
B1-2	7.10	9743.0	1.55	0.16	29.35	<0.00	<0.00	2.53	0.75	10.23	15.43	58.71	2.86	1.27
B2	7.90	4015.0	1.95	0.21	12.85	<0.00	0.16	1.84	0.47	3.27	4.57	27.32	1.51	0.79
C1	7.40	2258.0	2.45	0.16	49.69	<0.00	0.81	3.90	0.38	1.36	1.97	16.16	1.26	0.28
C1-2	7.70	5941.0	1.70	0.21	53.36	<0.00	0.10	4.08	0.41	5.65	7.86	35.22	2.30	0.56
C2	7.50	4561.0	4.20	0.74	31.83	<0.00	0.66	1.45	0.26	6.16	7.58	19.15	2.51	1.28

3.4. Discussion

Geochemical properties provide information about the conditions of formation and a channel through which climate shifts may be unravelled. Several geochemical signatures may be preserved while others are altered or even erased under progressively increasing arid climate. Such geochemical traits are common within the Vaalputs palaeosols. These geochemical signatures obtained from each horizon of both trench profiles (B(1,1) and C(1,5)) and those of the entire profiles are being used to infer palaeoclimate conditions with geochemical implications.

The bulk chemistry of the soil horizons shows some distinct chemical associations. The concentration of SiO_2 shows a negative correlation with CaO. This phenomenon is observed throughout the soils of Vaalputs (Figure 3.9 and Figure 3.10). These observations are specially pronounced within the laminated H-L and V-L materials (Table 3.1 and Table 3.2). Sediments in Vaalputs are derived from weathering of underlying basement granite-gneiss (Desmet, 2007). Evidence from this study also supports these observations, thus high SiO_2 content is expected. The confusing issue is the source of Ca^{2+} in such a host material and/or even parent material. In an environment that appears to have been as arid as long as Vaalputs, an external source of CaO is necessary however so far there has been no evidence of any feature in proximity that could have been a potential source. Durand *et al.*, (2006) described the development of calcretes above silicate rocks. The study conducted by Durand *et al.* (2006) reviewed pathways through which calcretes may develop on weathered silicate rocks: these requirements include "(i) the source rock should contain Ca-bearing primary minerals from which sediments can be derived, (ii) lateral transfer of Ca^{2+} at landscape scale from neighbouring Ca-rich source-rocks via laterally moving ground- and soil waters, in solution (Ca and HCO_3^- ions), or by mechanical erosion and deposition of limestone clasts; (iii) an allochthonous origin of Ca through atmospheric input; and (iv) the deposition and reworking of shallow lacustrine or palustrine carbonates"..

The onsite basement granite gneiss may contain up to 2wt% calcium concentration (Andreoli, pers. comm). However, high calcium concentrations (up to 26wt%) were detected within Vaalputs sediments. Thus the low calcium concentration of the basement geology alone is probably not enough to account for the high calcium concentrations measured in the Vaalputs sediments. A study of Proterozoic granulite facies terrane by Albat (1984) (around Kliprand, ~50 km south east of current study area, Vaalputs) described several outcrops

hosting calc-silicate minerals and compiled a geological map (18°30'E, 29°30'S and 19°00'E, 31°00'S) in which Vaalputs falls. The occurrences of calc-silicate gneiss outcrops in this map are indicated no more than 30 km SE of Vaalputs. A larger area upon which these calc-silicate gneiss outcrop occurs further NE (~100 km) of Vaalputs. It is therefore possible that these calc-silicate gneisses (or even those compositionally similar) are sources of Ca^{2+}. Thus allochthonous origin and atmospheric input are likely to be responsible Ca^{2+} accumulation in Vaalputs.

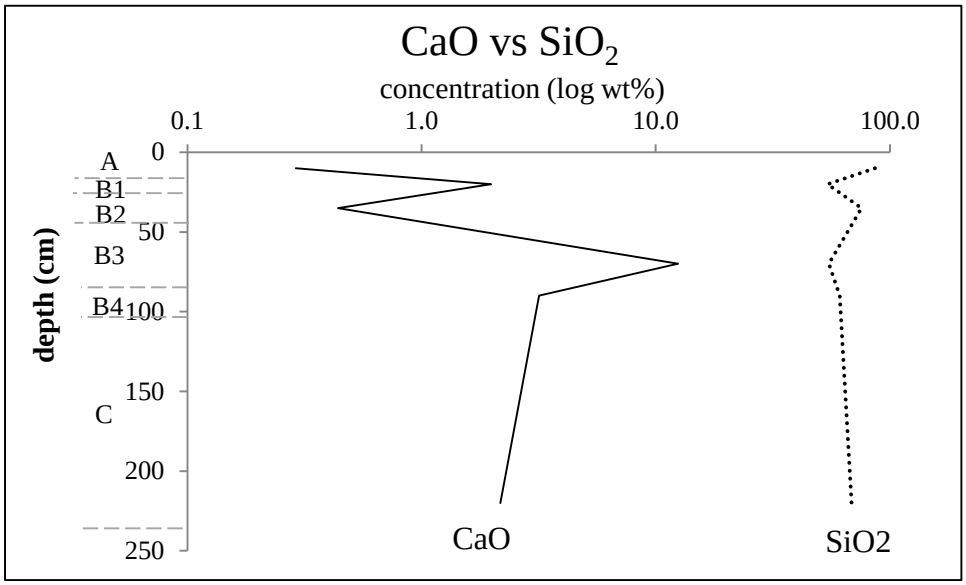

Figure 3.9: The distribution of CaO plotted against SiO_2 on B(1,1) trench from the top to the bottom of the profile. The concentration is given as log of wt% and the depth is measured in cm.

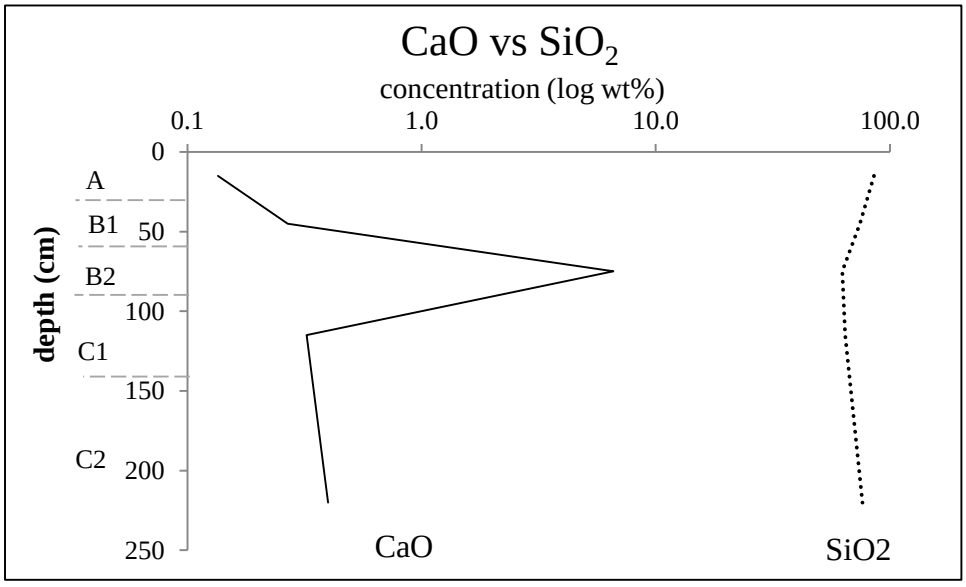

Figure 3.10: CaO distribution of plotted against SiO_2 on C(1,5) trench from the top to the bottom of the profile. The concentration is given as log of wt% and the depth is measured in cm.

The H-L and V-L laminations show an extreme enrichment in CaO and depletion in SiO_2 (Table 3.3 and Table 3.4). The extremely high LOI (Table 3.1 and Table 3.2) accompanying

high concentration of CaO within the H-L and V-L suggests that the white bands (Figure 3.1) of the laminations are predominantly $CaCO_3$.

Dorbank horizons in South Africa are known for their highly indurated nature where SiO_2 acts as the primary cementing agent (Ellis & Schloms, 1982; Francis, 2008). Calcium carbonate has also been reported as to form secondary cement within dorbank horizons. Several authors (Ellis & Schloms, 1982; Francis, 2008; Fey, 2010) suggest slaking tests as a useful tool to distinguish whether amorphous SiO_2 or secondary $CaCO_3$ is the dominant cementing agent on such indurated horizons. The distinction between the two cementing agents is based on the fact that materials cemented by amorphous SiO_2 will disintegrate when exposed to strong NaOH solution whereas samples that are cemented by $CaCO_3$ will disintegrate when exposed to strong HCl solution (Francis, 2008; Ellis & Schloms, 1982). Since both SiO_2 and $CaCO_3$ coexist throughout the trench profiles in Vaalputs slaking tests were executed to determine which of these cementing agents dominates. The results indicate that several horizons of trench B(1,1) (B1, B2L and B4) and C(1,5) (B1 and B2) disintegrated exposed only to warm NaOH (Table 3.9). This suggests that these indurated soils are predominantly SiO_2 cemented. None of the horizons slaked entirely in HCl alone. After alternating HCl - NaOH treatments were applied (Table 3.10) further samples from trench B(1,1) (B2, H-L and C) and C(1,5) (B1-2) expressed complete slaking. This suggests that these samples are cemented by both SiO_2 and $CaCO_3$. Samples that did not slake (Table 3.11) after being treated with both HCl and heated NaOH solutions (B3E, B3W, and V-L) suggest an alternative cementing agent, probably palygorskite (Francis, 2008). Samples that slaked only in strong basic solution confirmed their classification as dorbank horizons rather than silcrete horizons. The latter has been proved not to show substantial slaking in heated NaOH (Francis, 2008). Nash & Shaw (1998) described silcrete-calcrete duricrust intergrades in Kalahari and attributed their precipitation to a combination of evaporation and pH changes as well as salinity levels. In the current study, samples that showed complete slaking only after the application of alternating HCl - NaOH treatments would thus classify as calcareous-dorbank (cal-dorbank).

In order to establish if dorbank formation is a current pedogenic process milled samples were equilibrated in water and the resulting solution was analysed for chemistry (Table 3.12). Francis (2008) suggested a combination of high soil pH conditions (to increase silica solubility) and low rainfall environments (to ensure that leaching of soluble silica would be limited only to the subsoil) are necessary to produce dorbank horizons. In the current study

pH levels measured throughout trench B(1,1) are slightly alkaline (7.10 - 8.24). The only exception to this is the B1 horizon which has a solution pH of 9.16. The pH measured from trench C(1,5) fall in a narrow circumneutral range (6.70 - 7.90). Therefore the circumneutral equilibrium pH of the soil solutions suggests that silica mobilization is unlikely which further suggests that current day formation of dorbank is also unlikely, except possibly in the upper dorbank horizon (B1) of profile B(1,1). Francis (2008) measured elevated Na^+ concentrations within the dorbank horizons along the west coast of South Africa and stressed that Na^+ is important in dorbank formation, not only does it elevate the pH but it also promotes dispersion in the matrix which slows solution movement down so that silica from the soil solution precipitates out. Concentrations of Na^+ within Vaalputs sediments (Table 3.12) are much lower than those of Francis (2008) thus further suggesting that conditions necessary for dorbank formation have been highly reduced under current day climate.

High Ba concentration was measured from the A horizon of trench B(1,1) but nowhere on trench C(1,5) (Table 3.12). It is therefore difficult to explain high Ba concentrations within trench B(1,1) thus further sampling is needed.

In order to determine the spatial distribution of the major elements within the laminated zone elemental maps of no more than 2 mm^2 regions were collected (Figure 3.2 to Figure 3.8). Imaging and elemental mapping using PIXE and SEM provide comprehensive details about chemical distributions and associations. Throughout the solum, relative distributions of Si and Ca show that for the most part, these two elements indicate a negative association (Figure 3.9 and Figure 3.10). This is specially observed within white bands of the laminated H-L and V-L materials (Figure 3.1). Nash & Shaw (1998) described wavy laminae of calcite interlayered silica and attributed this to the opposing pH conditions needed for calcite and silica precipitation. The elemental maps (Figure 3.2, Figure 3.3, Figure 3.7 and Figure 3.8) further revealed that the thinly developed brown bands of the laminated H-L and V-L materials (Figure 3.1) are dominated by Si, Al, Fe and K. The association of Si, Al, K and Fe represented on these elemental maps is indicative of illite accumulation. There is little overlap between the Ca distribution and these illite associated elements. The illite accumulations correspond to the brown laminations that are observed within the white calcite matrix (Figure 3.1). A strong correlation between Al, Fe and K measured on the bulk analysis (Figure 3.11) suggests that illite is the dominant clay mineral throughout the solum, thus the illite within the laminations is likely to be derived from the soil matrix rather than forming within the lamination itself. Numerous studies have reported laminations on pedogenic calcite

as well as on calcretes. More recently (Brock-Hon *et al.*, 2012) reported similar features occurring as infill of calcium carbonate lamina. These laminae were described along sub-vertical cracks on a near surface petrocalcic horizon in Mormon Mesa, Nevada USA however no illite – calcite laminations were reported. The alternating illite-calcite laminations in Vaalputs (Figure 3.1) occurring as infill along vertical cracks within the B3 horizon are somewhat difficult to interpret. However a possible explanation is that the calcite precipitation occurred between adjacent clay coatings while gradually displacing clay cutans into 'islands' within a continuously increasing calcite matrix (Chapter 2). Evidence from elemental distribution maps (PIXE) and bulk analyses (XRF) of the laminations (H-L and V-L) suggest that the calcic bands (white) originated through chemical precipitation. Elemental maps indicating illite distribution within a Ca rich zone further suggest that $CaCO_3$ accumulation occurred in a clay dominant region thus illite pre-dates $CaCO_3$ precipitation.

Scanning electron microscope mapping allows the detection of lighter elements, such as Mg. Magnesium shows an equal distribution throughout the Si and Ca dominating regions thus the overlapping Si and Ca may imply sepiolite or palygorskite accumulations within a calcite matrix. Such clay minerals are commonly associated with calcretes in Namaqualand and can neoform with a calcrete matrix (Francis *et al.*, 2007; Francis, 2008).

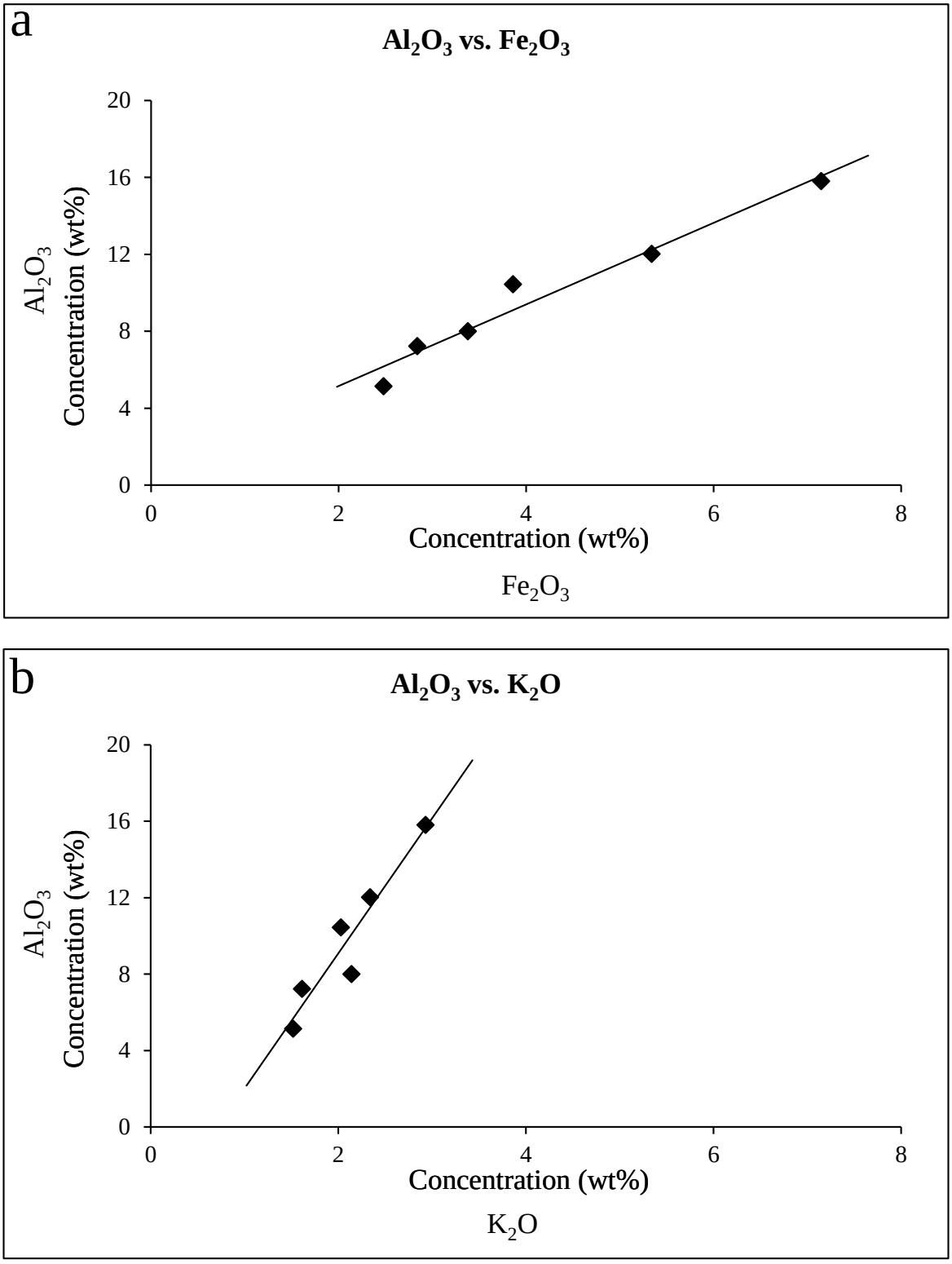

Figure 3.11: Graphical representation of elemental correlations (a) Al_2O_3 vs. Fe_2O_3 and (b) Al_2O_3 vs. K_2O within the horizons of trench B(1,1).

The trace element assembly of the Vaalputs soils is of interest due to the anomalously high Ba concentrations reported by Andreoli (pers. comm) in the soils. For general comparison of trace element composition the 25th, 75th percentile and mean have been provided for numerous elements as calculated from the regional geochemical dataset of the Springbok

2916 1:250 000 map sheet compiled by the Council of Geoscience (CGS) (Hansen, (unpublished data)). Although the study area falls outside this map, Springbok and Vaalputs are approximately 100km apart and the overall geology between these two locations shows a number of similarities. The overall geochemistry would therefore be expected to remain relatively similar. The trace element composition of the Vaalputs palaeosols compares well to the regional geochemical data (Table 3.5 and Table 3.6). There are however three exceptions to this and these include Cu, Sr and Ba concentrations. The Cu concentrations are elevated above the 75th percentile for all horizons throughout the B(1,1) trench profile whereas Sr and Ba are significantly enriched within the laminated zones. High Cu concentrations within the soils of Bushmanland terrane are expected as a consequence of the regional geology which hosts high Cu concentrations especially within the adjacent Okiep terrane (Reid *et al.*, 1987). The diorite series of the Koperberg Suite (near Okiep) have demonstrated high Ba concentrations (up to 4800ppm). Further north east of Vaalputs (Aggeneys terrane), Reid *et al.* (1987), Stalder & Rozendaal (2005) and Lacassie *et al.* (2006) have reported that the underlying basement geology is enriched in Ba.. The immediate basement granite gneiss hosting Vaalputs sediments has limited published geochemical data, however, the regional geology (Bushmanland terrane) is well studied and largely reported with high barite concentration. The high Sr concentration in Vaalputs are likely to result from the basement granite gneiss however its association with high Ba concentrations in soils is likely to be the result of the celestobarite (Sr, $BaSO_4$) solid solution series between these two elements (Stoop & Zavaleta, 1978; Sullivan & Koppi, 1995). The parallel concentrations of Sr and Ba suggest coexistence of both celestine ($SrSO_4$) and barite ($BaSO_4$) end-members of the isostructural series within Vaalputs palaeosols.

Barium, reported in an earlier study of Majodina (2010), was detected using XRF method on composite laminated materials of B3L and B1-2 from trench B(1,1) and C(1,5), respectively. In the current study, spatial distribution of Ba is investigated. The low concentrations (Table 3.5) and ERs (Table 3.7) of Ba within the laminated (V-L/H-L) materials (Figure 3.1) relative to the composite B3L suggest that Ba is associated with the clayey regions most adjacent to the H-L/V-L and not with the actual laminated H-L/V-L zone, as originally thought (Majodina, 2010). Elemental maps confirmed that these clayey regions have indicated elevated Ba concentration (Table 3.5 and Table 3.6). The clayey B2L also measured a high Ba concentration which suggests that high Ba compositions occur along high clay regions supporting findings within the B3L. The Ba concentrations within these clayey regions are

much higher than the 75th percentile of the regional geochemistry (Hansen, (unpublished data)). Although celestobarite solid solution is possible in Vaalputs, Sr shows slightly different enrichment patterns relative to Ba. Concentrations (Table 3.6) and ERs (Table 3.7) of Sr suggest elevation within the clayey B2L and B3L as well as within the H-L and V-L materials relative to the surrounding matrices.

The spatial resolution of the Ba was investigated using PIXE (Figure 3.4d and Figure 3.5c), SEM (Figure 3.6, Figure 3.7 and Figure 3.8) and XRT (Figure 3.12 and Figure 3.13). The association of Ba, S and O detected with SEM and PIXE confirmed mineral barite. The distribution of barite mapped using PIXE and SEM techniques were completed on thin sections. Barite could only be identified within clay (illite) dominated regions most adjacent to the calcite dominated laminations throughout the B3 horizon. At micro scale barite accumulation appears to be restricted to linear voids and on rims of circular pores. A recent study of (Brock-Hon *et al.*, 2012) describes similar occurrence of barite in palaeosols of the Marmon mesa where barite was largely found in association with linear voids and circular pores and in some cases barite would be found along boundaries between clay dominated and carbonate dominated matrices. Brock-Hon *et al.,* (2012) further describe five mechanisms through which barite may accumulate in soils. These processes include (i) "detrital barite crystals weathered from parent materials, (ii) precipitation of pedogenic barite crystals in humid, clay rich soils under acidic conditions, (iii) non-pedogenic precipitation from high-saline groundwater, (iv) biomineralisation by bacteria and in the rhizosphere and (v) rarely as pedogenic crystals in soils and palaeosols of arid climates where barium ions are supplied to solutions by parent material or dust". They concluded that the ability of the fibrous clays (with which barite is associated) to attract water and ions may have facilitated inorganic and/or organic accumulation of barite.

Barite distribution was further analysed on consolidated hand samples from trench B(1,1) (B1, B2, B3 and B3L) and trench C(1,5) (B1-2) using XRT. High barite concentrations were only identified within the B3 and B3L horizons. Barite showed preferential accumulation within interconnected (Figure 3.12b) and isolated micro-pores (Figure 3.12a) along contact surfaces of the calcic-argillic laminated material and B3 dorbank horizon. The interconnected pore spaces hosting Ba forms a network of micro-veins whereas the isolated pores forms a nodular concentration of Ba. Elemental maps produced from PIXE and SEM analyses show that Ba accumulation occurs along inner surfaces of circular pores (Figure 3.4d, Figure 3.5c

and Figure 3.6b and c) which in turn indicate that barite is not an infill but a coating along the walls of veinlets.

Similar to other sites in the world, the occurrence of pedogenic barite in Vaalputs suggests implications for palaeo-geochemical conditions.

It is difficult to say how Ba was deposited in Vaalputs however it is likely that it came as part of primary minerals along with sediment supply from the local geology. The current distribution (in micro-nodule and micro-veins) of barite within Vaalputs palaeosols suggest that at one stage Ba was mobilised and later re-precipitated as pedogenic barite. The mobilisation of Ba^{2+} is likely to have occurred during much wetter environments under anaerobic conditions when SO_4^{2-} was reduced to sulphide species. Such conditions were most likely prominent during the period of sedimentation in and around Vaalputs. The drying of sediments during the onset of arid climate facilitated more aerobic soil conditions while the sulphides was oxidised to SO_4^{2-} which promoted barite precipitation. The preferential accumulation of barite in micro-veins and micro-nodules may be related to one or two major processes (i) the SO_4^{2-} rich water concentrated in pore spaces and (ii) bio-degradation of primary barite during sulphate reduction released and increased Ba concentration along micro-vein walls (Figure 3.6b-c, Figure 3.12 and Figure 3.13). Under anaerobic conditions bacterial solubilisation of barite has a potential to increase Ba ions to concentrations greater than expected (Alberta *et al.*, 2009). Bolze *et al.*, (1974) conducted a laboratory investigation of microbial mobilisation of barite and concluded that Ba can be mobilised from barite during sulphate reduction. Therefore the accumulation of Ba on walls of micro-veins in Vaalputs could be related to microbial placement during the SO_4^{2-} reduction from primary barite under anaerobic conditions and was later re-precipitated during the reoxidation of anaerobic sediments. This may mark the transition from humid conditions to driers conditions when arid climate set in. It is also possible that the preferential accumulation of Ba within micro-veins and micro-nodules resulted from the desiccation event which gave rise to the development of polygonal ped units. The development of the desiccation cracks resulted to hydraulic gradient from which solute laden water were drawn to the ped surfaces where the required conditions of barite precipitation were met.

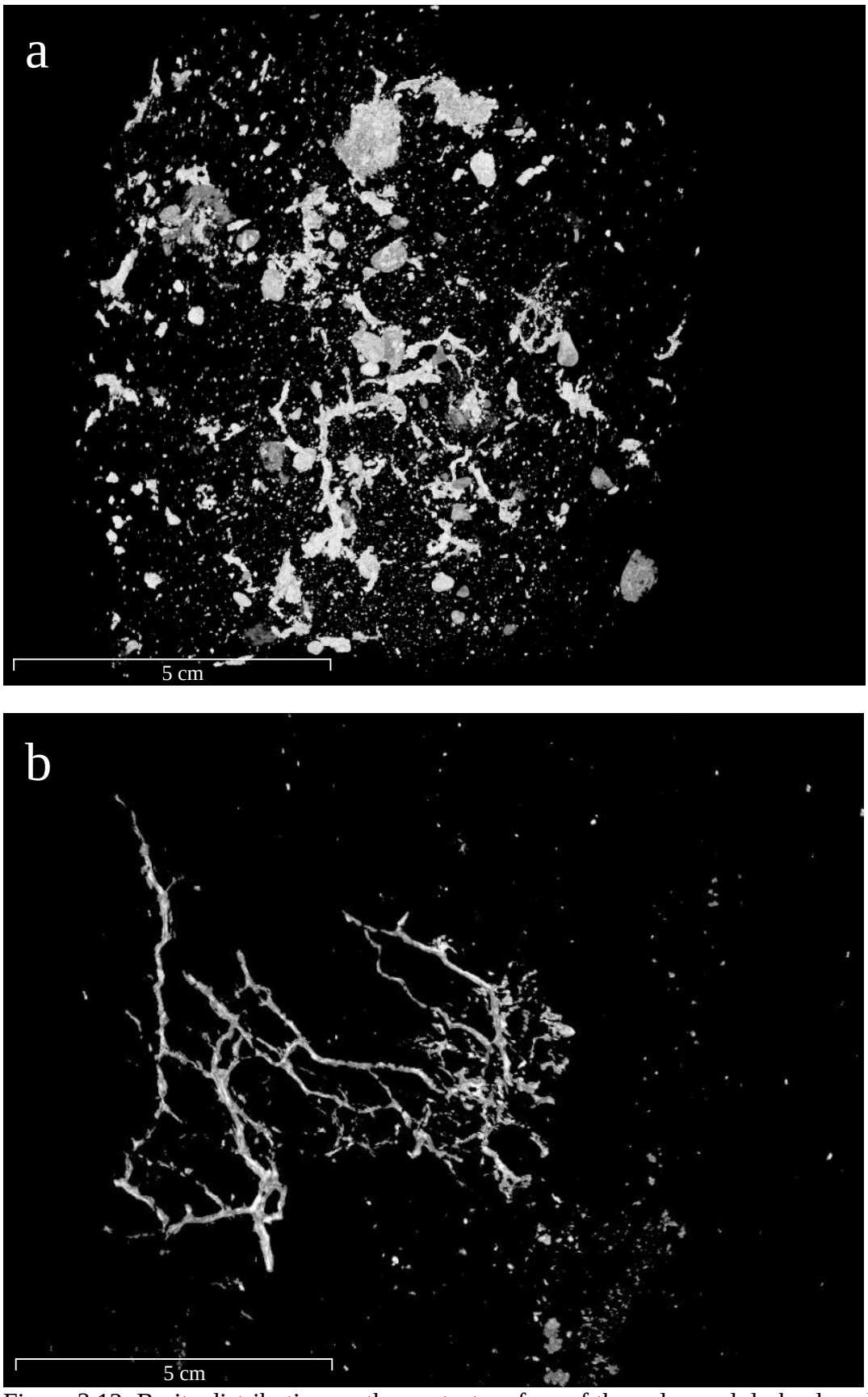

Figure 3.12: Barite distribution on the contact surface of the polygonal dorbank ped units and the calcareous laminations of H-L and V-L showing (a) interrupted micro pore spaces coated with barite (b) interconnected pore spaces forming a network of micro-veins containing barite.

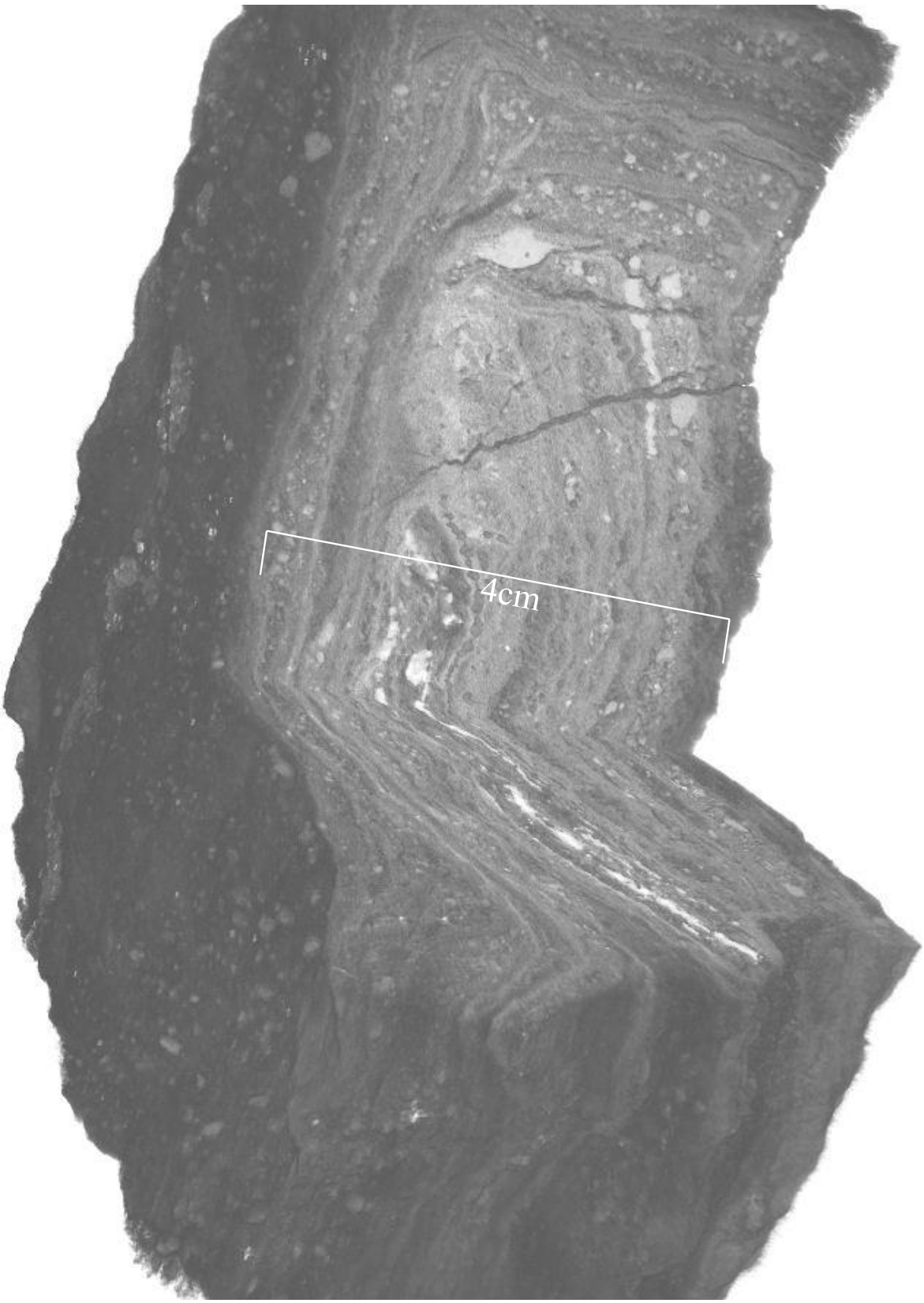

Figure 3.13: Hand sample of figure 3.12b analysed with XRT displaying barite distribution (bright white regions) along the contact zone of dorbank ped and its associated laminated material.

3.5. Conclusions

Geochemical signatures of Vaalputs palaeosols represent palaeo and current soil environmental conditions in and around Vaalputs. The Ca^{2+} content is derived from surrounding cal-silicate bearing gneisses and precipitates in Vaalputs as calcite. The disintegration of numerous horizons in strong alkaline solution indicates that amorphous silica is the dominant cementing agent whereas secondary calcite acts as a secondary cementing agent within the dorbank horizons. The inability of HCl and NaOH solutions to slake the white bands of H-L and V-L laminations along with elevated Mg measured with XRF within these white bands suggests that sepiolite in association with palygorskite may be present as the cementing agents. High pH conditions would precipitate calcite while dissolving and mobilising silica. Numerous horizons in Vaalputs measured relatively low Na^{+} concentrations accompanied by circumneutral pH conditions however it appears that calcite precipitation and silica dissolution may still continue at much reduced rates.

Apart from the surface A horizon all subsurface horizons contain elevated total Ba concentrations (measuring above regional trace metal background). This is related to the local geology (Bushmanland terrane) from which the sediments in Vaalputs and the surroundings are derived. Anaerobic conditions prevailed around the time of deposition of Ba-rich sediments. This resulted to the release and mobilisation of Ba from Ba rich primary minerals. The accumulation of authigenic barite may be related to the desiccation event when solutes laden water were drawn to ped surfaces.

The observed calcite and amorphous silica accumulations as well as authigenic barite in Vaalputs may indicate an overall climate shift from wet to dry.

4. Chapter 4: Mineral composition and spatial distribution within Vaalputs

4.1. Introduction

Mineral assemblages of palaeo-pedons and -sediments are commonly used as indicators of palaeoclimates under which they formed. Few publications exist relating to the soils within Namaqualand region. Detailed soil mineralogy studies of (Singer *et al.*, 1995; Francis, 2008) are among the few that exist for Namaqualand region. In both studies, mineral compositions have been used to infer palaeoclimates. The arid climate in which Vaalputs occurs is a perfect medium through which mineral assemblages may be preserved. It is these preserved minerals that may be studied to provide information about the local conditions of both the past and present.

The aim of this chapter is to determine the composition of clay (< 2µm) minerals in Vaalputs and infer palaeoclimates of formation.

4.2. Materials and Methods

Clay mineralogy was largely determined using X-ray diffraction (XRD) instruments. The clay analyses were performed on clay separates (<2 µm) at the University of Stellenbosch and iThemba LABS. Clay separates were prepared by dispersion followed by sedimentation. After drying the sedimented clay extracts were powdered and placed onto a glass slide for analysis in random clay orientation. The XRD analyses were performed with a BRUKER AXS (Germany). The instrument is composed of several components including a D8 advance diffractometer uses Cu-Kα radiation of 1.5406 Å as well as PSD Vantec-1 gas detector with 1600 channels. The measurements were taken at a tube voltage of 40 kV and a current of 40 mA while using a V20 variable slit. The 2θ angular range of 4.5 to 60° was maintained over the measurement period of approximately 1second per step. Mineral identification was done with the help of PANalytical X'Pert HighScore Plus software.

To resolve uncertainties regarding clay mineralogy throughout B(1,1) and C(1,5) SEM and PIXE were used.

Results obtained from equilibrated soil pastes were modelled using Phreeqc Interactive version 2.17.4468 for saturation index (SI) calculations. These calculations were run with database file *phreeq.dat* to predict minerals that may in equilibrium with current climate conditions.

4.3. Results

4.3.1. Mineral composition and distribution

X-ray diffractograms of the clay fraction from each horizon of trench B(1,1) and C(1,5) are shown in Figure 4.1 and Figure 4.2, respectively. Several clay minerals are identified including palygorskite, illite ($K_{0.6\text{-}0.85}(Al,Mg)_2(Si,Al)_4O_{10}(OH)_2$) and minor amounts of kaolinite ($Al_2Si_2O_5(OH)_4$) throughout the B(1,1) trench profile. The presence of palygorskite is identified on diffractograms with d-spacings of 3.24 Å, 4.47 Å and 10.50 Å. Illite peaks are well developed at d-spacings of 2.56 Å, 4.49 Å and 10.01 Å whereas kaolinite is identified at 1.66 Å, 3.58 Å and 7.16 Å d-spacings. Other minerals identified from the clay fraction include calcite (2.84 Å, 3.03 Å, 3.85 Å) and quartz (2.46 Å, 3.34 Å, 4.26 Å). Both quartz and calcite are present and dominate the clay mineral composition throughout B(1,1) and C(1,5) trench profiles.

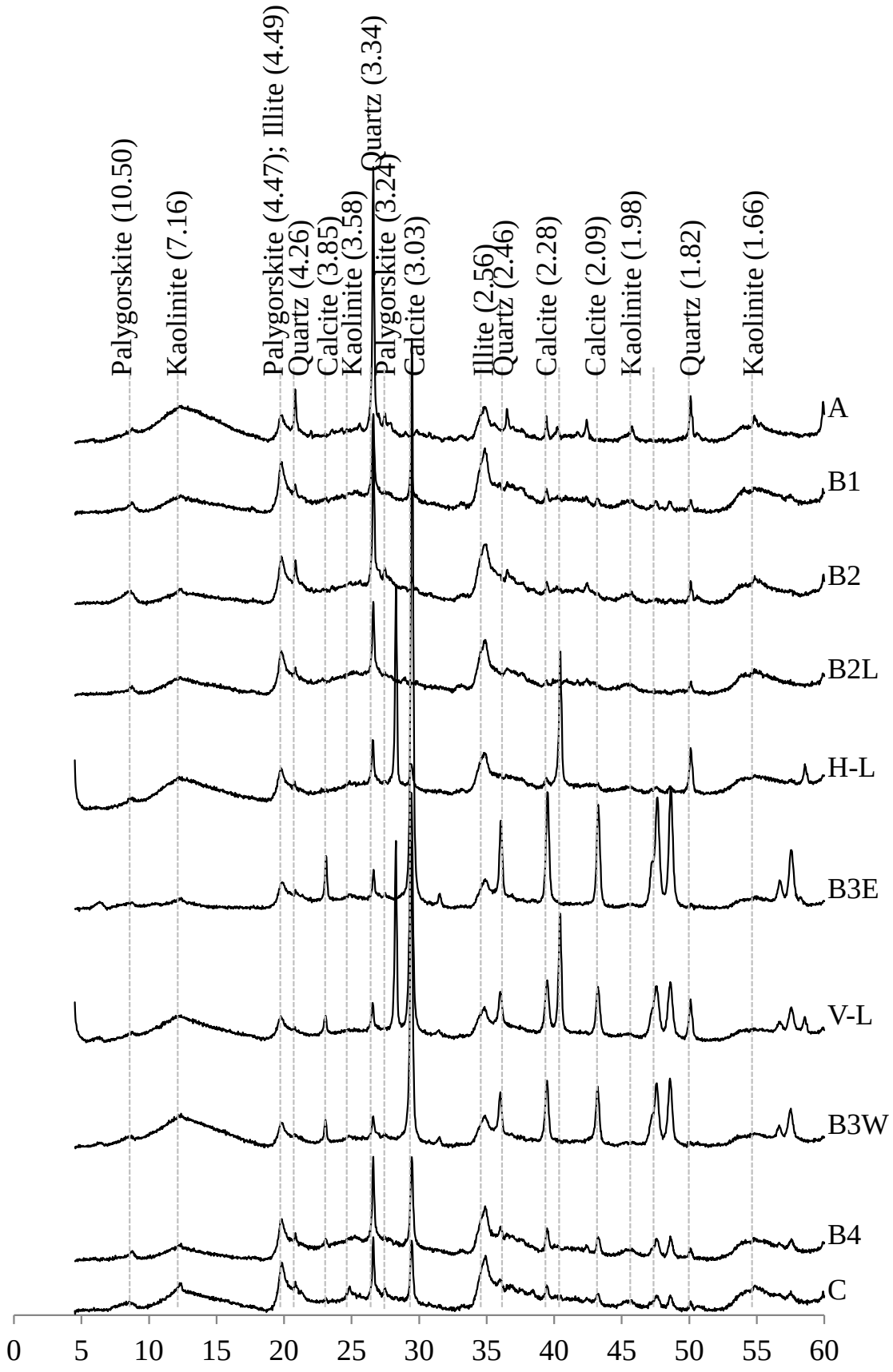

Figure 4.1: X-ray diffractograms of clay extracts taken from all horizons and laminations from trench B(1,1). The d-spacings are measured in Å.

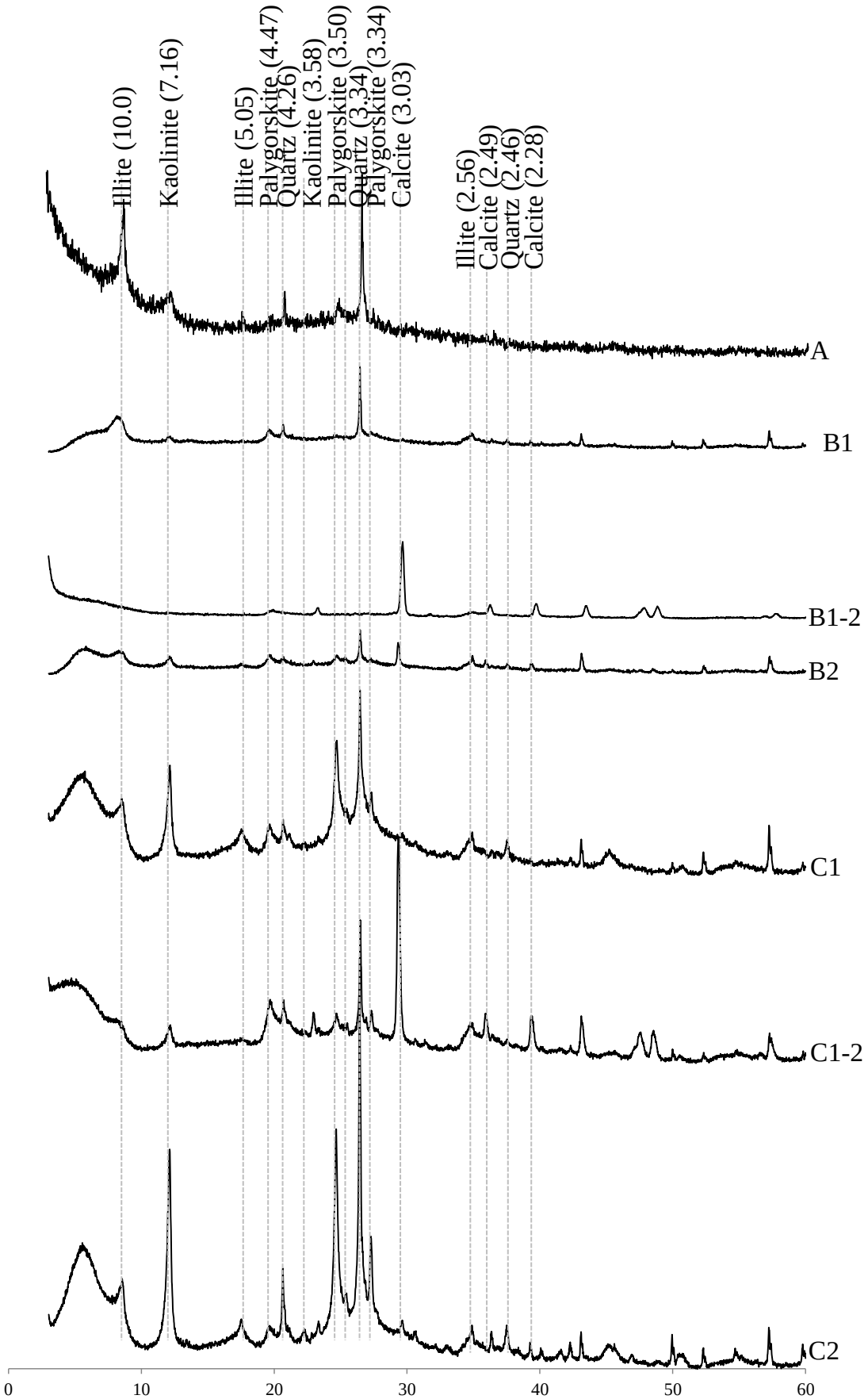

Figure 4.2: X-ray diffractograms of clay extracts taken from all horizons and laminations of trench C(1,5). The d-spacings are measured in Å

4.3.2. Mineral equilibria under current climate

Saturated paste extracts (Chapter 3) were modelled using Phreeqc Interactive 2.17.4468 to determine possible mineral equilibria within the B(1,1) and C(1,5) trench profiles. Saturation indices were calculated as log (ion activity product (IAP)/Keq). Negative values of SI indicate that IAP is less than Keq suggesting undersaturation of phase with respect to the horizon in question. Cases where SI = 0 indicate that IAP equals Keq which suggests equilibrium with respect to the mineral in question. Positive SI values indicate that Keq is less than IAP which suggests supersaturation with respect to the phase in question. Mineral equilibrium models of the soil horizons are displayed in Figure 4.3. On these models illite and kaolinite are supersaturated with respect to all horizons throughout trench B(1,1). Calcite is also supersaturated with respect to the entire B(1,1) trench with an exception to the top A horizon (Figure 4.3a). Saturation indices of amorphous silica throughout trench B(1,1) measures below zero (undersaturated) (Figure 4.3a-f). Sepiolite is undersaturated with respect to several horizons including A, B1, H-L, V-L and C (Figure 4.3a-f) and supersaturated with respect to B2, B3E, B3W and B4 of trench B(1,1). Palygorskite is only measured on A and V-L horizons and it is undersaturated with respect to these horizons. The rest of the horizons did not indicate any palygorskite. Mineral equilibrium models of trench C(1,5) are provided in Appendix 1 however trends similar to those of trench B(1,1) are observed.

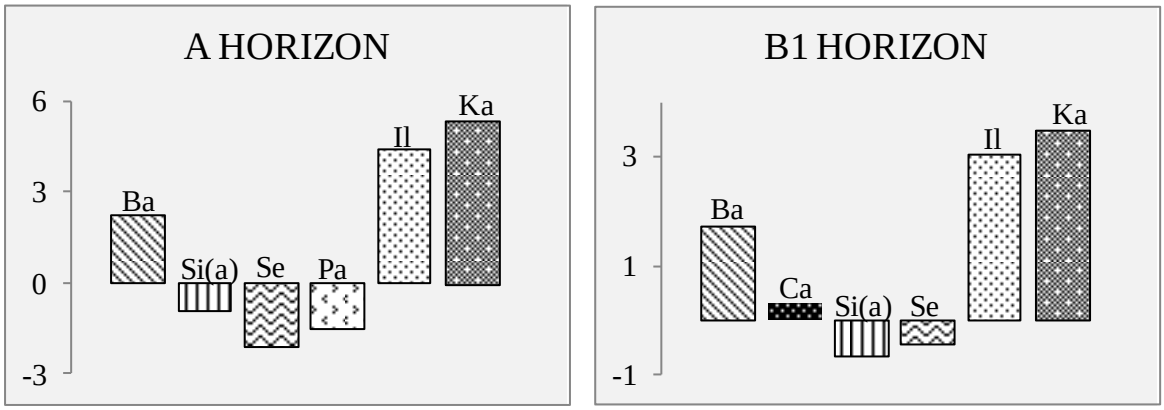

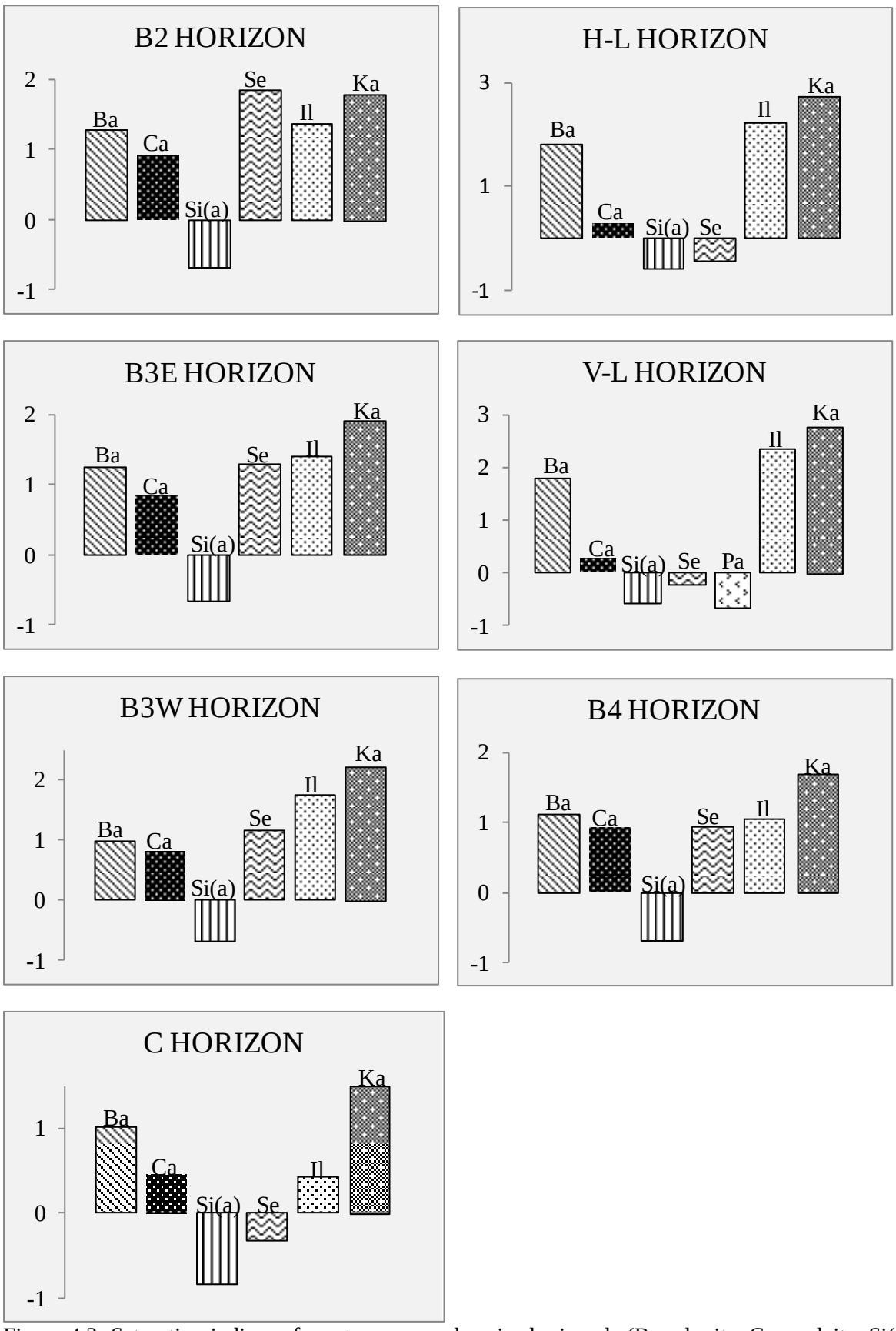

Figure 4.3: Saturation indices of most common clay sized minerals (Ba – barite, Ca – calcite, Si(a) – amorphous silica, Se – sepiolite, Pa – Palygorskite, Il – illite and Ka – kaolinite) on each horizon of trench B(1,1) in Vaalputs.

4.4. Discussion

4.4.1. Clay mineralogy of Vaalputs

The clay fraction (<2 µm) the Vaalputs palaeosols is largely dominated by palygorskite, illite, kaolinite, calcite and quartz. Due to the currently persisting arid climate within and around Vaalputs, clay mineral assemblage conveys physico-chemical conditions of formation.

Palygorskite is one of the most dominant clay minerals in Vaalputs and may be accompanied by sepiolite on occasion. Sepiolite could not be conclusively identified on diffractograms of all horizons however its identification was aided with SEM (Figure 3.7). Palygorskite was first identified and described near the town of Palygorsk in the Perm District in Russia. Ever since its discovery, palygorskite has been described in various geological settings (Callen, 1984; Post & Crawford, 2007).

The formation of mineral palygorskite was initially thought to be only restricted to few environments such as hydrothermal vein and ore-body alteration zones (Callen, 1984). Palygorskite minerals are now known to exist widely in environments such as: (1) epicontinental and inland seas and lakes (2) basaltic material or volcanic sediments by hydrothermal alteration and in clays of open oceans with fore-arc and oceanic rise (3) calcareous soils through precipitation (Callen, 1984). Relic palygorskitic fibrous textural features of have also been described on silcretes where they were interpreted as replacement of palygorskite-bearing palaeocalretes (Mees, 2010). The occurrence of palygorskite within the soils of Vaalputs therefore suggests a slightly different environment of formation compared to current climate where palygorskite occurs on dorbank horizons. Generally in soils, palygorskite occurs almost exclusively in very dry (aridic) environments where potential evapo-transpiration largely exceeds precipitation (Singer *et al.*, 1995; Singer *et al.*, 2003). Vaalputs is located within a dry region since early Miocene period (Chapter 2) therefore these soils have been a potential host of palygorskite and sepiolite since that period.

Further, high pH (alkaline conditions), high Si and Al, and relatively low Mg activities are conditions specified for the formation of mineral palygorskite (Francis, 2008). Moderate pH levels were measured throughout trench B(1,1) and C(1,5) thus high pH soil conditions required to form palygorskite and sepiolite no longer exist in Vaalputs. Singer (1980) and Callen (1984) indicated that many of the palygorskite containing soils are thought to be very

old and relic thus the widely distributed palygorskite in Vaalputs may be a relic feature. The scattered palygorskite and sepiolite minerals are largely observed on the calcareous dorbank (B1, B2, and B3) horizons and further observed on the lower most C horizon in a flake form. The most common occurrences of palygorskite are in the form of cutanic rims of orientated fibres along ped surfaces and grain skeletons (Callen, 1984). Coatings of palygorskite have been observed as part of infillings of desiccation cracks where these features were described as zones of recrystallisation (Mees, 2010). High concentrations of palygorskite and sepiolite minerals in Vaalputs are found adjacent to calcite dominated regions (white) of the H-L and V-L materials which are in turn infill to desiccation cracks of B3 dorbank horizon. These are similar findings to those of Callen (1984) who reported that palygorskite deposits are generally in association with carbonate facies such as calcretes, dolomites, and limestones. Callen (1984) further stated that palygorskite deposits are often found in close association with anomalous barium and strontium concentrations. High Ba and Sr concentrations (above regional background levels) are demonstrated throughout Vaalputs soils (Table 3.5). The association of palygorskite with high Ba concentrations is described by Brock-Hon *et al.*, (2012) as the ability of palygorskite to absorb water while attracting metals in solution.

In southern Africa nearly all the sepiolite and palygorskite occurrences are found in the Kalahari and are related to the calcrete formations (Singer *et al.*, 1995). In Namaqualand these fibrous clay minerals have been documented in Alexandra Bay, Springbok, Warmbad, Loeriesfontein (Singer *et al.*, 1995) and within Kleinzee areas (Francis *et al.*, 2007 and Francis, 2008). Within this region sepiolite containing soils occur more commonly on lower elevations (<200 masl) and along the west coastal region whereas the palygorskite containing soils occur more inland at higher elevations (approximately 600 – 900 masl) (Singer *et al.*, 1995; Francis *et al.*, 2007). The Vaalputs area occurs at an elevation of approximately 1000m above mean sea level (Brandt *et al.*, 2005) where both palygorskite and sepiolite coexist. This suggests that Vaalputs is likely to be allocated in a transition zone (coastal to inland) where both sepiolite and palygorskite dominate.

As evident from the XRD patterns calcite occurs in most soil horizons and materials. Calcite is very common in Vaalputs and its accumulation is described in Chapter 2 and Chapter 3.

Barite was not identified in the XRD patterns. This may result in the high detection limit (>5 wt%) of the XRD instrument. However the use of SEM confirmed preferential barite

accumulations (Figure 3.4, Figure 3.5, and Figure 3.12) within clayey zones of polygonal peds of dorbank horizons most adjacent to the H-L and V-L infill.

4.4.2. Modelling of current environment

Phreeqc models of saturated paste extracts are used to determine possible mineral equilibria within the B(1,1) and C(1,5) profiles. Due to high cation-anion balance errors on horizons of trench C(1,5) only A, B1, C1-2 and C2 horizons could be modelled with confidence whereas all horizons of trench B(1,1) measured low cation-anion balance errors allowed mineral equilibria models.

Mineral equilibria models of Vaalputs soils indicate that the soil solutions are supersaturated with respect to barite in all horizons. Although barite was not confirmed in all horizons (when using other analytical methods such as XRD, PIXE, SEM and XRT), where Ba was detected elevated concentrations above background levels were however measured. This suggests that current soil conditions in Vaalputs are conducive to barite accumulation. All horizons are supersaturated with respect to calcite conversely all horizons are undersaturated with respect to amorphous silica. This suggests that under current soil conditions dissolution of amorphous silica coupled with calcite precipitation should be expected (Chapter 3) and indicates that dorbank formation is no longer in phase with current conditions. The mineral equilibria models further suggest that soils in Vaalputs are largely undersaturated with respected to palygorskite and sepiolite in few cases. The occurrence of calcite along palygorskite and sepiolite dominated regions in Vaalputs suggests a possible dissolution of the latter minerals by calcite precipitation as suggested by Mees (2010). This confirms the proposal of Singer *et al.* (1995) that palygorskite and sepiolite formation is out of phase with current soil forming conditions.

4.5. Conclusions

Clay fraction in the Vaalputs soils is largely dominated by palygorskite and sepiolite which suggest formation under arid climates. The occurrence of palygorskite and sepiolite minerals suggests that Vaalputs lies on a transition zone from coastal region to inland where sepiolite would be expected to occur along coastal regions and palygorskite to occur more inland. The occurrence of sepiolite and palygorskite in close association with calcite suggests replacement trough chemical precipitation. Undersaturated palygorskite and sepiolite suggests that environmental conditions no longer favour precipitation.

Soils of Vaalputs are undersaturated with respect to amorphous silica (dissolving) suggesting that current environmental conditions do not favour formation of dorbank horizons. Since dry climate prevails in Vaalputs the dissolving amorphous silica is not expected to leach through the profile. The percolation of dissolved silica through the profile is further prevented by the extremely indurated subsurface dorbank horizon which is impermeable to water. Therefore the minor amount of leached silica (during wet season) is deposited within the surface A horizon. Thus the A horizon becomes cemented in certain areas. All horizon of trench B(1,1) and C(1,5) are supersaturated with respect to barite as a result of oxic conditions today.

5. Chapter 5: The genesis and evolution of Vaalputs palaeosols and palaeoclimate implications

Vaalputs is situated in an arid region thus soil features occurring within this area are likely to have developed over the increasingly dry climate. These soils may even be preserved features from previous climate. From the top to the bottom of the B(1,1) and C(1,5) trench profiles various physical, mineralogical and chemical structures of macro and micro scales are encountered. The understanding of each feature has presented a unique opportunity to unravel environmental conditions that may have produced that specific occurrence. Combining all past events will further provide a tentative overview of palaeo-environments that shaped Vaalputs soils and sediments.

Geomorphic studies of southern Africa (Partridge & Maud, 1987) described the accumulation of sediments around Namaqualand region as litholic (rock derived) in origin rather than catenal (soil derived). The latter study identified and described three African erosion cycles which peaked during early Cretaceous to early Miocene (African cycle), early mid-Miocene to late Pliocene (Post-African cycle I) and late Pliocene to Holocene period (Post-African cycle II). According to (Partridge & Maud, 1987; Partridge *et al.*, 1996) sediments around Namaqualand were generated during the Post-African Surface I cycle.

Throughout this study, observations have been described from top to bottom however in order to infer palaeoenviroments (chronologically) that may have existed in Vaalputs when sediments were deposited and pedologically altered it is necessary to view horizons from bottom to top. With no real age constraints, palaeo-environmental deductions in this study are related to existing literature. During the Post-African Surface I cycle (Partridge *et al.*, 1996) large volumes of sediments were derived and deposited within the Namaqualand region. This is expressed by a thick sedimentary package that can be as deep as 16m below surface in Vaalputs.

The elevated Ba in the Vaalputs soils is likely to originate from the sediments since the sediments were generated from barite rich rocks of the Bushmanland terrane described by Stalder & Rozendaal (2005). Although less likely, it is also possible that Ba came from Ba-containing primary minerals within the sediments. The varying grain sizes within

sediments of Vaalputs suggests that coupled with commonly observed redoxymorphic mottles on subsurface horizons in Vaalputs suggest that these sediments were deposited under prevailing wet soil conditions. The waterlogged sediments in Vaalputs did not only produce soil mottles but also anoxic soil conditions. Barium was probably released under these reduced conditions from primary minerals and later concentrated within micro-nodules and micro-veins to precipitate out of solution as secondary barite when sediments began to dry out during the onset of arid climate.

The massive dorbank horizon is an extensive feature in Vaalputs. This horizon shows marked vertical desiccation cracks forming large polygonal peds which no other horizons show. This suggests a short lived desiccation event may have occurred soon after the deposition of soil material, which now makes up the massive dorbank horizon. This desiccation event may have produced oxic conditions especially along the developed cracks where secondary mineral barite permitted to precipitate out of solution.

The deposition of a fine textured platy dorbank horizon (mottle free) followed suggesting that sediments were deposited under a low energy system (Boggs, 2006). The occurrence of a stone-line above the fine textured platy dorbank horizon in Vaalputs suggests that the underlying horizon was at one stage overlain by a coarse texture horizon which was later eroded leaving a residual stone-line to accumulate.

According to Partridge & Maud (1987) and Partridge *et al.*, (1996) the climate of the western regions began to dry out during early Miocene period. This suggests that fairly soon after the sediments were deposited the western climate became increasingly arid. The sedimentation layers of the platy dorbank horizon of the current study attests to the fact that there was limited pedogenesis on these sediments prior to the onset of aridity. With continuous desiccation and increasing soil pH conditions amorphous silica, palygorskite and sepiolite began to accumulate within all soil horizons and along desiccation cracks of the massive dorbank horizon in Vaalputs. The composition of the solution chemistry suggests that none of these three phases are forming under current day conditions, thus the major dorbank units, palygorskite and sepiolite can be considered relic features.

Occasionally the topmost unconsolidated horizon is slightly indurated which suggests that silica cementation may still be active under current climate. The relatively low pH and low Na^+ content coupled with the cemented surface horizon may suggest that conditions conducive to dorbank formation have dramatically slowed down. These observations are

further supported by soil solution models which indicate that all horizons in Vaalputs are slightly under saturated with respect to amorphous silica.

The period and mechanism through which the surface horizon was deposited are indefinite however this horizon consists almost entirely of equigranular coarse sand texture which suggests residual accumulation through aeolian activities (McCarthy *et al.,* 1985). The soils in Vaalputs show an extreme accumulation of Ca whereas the sediment source is depleted in Ca. This depletion from source rock suggests input from external sources through possibly aeolian activities. The precipitation of calcite appears to occur at an expense of silica and palygorskite dissolution especially within the desiccation cracks of the massive dorbank horizon thus SiO_2 concentration is inversely proportional to those of CaO.

Soils of Vaalputs have been subject to increasingly arid climate however their dominant grain size distribution varies largely from fine sand to coarse sand and sometime pebbly. This indicates that a large portion of Vaalputs sediments were deposited through fluvial activities of relatively high energy, indicative of wet climate. The soil mottles within dorbank horizons in Vaalputs suggest that a vastly wet climate prevailed which produced anoxic conditions over extended periods when sediments were still unconsolidated. This probably resulted in the release and mobilisation of Ba from primary Ba-bearing minerals under low sulphate condition. The sedimentation layering observed on the subsurface platy dorbank horizon may have been preserved as a result of minimum pedogenesis under changing climate from wet to dry. The desiccation cracks of the subsurface massive dorbank horizon suggest that an increasingly arid climate occurred in Vaalputs. The preferential accumulation of secondary barite within micro-veins and micro-nodules suggests a redistribution of Ba and barite precipitation may have occurred under oxic soil conditions which are likely to have prevailed under progressively drying climate. The high concentrations of dust deposited Ca in Vaalputs indicates an accumulation under current arid climate. The observed occurrences of palygorskite, sepiolite and dorbank horizons are difficult to interpret, however, this suggests that marine fogs may have penetrated further inland than what occurs today resulting in Na deposition (required to raise pH and promote clay dispersion). Sodium and pH are relatively low under current day climate which suggests that most of the Na has been leached out, which may indicate a decrease marine influence.

A tentative timeline of Vaalputs events is given below (Figure 5.1). This addresses major events that may have led to the development of features observed with Vaalputs palaeosols.

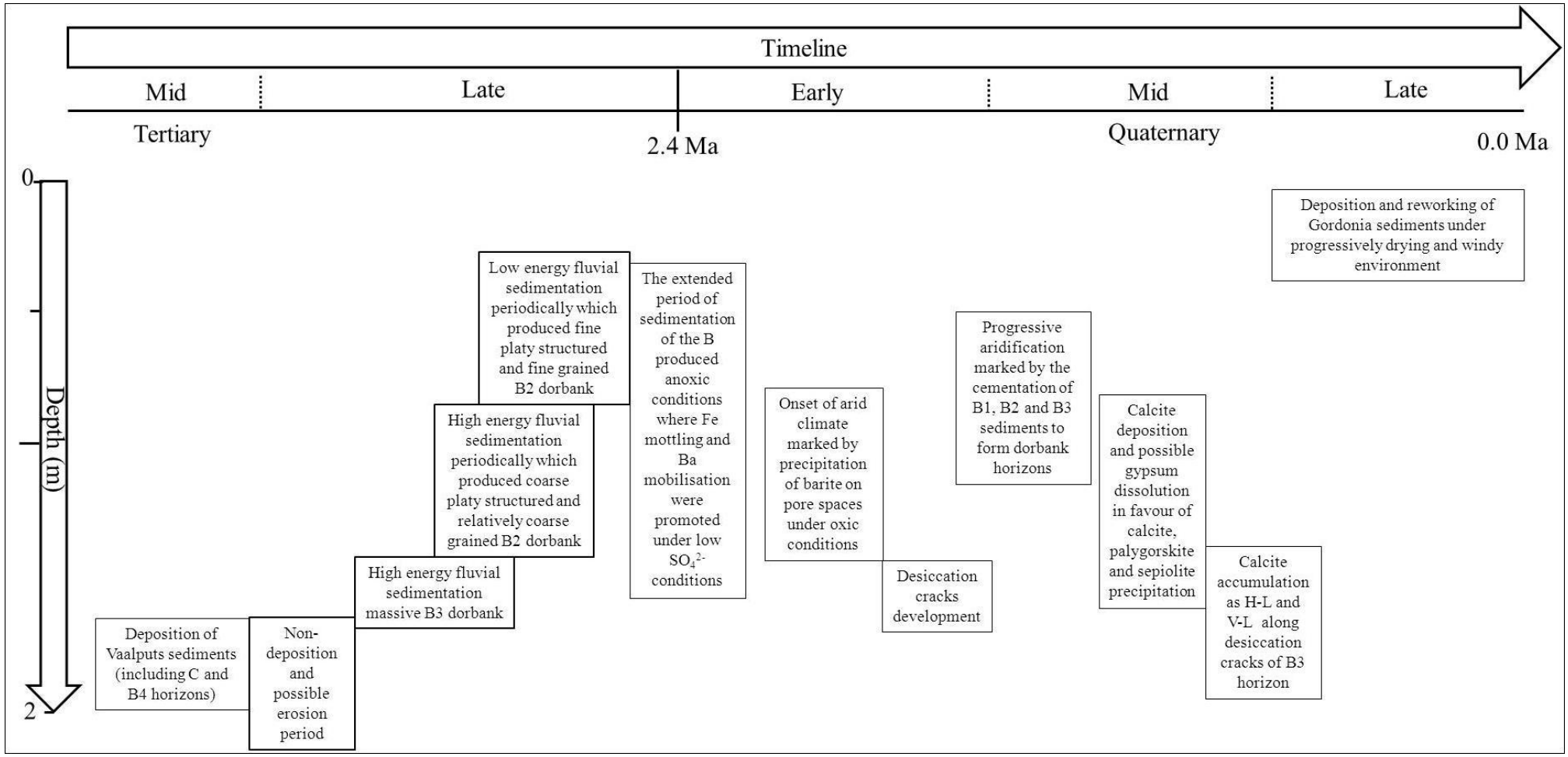

Figure 5.1: A tentative timeline of major events in Vaalputs given in depth (m) vs. time (Ma).

6. Chapter 6: Conclusions

- Petrographic analyses indicate that soil material in Vaalputs is generated from proximal local geology probably derived during the early Miocene to late Pliocene periods.
- The sediments were deposited through fluvial activities which appear to have persisted over extended periods and lead to waterlogging of sediments.
- The waterlogged sediments resulted to mottle formation under anoxic soil condition. However not all soil mottles in Vaalputs are palaeo-features; the accumulation of Mn and the gleying of Fe along root traces confirm current day formation which further suggest that redoxymorphic features have been occurring over a long time in Vaalputs.
- The pebble sized material accumulating as a stone-line (between the indurated B2 horizon below and the largely unconsolidated A horizon above) indicates formation from residual material of weathered sediments which the stone were hosted.
- Barium occurs in high concentrations throughout the subsurface horizons in Vaalputs which suggest input with host sediments. The mobilisation of barium is likely to have occurred under those anoxic conditions related to the formation of soil mottles. Barite precipitation coupled with the preservation of the layers of B2 horizon mark the abrupt climate transition from wet to dry.
- Progressive aridity in Vaalputs resulted to the formation of palygorskite and sepiolite and later promoted the formation dorbank horizons through the dissolution and precipitation of silica under high pH and high Na^+ concentrations. Although current day soil chemistry indicates that dorbank formation is limited in Vaalputs, the A horizon is occasionally indurated which confirms that silica cementation is still active possibly at reduced rates.
- The addition of Ca through dust deposition indicates arid condition where Ca precipitates as calcite while replacing palygorskite and sepiolite and promoting further dissolution and mobilisation of silica. Mineral equilibration models also suggest that all horizons are undersaturated with respect to amorphous silica. This further indicates that the subsurface dorbank horizons are relic features whereas the surface horizon marks a current day formation of dorbank.

Further work

- Vaalputs palaeosols are highly complex soil systems to fully understand which features are relics and which are current day formations, further studies are required. The study has described numerous features and may serve as a suitable starting point.
- One of the biggest challenges in Vaalputs is that there is a high degree of spatial variation therefore both large and small scale studies are necessary.
- Precise dates of sediment depositions are also necessary for further palaeoclimate reconstruction in Vaalputs.

7. References

Achyuthan, H., 2003. Petrologic analysis and geochemistry of the Late Neogene-Early Quaternary hardpan calcretes of Western Rajasthan, India. Quaternary International, 106-107:3-10.

Albat, H., 1984. The Proterozoic Granulite Facies Terrane Around Kliprand, Namaqualand Metamorphic Complex. University of Cape Town, Dept. of Geology, Chamber of Mines Precambrian Research Unit, [Cape Town], pp1 - 50.

Alberta, A.E., Canadian Association of Petroleum,Producers Staff, Environmental, A. and Canadian Association of, P.P., 2009. Soil Remediation Guidelines for Barite: Environmental Health and Human Health. Alberta Environmental Farm Plan, pp1 - 44.

Andreoli, M.A.G., Hart, R.J., Ashwal, L.D. and Coetzee, H., 2006. Correlations between U, Th content and metamorphic grade in the Western Namaqualand belt, South Africa, with Implications for radioactive heating of the crust. J. Petrol., 47:1095-1118.

Bai Haifeng, Li Pinfang, Zhang Biao and Eneji, A.E., 2011. The illuviation of CaCO3 and the deposition of clay in cal-ustic Isohumisols. Electronics, Communications and Control (ICECC), 2011 International Conference on. , pp. 2359-2362.

Bettenay, E. and Churchward, H.M., 1974. Morphology and Stratigraphic Relationships of the Wiluna Hardpan in arid Western Australia. Journal of the Geological Society of Australia, 21:73-80.

Blank, R.R. and Fosberg, M.A., 1991. Duripans of the Owyhee Plateau region of Idaho: genesis of opal and sepiolite. Soil Sci., 152:116-133.

Boggs, S., 2006. Principles of Sedimentology and Stratigraphy. Upper Saddle River, N.J. Pearson Prentice Hall, Upper Saddle River, N.J. pp - 75, 112.

Bolze, C.E., Malone, P.G. and Smith, M.J., 1974. Microbial mobilization of barite. Chem. Geol., 13:141-143.

Brandt, D., 1998. The Recent Morpho-Tectonic History of the Vaalputs Radioactive Waste Depository and Environs. (PhD(Geol))--University of the Witwatersrand. pp 134 - 152.

Brandt, D., Andreoli, M.A.G. and McCarthy, T.S., 2005. The late Mesozoic palaeosoils and Cenozoic fluvial deposits at Vaalputs, Namaqualand, South Africa: Possible depositional mechanisms and their bearing on the evolution of the continental margin. South African Journal of Geology, 108:271-284.

Brandt, D., Andreoli, M.A.G. and McCarthy, T.S., 2003. Mesozoic fluvial deposits on a rifted continental margin near Vaalputs, Namaqualand, South Africa. South African Journal of Geology, 106:11-16.

Braucher, R., Lima, C.V., Bourlés, D.L., Gaspar, J.C. and Assad, M.L.L., 2004. Stone-line formation processes documented by in situ-produced 10Be distribution, Jardim River basin, DF, Brazil. Earth Planet. Sci. Lett., 222:645-651.

Brewer, R., 1972. The basis of interpretation of soil micromorphological data. Geoderma, 8:81-94.

Brock, A.L. and Buck, B.J., 2005. A new formation process for calcic pendants from Pahranagat Valley, Nevada, USA, and implication for dating Quaternary landforms. Quatern. Res., 63:359-367.

Brock-Hon, A.L., Robins, C.R. and Buck, B.J., 2012. Micromorphological investigation of pedogenic barite in Mormon Mesa petrocalcic horizons, Nevada USA: Implication for genesis. Geoderma, 179–180:1-8.

Bronger, A., Bruhn-Lobin, N. and Heinkele, T., 1993. Micromorphology of paleosols - genetic and paleoenvironmental deductions: Case studies from central China, south India, NW Morocco and the Great Plains of the USA. In: Anonymous Developments in Soil Science. Elsevier, pp. 187-206.

Brown, D.J., McSweeney, K. and Helmke, P.A., 2004. Statistical, geochemical, and morphological analyses of stone line formation in Uganda. Geomorphology, 62:217-237.

Callen, R.A., 1984. Clays of the Palygorskite-Sepiolite Group: Depositional Environment, Age and Distribution. Developments in Sedimentology, 37:1-37.

Chadwick, O.A., Hendricks, D.M. and Nettleton, W.D., 1987a. Silica in duric soils: I. A depositional model. Soil Sci. Soc. Am. J., 51:975-982.

Chadwick, O.A., Hendricks, D.M. and Nettleton, W.D., 1987b. Silica in duric soils: II. Mineralogy. Soil Sci. Soc. Am. J., 51:982-985.

Chartres, C.J., 1985. A preliminary investigation of hardpan horizons in north-west New South Wales. Aust. J. Soil Res., 23:325-337.

Chartres, C.J. and Fitzgerald, J.D., 1990. Properties of Siliceous Cements in some Australian Soils and Saprolites. Developments in Soil Science, 19:199-205.

Conradie, J.A. and Schoch, A.E., 1986. Petrographical characteristics of the koperberg suite, South Africa — an analogy to massif-type anorthosites? Precambrian Res., 31:157-188.

Cowling, R.M., Esler, K.J. and Rundel, P.W., 1999. Namaqualand, South Africa: An Overview of a Unique Winter-Rainfall Desert Ecosystem. Plant Ecol., 142:3-21.

Currie, L.A., 1968. Limits for qualitative detection and quantitative determination: Application to radiochemistry. Anal. Chem., 40:586-593.

Daley, B., 1967. Pseudomorphs after gypsum from the Bembridge Marls. Proceedings of the Geologists' Association, 78:319-IN10.

Desmet, P.G., 2007. Namaqualand—A brief overview of the physical and floristic environment. Journal of Arid Environments, 70: 570 - 587.

Drees, L.R. and Wilding, L.P., 1987. Micromorphic record and interpretations of carbonate forms in the Rolling Plains of Texas. Geoderma, 40:157-175.

Duchesne, J., Auwera, J.V., Liégeois, J., Barton, E.S. and Clifford, T.N., 2007. Geochemical constraints of the petrogenesis of the O'okiep Koperberg Suite and granitic plutons in Namaqualand, South Africa: A crustal source in Namaquan (Grenville) times. Precambrian Res., 153:116-142.

Durand, N., Gunnell, Y., Curmi, P. and Ahmad, S.M., 2006. Pathways of calcrete development on weathered silicate rocks in Tamil Nadu, India: Mineralogy, chemistry and paleoenvironmental implications. Sediment. Geol., 192:1-18.

Ellis, F., 1988. Die gronde van die Karoo. (Ph.D. Agric.)--Universiteit van Stellenbosch, 1988.

Ellis, F. and Schloms, B.H.A., 1982. A note on the dorbanks (douripans) of South Africa. Palaeoecology of Africa, vol.15.Proc.6th conference Southern African Society for Quaternary Research, Pretoria, 1981, :149-157.

Fey, M.V., 2010. Silicic soils in: soils of south africa. In: Anonymous Soils of South Africa: Their Distribution, Properties, Classification, Genesis, use and Environmental Significance. Cambridge University Press, Cape Town, pp. 53-54.

Francis, M.L., Fey, M.V., Prinsloo, H.P., Ellis, F., Mills, A.J. and Medinski, T.V., 2007. Soils of Namaqualand: Compensations for aridity. J. Arid Environ., 70:588-603.

Francis, M.L., 2008. Soil formation on the Namaqualand coastal plain. Dissertation (PhD(Agric))--University of Stellenbosch, 2008. pp 5 - 43, 90 - 114, 198 - 231.

Gee, G.W. and Bauder, J.W., 1986. Particle-size Analysis: in Methods of Soil Analysis Part 1. A. Klute (edi.), Soil Science Society of America Book Series 5, Madison, Wisconsin, USA. pp - 383-411.

Gile, L.H., Peterson, F.F. and Grossman, R.B., 1966. Morphological and Genetic Sequences of Carbonate Accumulation in Desert Soils. Soil Sci., 101:347-360.

Glaser, B. and Zech, W., 2005. Reconstruction of climate and landscape changes in a high mountain lake catchment in the Gorkha Himal, Nepal during the Late Glacial and Holocene as deduced from radiocarbon and compound-specific stable isotope analysis of terrestrial, aquatic and microbial biomarkers. Org. Geochem., 36:1086-1098.

Goss, D.W., Smith, S.J. and Stewart, B.A., 1973. Movement of added clay through calcareous materials. Geoderma, 9:97-103.

Gunal, H. and Ransom, M.D., 2006. Clay illuviation and calcium carbonate accumulation along a precipitation gradient in Kansas. Catena, 68:59-69.

Hansen, R.N., (unpublished data). Non-parametric statistical analysis and spatial distribution of the regional geochemical data of the Okiep Copper District, Namaqualand, South Africa: Implications for anthropogenic influence and risk assessment. pp 1 - 30.

Hoffman, J.W. and De Beer, F.C., 2012. Characteristics of the Micro-Focus X-ray Tomography Facility (MIXRAD) at Necsa in South Africa. 18th World Conference on Nondestructive Testing. Durban, South Africa.

Pretorius H. C.F., 2012. The content and behaviour of natural radionuclides in basement-hosted groundwater from Vaalputs, Namaqualand, South Africa. Dissertation (MSc(Geology). University of Free State. pp1 - 39.

Johnson, D.L. and Balek, C.L., 1991. The genesis of Quaternary landscapes with stone-lines. Physical Geography, 12:385-395.

Johnson, D.L., 1989. Subsurface Stone Lines, Stone Zones, Artifact-Manuport Layers, and Biomantles Produced by Bioturbation via Pocket Gophers (Thomomys Bottae). American Antiquity, 54:pp. 370-389.

Kent, L.E. and Gribnitz, K.H. (1985). Freshwater shell deposits in the northwestern Cape Province:further evidence for a widespread wet phase during the late Pleistocene in southern Africa. South African Journal of Science, 81, 361-370.

Khormali, F., Abtahi, A., Mahmoodi, S. and Stoops, G., 2003. Argillic horizon development in calcareous soils of arid and semiarid regions of southern Iran. Catena, 53:273-301.

Kleber, A., 2000. Compound soil horizons with mixed calcic and argillic properties - Examples from the northern Great Basin, USA. Catena, 41:111-131.

Konstantin E., P., 2002. Pedogenic carbonate cutans on clasts in soils as a record of history of grassland ecosystems. Palaeogeogr. , Palaeoclimatol. , Palaeoecol., 177:199-214.

Land Type Survey Staff, 1989

Lacassie, J.P., McClung, C.R., Bailie, R.H., Gutzmer, J. and Ruiz-Del-Solar, J., 2006. Geochemical patterns of schists from the Bushmanland Group: An artificial neural networks approach. J. Geochem. Explor., 91:81-98.

Le Roux, P.A.L., Hensley, M. and Van Huyssteen, C.W., 2010. Advances in pedology in South Africa. South African Journal of Plant and Soil, 27:1-8.

Lynn, W.C., Tu, H.Y. and Franzmeier, D.P., 1971. Authigenic Barite in Soils1. Soil Sci. Soc. Am. J., 35:160-161.

Majodina, T.O., 2010. Geochemical characterisation of paleosols at Vaalputs. Dissertation (Hons(Geol))--University of Stellenbosch, pp1 - 38.

McCarthy, P.J., Martini, I.P. and Leckie, D.A., 1998. Use of micromorphology for palaeoenvironmental interpretation of complex alluvial palaeosols: an example from the Mill Creek Formation (Albian), southwestern Alberta, Canada. Palaeogeogr. , Palaeoclimatol. , Palaeoecol., 143:87-110.

McCarthy, T.S., Moon, B.P. and Levin, M., 1985. Geomorphology of the Western Bushmanland Plateau, Namaqualand, South Africa. South African Geographical Journal, 67:160-178.

Mees, F., 2010. 22 - Authigenic Silicate Minerals – Sepiolite-Palygorskite, Zeolites and Sodium Silicates. In: Anonymous Interpretation of Micromorphological Features of Soils and Regoliths. Elsevier, Amsterdam, pp. 497-520.

Morrás, H., Moretti, L., Píccolo, G. and Zech, W., 2005. New Hypotheses and Results About the Origin of Stonelines and Subsurface Structured Horizons in Ferrallitic Soils of Misiones, Argentina. Geophysical Research Abstracts, 7.

Mortlock, R.A. and Froelich, P.N., 1989. A simple method for the rapid determination of biogenic opal in pelagic marine sediments. Deep Sea Research Part A.Oceanographic Research Papers, 36:1415-1426.

Nash, D.J. and Shaw, P.A., 1998. Silica and carbonate relationships in silcrete-calcrete intergrade duricrusts from the Kalahari of Botswana and Namibia. J. Afr. Earth Sci., 27:11-25.

Norton, L.D., 1993. Micromorphology of silica cementation in soils. In: Anonymous Developments in Soil Science. Elsevier, pp. 811-824.

Pal, D.K., Srivastava, P. and Bhattacharyya, T., 2003. Clay illuviation in calcareous soils of the semiarid part of the Indo-Gangetic Plains, India. Geoderma, 115:177-192.

Patridge, T.C., de Villiers, J.M., Fitzpatrick, R.W. and Maud, R.R., 1996. Soil-Lanhscape-Climate Relations in Southern Africa. Catena (in press), :1-24.

Patridge, T.C. and Maud, R.R., 1987. Geomorphic evolution of Southern Africa since the mesozoic. South African Journal of Geology, 90:179-208.

Pickford, M., Eisenmann, V. and Senut, B., 1999. Timing of landscape development and calcrete genesis in northern Namaqualand, South Africa. S. Afr. J. Sci., 95:357-359.

Podwojewski, P., 1995. The occurrence and interpretation of carbonate and sulfate minerals in a sequence of Vertisols in New Caledonia. Geoderma, 65:223-248.

Post, J.L. and Crawford, S., 2007. Varied forms of palygorskite and sepiolite from different geologic systems. Appl. Clay. Sci., 36:232-244.

Prozesky, V.M., Przybylowicz, W.J., van Achterbergh, E., Churms, C.L., Pineda, C.A., Springhorn, K.A., Pilcher, J.V., Ryan, C.G., Kritzinger, J., Schmitt, H. and Swart, T., 1995. The NAC nuclear microprobe facility. Nuclear Inst.and Methods in Physics Research, B, 104:36-42.

Przybylowicz, W.J., Mesjasz-Przybylowicz, J., Pineda, C.A., Churms, C.L., Springhorn, K.A. and Prozesky, V.M., 1999. Biological Applications of the NAC Nuclear Microprobe. X-Ray Spectrom., 28:237-243.

Ransom, M.D. and Bidwell, O.W., 1990. Clay Movement and Carbonate Accumulation in Ustolls of Central Kansas, U.S.A. Developments in Soil Science, 19:417-423.

Reheis, M.C., 1987. Climatic implications of alternating clay and carbonate formation in semiarid soils of South-Central Montana. Quatern. Res., 27:270-282.

Reid, D.L., Welke, H.J., Erlank, A.J. and Betton, P.J., 1987. Composition, age and tectonic setting of amphibolites in the central Bushmanland Group, Western Namaqua Province, southern Africa. Precambrian Res., 36:99-126.

Retallack, G.J., 2001. Soils of the Past : An Introduction to Paleopedology. Boston, Mass. : Unwin Hyman, Boston, Mass.

RSA Soil Classification Working Group, 1991.

Ruhe, R.V., 1959. Stone lines in Soils. Soil Sci., 87:223-231.

Ruhe, R.V., 1956. Geomorphic Surfaces and the Nature of Soils. Soil Sci., 82:441-456.

Ryan, C.G., 2000. Quantitative trace element imaging using PIXE and the nuclear microprobe. Int J Imaging Syst Technol, 11:219-230.

Ryan, C.G., Cousens, D.R., Sie, S.H. and Griffin, W.L., 1990a. Quantitative analysis of PIXE spectra in geoscience applications. Nuclear Inst.and Methods in Physics Research, B, 49:271-276.

Ryan, C.G., Cousens, D.R., Sie, S.H., Griffin, W.L., Suter, G.F. and Clayton, E., 1990b. Quantitative pixe microanalysis of geological matemal using the CSIRO proton microprobe. Nuclear Instruments and Methods in Physics Research Section B: Beam Interactions with Materials and Atoms, 47:55-71.

Ryan, C.G. and Jamieson, D.N., 1993. Dynamic analysis: on-line quantitative PIXE microanalysis and its use in overlap-resolved elemental mapping. Nuclear Inst.and Methods in Physics Research, B, 77:203-214.

Ryan, C.G., Jamieson, D.N., Churms, C.L. and Pilcher, J.V., 1995. A new method for on-line true-elemental imaging using PIXE and the proton microprobe. Nuclear Inst.and Methods in Physics Research, B, 104:157-165.

Schaetzl, R.J., 1957-, 2005. Soils : Genesis and Geomorphology. New York : Cambridge University Press, New York.

Shankar, N. and Achyuthan, H., 2007. Genesis of calcic and petrocalcic horizons from Coimbatore, Tamil Nadu: Micromorphology and geochemical studies. Quaternary International, 175:140-154.

Singer, A., 1980. The paleoclimatic interpretation of clay minerals in soils and weathering profiles. Earth Science Reviews, 15:303-326.

Singer, A., Ganor, E., Dultz, S. and Fischer, W., 2003. Dust deposition over the Dead Sea. J. Arid Environ., 53:41-59.

Singer, A., Kirsten, W. and Bühmann, C., 1995. Fibrous clay minerals in the soils of Namaqualand, South Africa: characteristics and formation. Geoderma, 66:43-70.

Stalder, M. and Rozendaal, A., 2005. Distribution and geochemical characteristics of barite and barium-rich rocks associated with the Broken Hill-type Gamsberg Zn-Pb deposit, Namaqua Province, South Africa. South African Journal of Geology, 108:35-50.

Stoops, G.J. and Zavaleta, A., 1978. Micromorphological evidence of barite neoformation in soils. Geoderma, 20:63-70.

Sullivan, L.A., 1993. Micromorphology and composition of silica accumulations in a hardpan. In: Anonymous Developments in Soil Science. Elsevier, pp. 845-853.

Sullivan, L.A. and Koppi, A.J., 1995. Micromorphology of authigenic celestobarite in a duripan from central Australia. Geoderma, 64:357-361.

Sullivan, L.A. and Koppi, A.J., 1993. Barite pseudomorphs after lenticular gypsum in a buried soil from central Australia. Aust. J. Soil Res., 31:393-396.

van Achterbergh, E., Ryan, C.G., Gurney, J.J. and Le Roex, A.P., 1995. PIXE profiling, imaging and analysis using the NAC proton microprobe: Unraveling mantle eclogites. Nuclear Inst.and Methods in Physics Research, B, 104:415-426.

Appendix 1

UNIVERSITEIT STELLENBOSCH UNIVERSITY

ENVIRONMENTAL GEOCHEMISTRY

Geochemical characterisation of paleaosols in Vaalputs

Honours Thesis 2010

STUDENT: MAJODINA OLWETHU 15177947

SUPERVISOR: DR. CLARKE CATHY

Abstract

Vaalputs radioactive waste disposal facility is situated in an arid region of Namaqualand that is characterised by low precipitation and high evaporation which is evident from the evaporative minerals such as gypsum, calcite, palygorskite that may be found as precipitates on the soils of the area. The radioactive waste is disposed into trenches excavated of 8 metres deep in canisters and then buried under the thick soil package. This site consists of a network of anomalous features such Barium-riched veins, makondos, calcrete nuggets (which may look like brecciated rocks when viewed from the trench). All of these features are hosted on the dorbank horizon which is largely cemented by silica and maybe calcite as a secondary cementing agent. These dorbank hosted veins do not only have high barium (Ba) concentration but they also have high trace metal concentrations compared to their surround dorbank matrix. The Ba concentrations measured from the C02 trench are as high as 8316 ppm.

Table of Contents

List of Figures

1. INTRODUCTION

1.1. Overview

In the mid 1970s, South Africa planned its first nuclear power station; as a result, the whole initiative introduced a need for a radioactive waste disposal facility. For a suitable waste disposal site to be found, strict site specific criteria had to be formulated. This included; low rainfall and extremely high evaporation, low agricultural, mining and economic growth potential, distance from international borders, low population density, deep water-table, stable seismic conditions, stable surface and groundwater conditions, minimal impact on surrounding nature reserve or ecologically sensitive systems and finally, the site must have thick clay-rich soils and sediments of low hydraulic conductivities. The search for a suitable waste disposal site commenced in the early 1980s and finally ended in the mid 1980s with the identification of the Vaalputs area which today occupies an area of about 10 000 ha which lies approximately 100 km SE of Springbok in the Northern Cape Province (Figure 1) (Logue, 2010). The first low and intermediate radioactive waste load was scheduled for delivery in the late 1986. Currently, the waste is disposed in trenches excavated to a depth of 8 m. The excavation of trenches and a large number of boreholes have revealed a complex system of colluvial sediments (Vaalputs and Dasdap Formations) which have been pedologically altered since the late Cretaceous, over a period of ca. 67 million years (Logue, 2010).

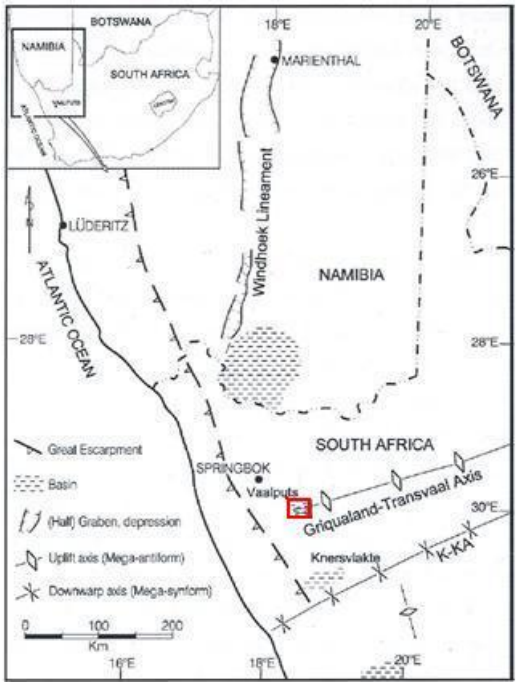

Figure 2: Location of the Vaalputs disposal site (inside the red square) within the Northern Cape Province including the location of regional depressions, basins, lineaments, the Great Escarpment and the Griqualand- Transvaal Axis of uplift (taken from Brandt et al., 2005; Logue, 2010).

The prolonged sedimentation of colluvial and fluvial deposition, followed by an extended period of paedogenesis, under varying climate conditions have resulted in numerous anomalous pedological features which include; 1) shear-like fractures on slightly consolidated sediments which generally appear to resemble displacement at shallow dipping angles,

2) horizontally and vertically banded barite-rich veins cutting through the petroduric (International Union of Soil Science (IUSS) classification system), also known as dorbank (South African classification system). In many occurrences, the barium-rich vein network system appears in an organised periodic spacing of about 40cm, in both horizontal and vertical directions (Figure 2a).

a

b

c

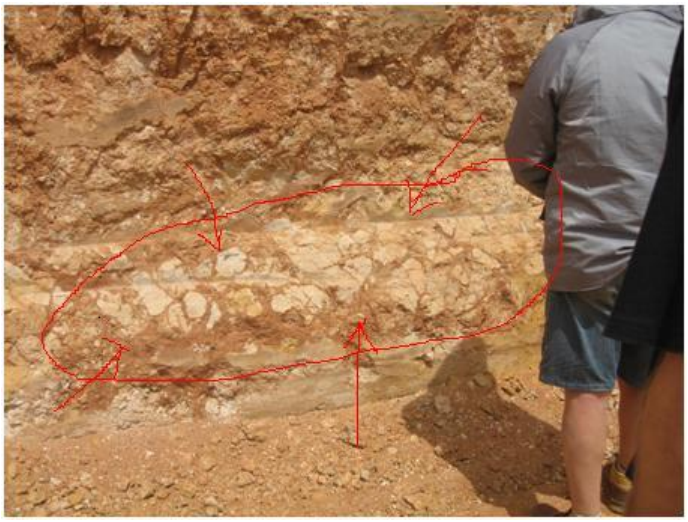

Figure 3: Some of the anomalous pedological features that are exposed at the waste disposal trenches in Vaalputs; (a) barium-rch veins hosted in dorbank matrix propagating in horizontal and vertical directions in trench B11 (b) Makondo feature on the dorbank horizon covered by younger and unconsolidated red sand of Gordonia Formation (c) Breccia like features (nodules) on soft soil sediments exposed on the walls of the domestic waste trench.

3) sporadic Makondo features (funnel shaped feature) on the dorbank covered by younger, unconsolidated sediments of the Gordonia sub-formation (Figure 2b).

4) the excavation of the domestic trench, situated 1500m south-east of the B trenches, has also revealed very prominent brecciated rock-like features on soft sediment (Figure 2c).

All of the anomalous sedimentary features reside on the Vaalputs formation which is suspected to have been deposited about 15000 years ago (Logue A, 2010).

Gaining an understanding of the physico-chemical that resulted in the formation of these anomalous soils is of twofold importance. Firstly, an understanding of geochemical processes that have occurred or are occurring in the soil are important for the provision of input data for modelling the resilience of nuclear waste canisters in these soils over time, as well as the rate of dispersion of radionuclides and the chemical interaction that may occur should the radionuclides be released to the soils. Secondly, understanding the formation of these features provides an opportunity to gain insights into the past climates that have shaped the palaeosols at Vaalputs. Whilst many soils in arid regions are considered geochemically inert, it is still important to understand the geochemical processes occurring especially during sporadic rainfall events, when highly soluble evaporite minerals may come into solution.

1.2. Aims and Objectives

The aim of this study is to characterize the chemical and mineralogical composition of the soil. To also determine the chemical cementing agents within the indurated soil horizons and features especially within the vein materials.

Based on the geochemical and mineralogical data, postulate a mechanism for the formation of the Barium-rich veins present in the upper dorbank horizons.

1.3. Regional Setting

The Vaalputs nuclear waste disposal site is located within the Bushmanland metamorphic Subprovince, approximately at 1000m above mean sea level within 30°08′ south and 18°53′ east (McCarthy et al., 1985 and Brandt et al., 2005 and Logue, 2010). To the west of the Vaalputs site lies the great escarpment (approximately 1200 to 1700 metres above mean sea level) that runs parallel, north-south, to the west coast of South Africa giving rise to a landward gently sloping surface. "Within the vicinity of the escarpment, prolonged fluvial activities have vastly exposed a variety of granitic-gneiss rocks, including the regional basement granite" (Andreoli et al., 2006; Eglington, 2006 and Logue 2010).

The site itself is riddled with NNE-SSW trending linear sand dunes with low amplitudes (Logue, 2010 and Brandt, 1998) (Figure 10 in the appendix B section).

To the east of the Vaalputs site, the surface is relatively flat and the dominating surface geology is of sedimentary origin such as sand cover, mud covered pans, drainage flats, pan-margin deposits, deflated gravel pavements and duricrusts (Brandt, 1998 and Logue, 2010).

1.4. Regional Geology and Soils

At Vaalputs waste disposal site, the stratigraphy is largely dominated by thick unconsolidated sedimentary package that may reach depths of approximately 17 metres from surface (Logue, 2010). To the west of Vaalputs waste site where the surface elevation increases towards the great escarpment, extensive basement granite is exposed due to intensive fluvial incision (Logue 2010). The basement lithology is dominated by the Namaqualand metamorphic complex which is subdivided into numerous formations such as Augen gneiss of Little Namaqualand Suite (~1200 Ma), various granitiods of Southern Megacrystic Suite dated at ~1060 Ma, the charnokites of Kliprand Charnokitic Suite of ~1060 to 1030 Ma and finally the dolerites, norites, hypersthernites and Enderbites of Koperberg Suite dated at ~1030 Ma (Logue, 2010; Andreoli et al. 2006) The basement granitic rock formation is (unconformably) overlain by a thick package of sedimentary units dated from Mesozoic to Cenozoic age (Brandt, 1998). The unit found stratigraphically overlying the basement granite is the Dasdap formation, which consists mainly of conglomerates and immature cross-bedded arkosic grits of ~67 Ma. Overlying the Dasdap is the White Clay formation that is largely composed of grey-white sandy to gritty clay, weathered basement and siliceous sandstones. The Vaalputs formation which are largely

composed of solid hard cemented sediments of silcrete (~15000 years ago) and calcrete upon which all of the above mentioned anomalies exist. The top most unit is an unconsolidated red sand of Gordonia formation (Figure 3and 4) (Brandt, 1998; Andreoli et al. 2006; and Logue 2010).

There is limited information on the soils of the Bushman land region. According to the Land Type survey maps (Land Type Survey Staff, 1987) the soils in the Vaalputs region are classified as deep (>300mm) red soils, with a high base status. A recent study by Francis (2008) looked at the mineralogy, morphology and paedogenesis of soils on the Namaqualand coastal plain.

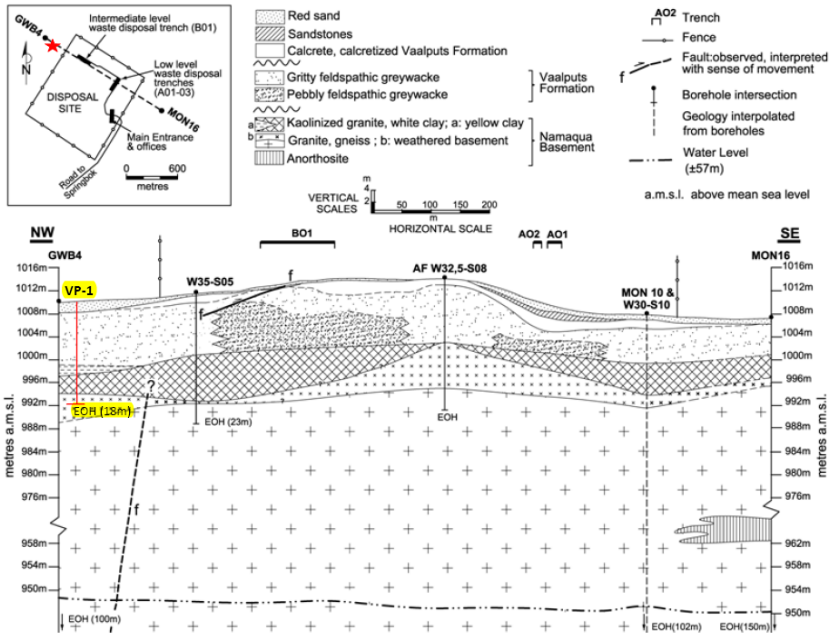

Figure 4: Simplified geological cross section of Vaalputs (taken from Logue, 2010)

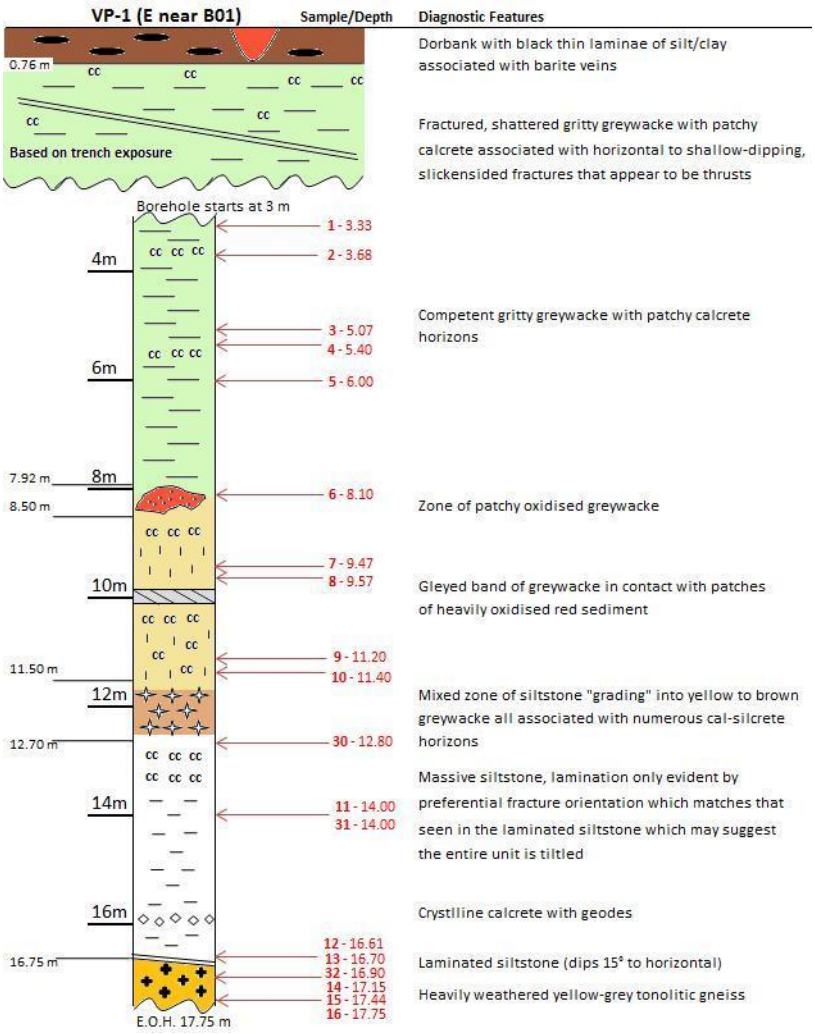

Figure 5: Simplified strigraphic column constructed from logging of drill core of borehole VP-1 at Vaalputs (taken from Logue, 2010)

2. MATERIALS AND METHODS

2.1. Sample collection

A soil profile from trench C02 of the NECSA waste disposal site (Figure 5) was identified as a representative profile displaying the typical vein systems. Despite the C02 trench being excavated to a depth of 8 m only the top 4 m were sampled due to limited access to the deeper sediments. The profile was classified following the South African Soil Classification system (Soil Classification Working Group, 1991). The complexity of the soil profile made classification difficult. Horizons were selected for sampling based on morphology as well as the degree of Dorbank consolidation. Samples were collected from matrix and vein materials within the Dorbank as well as the unconsolidated sediments to a depth of 3.9 m. A similar profile from the nearby B11 trench was also classified and sampled. Samples were collected from each horizon using a spade and a geological hammer and they were stored in plastic bags for transporting. Figure 3 shows a simplified geology across trench B01, east of trench B11. Figure 4 is a simplified core data derived from borehole VP-1 shown on figure 3.

To determine which soil profile (B11 or CO2) would be used for detailed chemical analysis, the vein material from each profile was analysed for Ba using X-ray Fluorescence (XRF). The C02 vein material showed the highest Ba concentration and thus trench C02 profile was used for detailed chemical analysis. The vein material from B11 was also used for selected for further analyses. Figure 5 is a trench map that illustrates the distribution of trenches and the sampled trenches, B11 and C02.

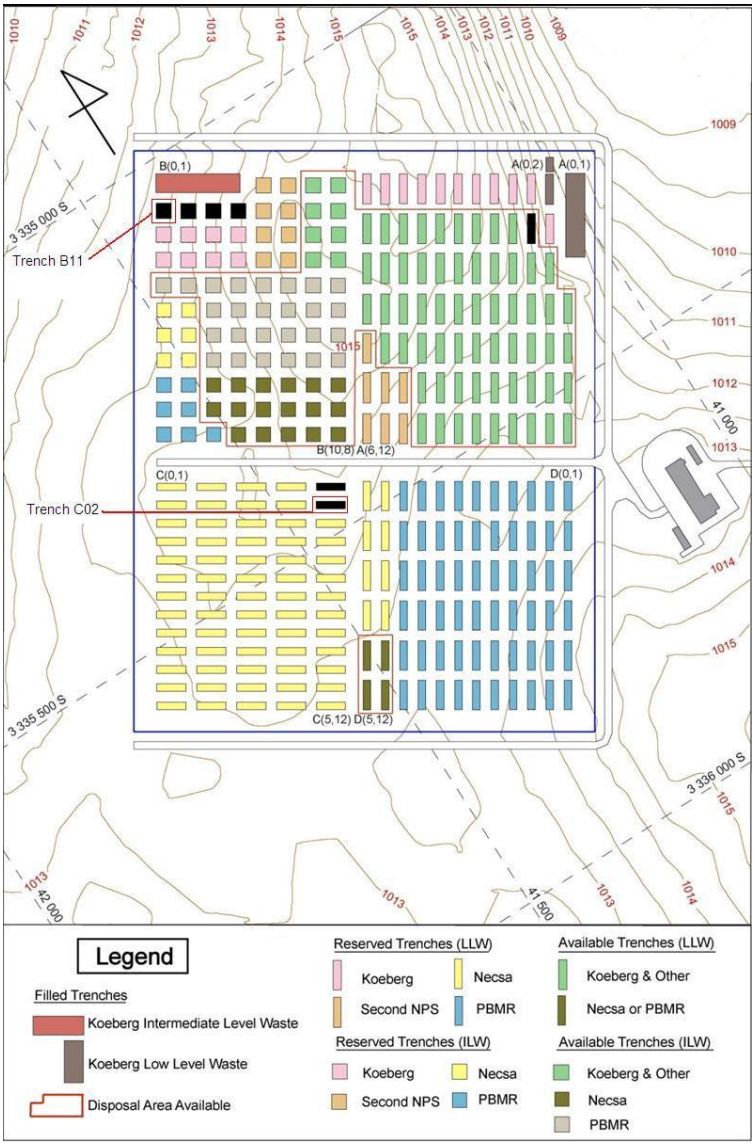

Figure 6: Trench map in Vaalputs and sampled trenches

2.2. Laboratory Methods

Major and trace element composition of the soil samples were determined by XRF analysis using an Axios from PANalytical with a 2.4kWatt Rh X-ray Tube. Samples were prepared by milling the samples to a fine powder using a tungsten mill.

Saturated paste extracts were prepared with the milled soil samples. Depending on the amount of sample available, about 250g of milled soil was added into a 500ml beaker and deionised water was slowly and carefully added while stirring with glass rod until the mixture became a paste. Using the parafilm, the beakers were sealed off and left for 18 hours to allow the water to equilibrate with the soil. The saturated paste water was extracted over 90 minutes using a Büchner funnel.

The saturated paste extracts were analysed for major anions using ion chromatography Dionex DX-120 IC instrument and metals using Varian Agilent 7700 ICP-MS, respectively. Dissolved inorganic silica was measured, using a modified molybdated-blue spectrophotometry (Land and Parsons, 1968). Alkalinity was determined by potentiometric titration using 0.001M HCl. The pH and EC were measured on the paste extracts as well as in 1:2.5 soil-water solutions.

Slaking tests were devised to distinguish between samples of calcrete, ferricrete and silcrete. This was performed by submerging a fragment of cemented material (B1, B1-2, B2, C1-2 and B11) in 5M HCl and, another fragment of the same material in 6M NaOH solution and ran simultaneously for 14 days. For samples that did not slake, alternate HCl and NaOH treatments were applied. Samples that did not slake in NaOH at room temperature were heated to 40 ℃.

Sample preparation for x-ray diffraction (XRD) analysis was also done on the same milled horizon material. Clay separates (<2µm) were prepared by dispersion followed by sedimentation onto a ceramic tile. Briefly, 30g soil material was suspended in 300 mL deionised (DI) water. The pH of the suspension was raised to pH 9.5 using 0.5 M Na_2CO_3. Soils were sonicated for 5 minutes in an ultrasonic bath and stirred rigorously before being left to settle for 4 hours. The suspended material was removed from the top 5 cm and placed in two 50 centrifuge tubes. The clay suspensions were then washed and flocculated with either $MgCl_2$ or KCl. After washing thoroughly with DI and ethanol to remove excess chlorides, the Mg and K saturated clay extracts were sedimented on ceramic tiles. Powder samples from the B11 and B1-2 Ba-rich veins were prepared by back pressing the powder in an aluminium sample holder. All patterns were run on a PANalytical X'Pert PRO MPD that uses Cu Kα radiation.

Data modelling was performed from equilibrated saturated paste extracts on phreeqc interactive, version 2.17.4468 using *phreeq.data* database files. Phreeqc models were designed to produce results that would be used to compare Saturation Indices (SI) of possible neoformation mineral for all samples.

3. RESULTS

Two trench profiles (C02 and B11) were sampled for this study. Due to clearer representation of different pedosedimentary horizons and extreme concentration of element Ba detected from XRF analysis, the trench C02 profile was selected for further detailed chemical analysis. Samples A, B1, B1-2, B2, C1, C1-2 and C2 were collected from trench C02. For the purposes comparison, the vein material from trench B11 profile was also sampled and analysed (Table 1).

3.1. Soil Characteristics

The top soil is unconsolidated and may consist of few roots. It commonly has a fine to medium grained sandy loam texture and is classified as 7.5YR 5/8 on the Munsell colour chart with massive apedal structure. The dorbank is massive and is largely segmented by Ba-rich veins both in the vertical and horizontal directions into blocks of similar size. The grain size is mainly of sand type although as may be expected, variations occur. Down the profile, the hard dorbank grades into less cemented soil package, generally referred to as greywacke in Vaalputs (Lounge, 2010). The dorbank hosted Ba-rich veins grade into calcite veins (Table 1, Figure 2a and Figure 6). The soils become less consolidated with decline in elevation along the C02 trench profile. The top most unit apart from A horizon is the dorbank which is the most cemented and hardest horizon on the studied profile and the C2 sample is loosely consolidated and consists of coarse grained fraction of pebbles and rock fractions.

Table 13: soil profile description of trench C02 (A, B1, B1-2, B2, C1, C1-2 and C2) samples and vein material from trench B11

Depth (cm)	Description	Horizon (sample name)	Munsell colour
0 - 30	Slightly moist, red colour, sandy loam, massive apedal structure, loose; few roots, no HCl reaction, abrupt transition from unconsolidated soil to	A	7.5YR 5/8
30 – 60	Dry, mottled pale red, red and cream colours, very coarse laminated structure, massive peds with few cracks, very hard and brittle (Dorbank), many vertical and horizontal cream laminated veins between peds; MnO_2 oxide band at 40 cm depth, abrupt transition, through vein to B2 sample	B1	7.5YR 7/4
30 - 90	Vein material found connecting sample B1 and B2. Deep red and cream colours, very fine grained and thin but hard, at natural conditions negative react with HCl, gradually grades to C1 – 2 sample at depth, much less compacted compared to vein sample of trench B11	B1 - 2	5YR 7/8
60 - 90	Dry, mottled pale red, red and cream colours, very coarse laminated structure, massive peds with few cracks, very hard (slightly less hard than B1) and brittle (Dorbank), substantially more calcite mottles than above horizon more vein material (B1 – 2) between peds, abrupt transition to	B2	7.5YR 5/6
90 - 140	Dry, olive green grey colour with abundant red mottles and few white mottles, hard (less than B2), massive, negative reaction with HCl, few MnO_2 mottles	C1	7.5YR 4/6
90 - 290	Dry, white horizontal and vertical veins, thin and soft, easily broken, vigorous HCl reaction	C1 - 2	7.5YR 7/6
140 - 290	Dry, olive green-grey colour with abundant red mottles and few white mottles, sandy loam, slightly hard (less than C1), massive, negative reaction with HCl, white horizontal and vertical veins hosts calcite veins that are generally spaced further apart than above B2,very coarse grained with pebbles and rock fragments	C2	7.5YR 6/6

30 - 60	Vein material hosted by the dorbank, deep red and cream colours, very fine grained and thin but hard, at natural conditions negative react with HCl, compared to B1 – 2, B11 is much more compacted and dense than the B1-2 vein material sampled from trench C02	B11	5YR 7/6

Figure 6 is a C02 trench profile picture that shows all the studied units and their relative distributions. As it may be evident from the profile picture, the red colour of the soils decreases with increasing depth. From B1 to C2, the level of consolidation was also noticed to decrease with increasing depth. Vertical veins were also observed to be hosted by horizons B1 and B2; horizontal veins are observed at the bases of the both horizons B1 and B2. Closer to the base of the profile, very coarse pebbles and rock fragments were found.

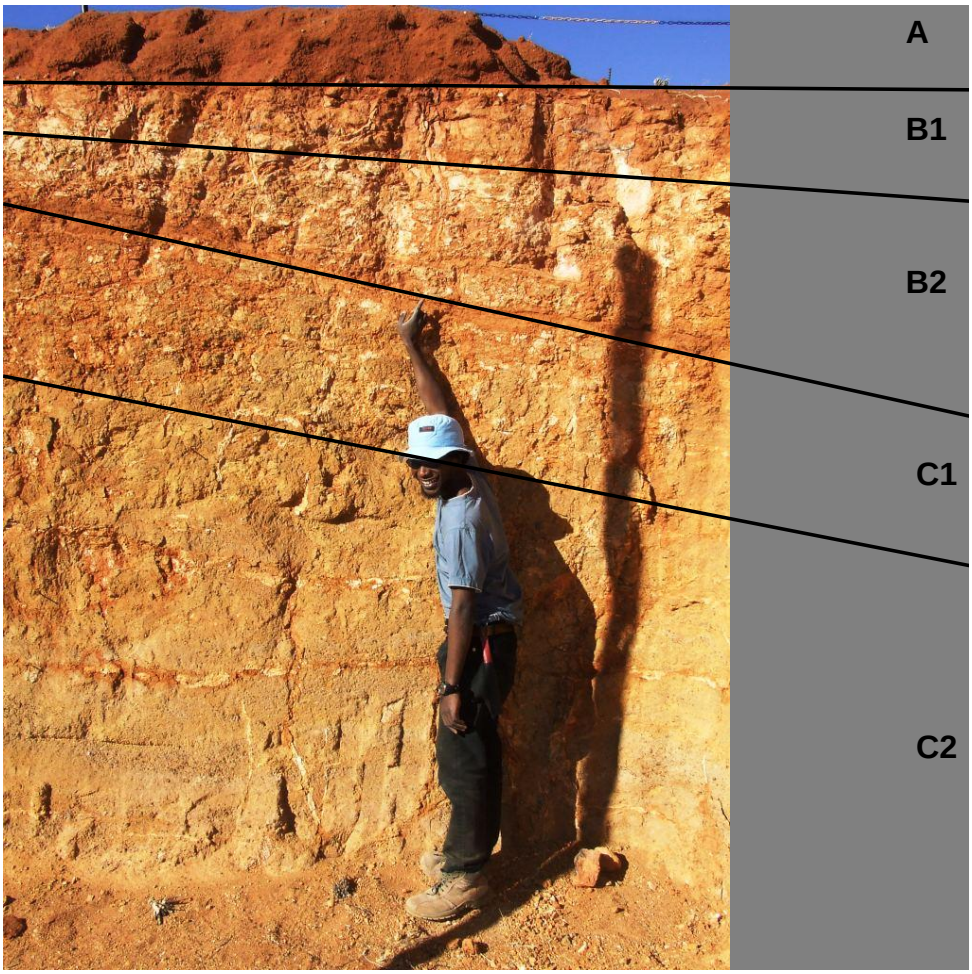

Figure 7: Profile picture of trench C02 indicating studied pedosedimentary horizons and their distribution vertically.

3.2. Chemical characteristics

Determining which trench profile (B11 or B1-2) would be used was based on the XRF analysis of trace metals of the barium-rich veins. The analysis indicated very high element barium (Ba) concentrations for both vein materials, although highest values (8316 ppm) were measured from B1-2. The Ba concentration measured from B11 was 2420 ppm, which is very high compared to the concentrations 803 ppm and 364 ppm, encountered in the dorbank matrix material of B1 and B2, respectively (Table 2). Although the strontium (Sr) soil concentrations are within a typical range in Vaalputs (Kabata-Pendias, 2001), both B1-2 and B11 barium-rich veins have relatively high Sr concentration values of 440 ppm and 466ppm, respectively compare to the B1 and B2 matrix materials of 84 ppm and 102ppm, respectively. Relative to C1 and C2 matrix material concentrations (316 ppm and 365 ppm, respectively), the C1-2 calcite vein is depleted in Ba (228 ppm) but enriched for Sr (139 ppm) (Table 2).

To compare the relative trace metal concentrations measured from the Ba-rich vein material (B1-2) with those measured from the matrix materials of the host dorbank (B1 and B2), enrichment ratio values were calculated (Table 3). Relative to the B1 dorbank matrix, the B1-2 vein material shows extreme enrichment ratios of 8.6, 5.2, and 10.4 in elements copper (Cu), Sr and Ba, respectively. Compared to sample B2, B1-2 is again much enriched in elements Sr and Ba by factors of 4.3 and 23.5, respectively. The enrichment ratios calculated for sample C1-2 relative to C1 and C2, are close largely close to 1. B1-2 and B11 horizons were depleted in chromium, nickel and zirconium with respect to C1 and C2 whereas C1-2 horizon is also depleted in these metals with respect to C1 and C2 horizon (Table 3).

Table 14: XRF data of trace element composition generated from each horizon in ppm

Sample name	V	Cr	Co	Ni	Cu	Zn	Ga	Rb	Sr	Y	Zr	Nb	Ba	La	Ce	Nd	Pb	Th	U
										ppm									
A	62	34	110	10	5	24	7	76	54	22	291	16	208	22	52	22	22	28	5
B1	45	58	63	68	5	26	10	100	84	34	183	11	803	32	83	33	27	19	3
B1-2	59	34	69	46	45	38	6	58	440	77	77	6	8316	70	210	77	23	10	4
B2	44	42	54	18	20	30	11	91	102	30	167	10	354	44	79	31	27	18	3
C1	68	42	69	24	17	46	17	165	81	66	211	14	316	78	138	57	37	26	6
C1-2	37	27	44	12	26	30	11	108	139	35	142	10	228	54	76	31	29	20	3
C2	58	36	92	13	14	24	11	123	68	28	220	14	355	47	91	36	34	30	6
B11	27	26	45	24	51	38	6	45	466	12	54	6	2420	11	65	22	30	6	3

Table 15: XRF trace element enrichment ratios

Sample Ratios	V	Cr	Co	Ni	Cu	Zn	Ga	Rb	Sr	Y	Zr	Nb	Ba	La	Ce	Nd	Pb	Th	U
B1-2/B1	*1.3*	*0.6*	*1.1*	*0.7*	**8.6**	*1.5*	*0.6*	*0.6*	**5.2**	2.3	*0.4*	*0.6*	**10.4**	2.2	2.5	2.3	*0.8*	*0.5*	*1.4*
B1-2/B2	*1.3*	*0.8*	*1.3*	2.5	2.3	*1.3*	*0.6*	*0.6*	**4.3**	2.5	*0.5*	*0.6*	**23.5**	*1.6*	2.6	2.5	*0.8*	*0.5*	*1.5*
C1-2/C1	*0.5*	*0.7*	*0.6*	*0.5*	*1.6*	*0.7*	*0.6*	*0.7*	*1.7*	*0.5*	*0.7*	*0.7*	*0.7*	*0.7*	*0.5*	*0.5*	*0.8*	*0.8*	*0.5*
C1-2/C2	*0.6*	*0.8*	*0.5*	*0.9*	*1.8*	*1.3*	*1.0*	*0.9*	2.1	*1.3*	*0.6*	*0.7*	*0.6*	*1.1*	*0.8*	*0.9*	*0.8*	*0.7*	*0.4*

less than 2
between 2 and 4
greater than 4

X-ray fluorescence analysis was performed to determine only trace metal concentrations for sample B11 whereas both trace metals and major cation concentrations were measured for samples of C02 trench. Table 4 shows that Al_2O_3 is present in almost equal concentrations for all soils sampled from Vaalputs with the A horizon sample having the least Al_2O_3 concentration value of 4.92 by weight percent (%wt), compared to 10.61%wt as the highest concentration value measured from C1 sample. Relative to all other horizons (A, B1, B2, C1 and C2), B1-2 and C1-2 veins have very high calcium (CaO) concentrations of 18.64%wt and 12.23%wt, respectively. Apart from sample B2, 6.59%wt, the rest of the samples have CaO concentrations that are measured as values below 1%wt. Iron (Fe_2O_3) and potassium (K_2O) concentrations generally increase slightly with depth from the top most unit, A, to the bottom C2 horizon. Magnesium (Mg) concentrations are relatively elevated in vein B1-2 with a value of 5.16%wt, whereas all other horizons are in the range of 0.17 to 1.79%wt. Silica (SiO_2) was, however in low concentrations in B1-2 vein material measuring 38.48%wt compared to the directly overlying A horizon that has a concentration of 85.48%wt. The total the loss on ignition (LOI) was relatively high for all the samples apart from the A horizon (1.95). The highest, 23.00%wt, LOI was measured from B1-2 vein material. Enrichment ratios are also calculated from major cations for B1-2/B1 and B1-2/C1-2 (Table 5). With respect to B1, B1-2 is highly enriched in CaO that results to an enrichment ration of 68.89. The MgO concentration in B1-2 gives an enrichment ratio of 3.26 relative to B1. B1-2/C1-2 also has an enrichment ratio of 3.28. Most of the enrichment ratios of B1-2/B1 and B1-2/C1-2 have values closer to 1 for some cations (Al_2O_3, Fe_2O_3, MnO).

Table 16: XRF data of major ions composition generated from each horizon in weight percentage

Sample name	Al_2O_3	CaO	Cr_2O_3	Fe_2O_3	K_2O	MgO	MnO	Na_2O	P_2O_5	SiO_2	TiO_2	LOI	H_2O	sum
	wt%	wt%	wt%	wt%	wt%	wt%	wt%	wt%	wt%	wt%	wt%	wt%	wt%	wt%
A	4.92	0.14	0.00	2.48	1.48	0.17	0.04	0.29	0.04	85.48	0.57	1.95	0.73	98.27
B1	6.88	0.27	0.01	2.73	1.81	1.58	0.02	0.33	0.03	74.49	0.39	6.97	3.57	99.08
B1-2	6.39	18.46	0.00	2.52	1.14	5.16	0.02	0.28	0.07	38.42	0.15	23.00	4.39	100.00
B2	7.39	6.59	0.00	2.93	1.65	1.79	0.02	0.18	0.04	62.52	0.38	12.60	3.54	99.64
C1	10.61	0.32	0.00	3.68	2.79	1.33	0.03	0.43	0.05	64.50	0.46	15.37	2.94	102.50
C1-2	7.90	12.23	0.00	2.89	2.12	1.65	0.02	0.29	0.05	60.02	0.34	8.47	4.00	100.00
C2	6.53	0.40	0.00	3.75	2.20	0.49	0.03	0.32	0.04	76.26	0.43	4.80	2.39	97.65

Table 17: RXF major element enrichment ratios

Sample name	Al_2O_3	CaO	Cr_2O_3	Fe_2O_3	K_2O	MgO	MnO	Na_2O	P_2O_5	SiO_2	TiO_2
Enrichment ratio B1-2/B1	0.93	68.89	0.58	0.92	0.63	3.26	1.16	0.86	2.16	0.52	0.38
Enrichment ratio B1-2/C1-2	0.85	1.59	1.33	0.92	0.57	3.28	0.96	1.01	1.43	0.67	0.45

Data from the saturated paste extracts is given in Table 6 and 7. Saturated paste extracts provided major cation and trace metal, as well as major anion concentrations that were equilibrated with the soils of A to C2 including B11. The pH measured in the 1:2.5 soil-water solution ranged between 7.10 and 8.90 and that measured from saturated paste extracts ranged between 6.70 to 7.87 meanwhile the electrical conductivities (EC) measured in the paste lowest in the A horizon (45.71 µS/cm) and highest in the vein materials (Table 6).

Concentrations of both Cl^- and SO_4^{2-}anions are depleted in the Ba-rich vein material of B1-2 compared to B1 matrix material whereas relative to B2 horizon (456.0 mg/L), the B1-2 sample has higher concentrations of these anions. The concentrations of Cl^- and SO_4^- measured from B11 (283.051 mmol/L and 8.042 mmol/L, respectively) sample are higher than those measured from B1-2 (29.391 mmol/L and 2.479mml/L, respectively). Calcium, Mg, Na, Sr, K and Ba ions are elevated in the Ba-rich veins (B1-2 and B11) with respect to B1 and B2 matrix materials, especially B11. In general, sample B11 has the highest major anion and cation concentrations.

The alkalinity was only present as bicarbonate species in all of the samples. A detailed table of ICP-MS data is provided in appendix B.

Table 18: pH and EC measured from 1:2.5 soil-water ratio and Saturated paste extracts

Sample Name	pH	EC (uS/cm)	pH	EC (uS/cm)
	1.0 : 2.5		Saturated paste	
A	7.10	45.71	6.70	419.1
B1	8.22	742.5	7.08	8138
B1-2	8.00	2552.0	7.05	9743
B2	8.70	1084	7.87	4015
C1	8.90	675.7	7.40	2258
C1-2	8.19	2155	7.66	5941
C2	8.14	1154	7.45	4561
B11	8.39	4235	7.11	23120

Table 19: Cation and anion analyses generated ICP-MS and ion chromatography prepared from saturated paste extracts in mmol/L
Alkalinity is present as HCO_3^- and Si represents dissolved Silica measure calorimetrically

Name	Si	Ca	Mg	Na	K	Ba	F-	Cl-	NO_3^-	PO_4^{3-}	SO_4^-	Alkalinity
						mmol/L						
A	0.321	0.307	0.250	1.498	1.134	0.000	0.000	1.410	0.081	0.000	0.542	1.050
B1	0.590	8.534	17.026	40.886	2.397	0.001	0.105	86.396	0.403	0.000	7.385	1.200
B1-2	0.750	10.232	15.236	58.738	2.856	0.001	0.158	29.391	0.000	0.000	2.479	1.550
B2	0.469	3.270	4.509	27.333	1.511	0.001	0.211	12.862	0.000	0.161	1.802	1.950
C1	0.377	1.362	1.943	16.165	1.262	0.000	0.158	49.756	0.000	0.804	3.823	2.450
C1-2	0.407	5.652	7.761	35.239	2.305	0.001	0.947	37.571	0.000	0.096	1.417	1.700
C2	0.261	6.160	7.486	19.162	2.510	0.001	0.737	31.873	0.000	0.652	1.417	4.200
B11	0.710	32.042	36.309	131.522	5.017	0.003	0.000	283.051	0.000	0.000	8.042	1.650

3.3. Mineral characteristics

3.3.1. Slaking Tests

Slaking tests were designed to determine the cementing agent of each horizon sample. Only horizon samples with consolidated sediments (B1, B1-2, B2, C1-2 and B11) were subjected to this test. The test was repeatedly carried out three times on the same samples. The (First, Second and Third) observations were made at the beginning of each test, when the acid or base solution was added into the beakers containing the test samples, while the (First, Second and Third) results were taken at the end of each the test after two weeks. The high temperature results were taken from exposing sample B1 and B2 to warm (40 °C) NaOH solution. The scale of 0-5 was used for both the observations and results. For the observations, the scale indicates the level of reactivity observed at the beginning of each test and for the results, it indicates the level of slaking at the end of each test.

When the 5M HCl acid solution was added into the beakers containing horizon samples, the C1-2 sample displayed a vigorous effervescence reaction and the B1-2 vein sample in NaOH solution began to slightly slake within a period of 4 hours. The rest of the samples did not show any reactivity in either HCl solution or in NaOH solution.

After 14 days, none of the samples had slaked to an appreciable extent but all samples in acid solution, apart from B11, had been strongly bleached in colour from red to grey. In order to quantify the results, further tests were conducted. Same samples were used; those initially subjected to NaOH for 14 days were swapped to HCl and those moved from HCl were placed in NaOH solution. When B1-2 and B11 vein materials were moved from the NaOH to the HCl, a strong effervescence reaction was observed along the white part of both veins. At the end of the second test, a gel-like fluid had developed around the acid treated samples of B1-2 and B11. A third test carried out on the B1-2 and B11 veins, further effervescence and slaking was observed.

The results of this test are summarised on Table 8. The detailed observations of the slaking test are provided in Table 9-11 ain the appendix B section

Table 20: Slaking tests and results of HCl and NaOH alternated samples

	First observations		First results		Second observations		Second results		Third observations		Third results		High Temperature Results
Sample name	5M HCl	6M NaOH	5M HCl	6M NaOH	5M HCl	6M NaOH	5M HCl	6M NaOH	5M HCl	6M NaOH	5M HCl	6M NaOH	Warm (40°C) 6M NaOH
B1	0	0	0	0	0	0	2	0	n.d.	n.d.	n.d.	n.d.	5
B1-2	0	0	0	1	4	0	3	4	n.d.	n.d.	n.d	n.d	n.d.
B2	0	0	0	0	0	0	1	1	n.d.	n.d.	n.d.	n.d.	5
C1-2	5	0	1	0	5	0	0	0	n.d.	n.d.	n.d.	n.d.	N.d.
B11	0	0	1	2	4	0	3	2	4	0	2	1	n.d.

n.d. = no data observations: 0 = no reaction 5 = strong reaction

results: 0 = no slaking 5 = complete slaking

The samples exposed to warm 6M NaOH solution were found to have completely slaked within a period of 5 days.

3.3.2. x-Ray Diffraction

X-ray Diffraction analyses of all the samples presented analytical problems with pattern peaks that would be slightly shifted from the angles which they would normally be expected to occur. This was due to differing clay thickness on the ceramic tile. The X-ray diffraction data generated from clay extracts (of all eight horizons) and bulk powder samples (of only the Ba-rich veins, B1-2 and B11) is shown in figures 7 and 8, respectively. Only the B1 and B2 samples indicated the presence of mineral smectite, $((Ca, Na, H)(Al, Mg, Fe, Zn)_2(Si, Al)_4O_{10}(OH)_2\ xH_2O)$ after they were treated with Mg-Glycerol, which resulted to the shift of the 14Å peak to 18Å. The C1 horizon was the only sample that indicated the presence of vermiculite, $(Mg,Fe,Al)_3(Al,Si)_4O_{10}(OH)_2•4(H_2O)$, (collapse of the 14Å to 10Å). All of the samples had prominent peaks for mineral illite, kaolinite and quartz whereas palygorskite was also measured in all samples apart from the unconsolidated A horizon. The mineral barite's peak was observed from all samples, except for those of A and B1 horizon, at a d-distance of 3.44Å. Its most intense peaks were observed from B11 and B1-2 samples. The calcite peak at 3.04Å was observed from sample B1-2, B2, C1, C2 and the most intense peak of calcite was observed from sample C1-2. Due to prior knowledge that, samples of B11 and B1-2 effervescences in the presence of 0.1 M HCl, an assumption that carbonates (calcite) were hosted in relatively large concentrations in these samples although the XRD patterns did not show credible

peaks. For this reason, further XRD analyses were conducted on the B11 and B1-2 vein materials. Milled bulk (clean vein) samples of both veins were analysed. The XRD patterns generated from the clean vein materials, in figure 8, were compared with those of clay extracts of the same vein materials, in figure 7. The resulting graphical patterns indicated very intense calcite peaks for both veins.

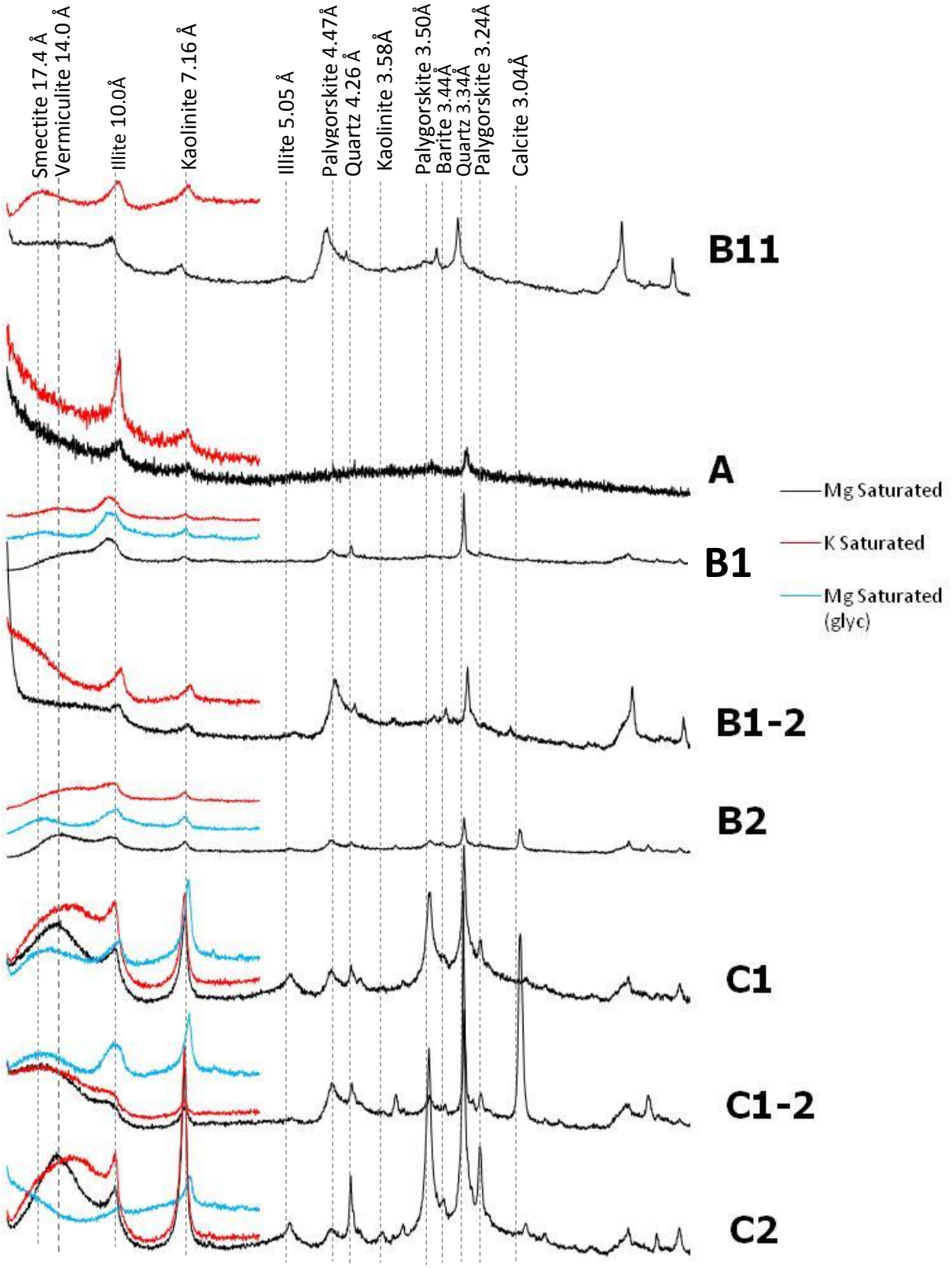

Figure 8: XRD patterns of all studied horizons

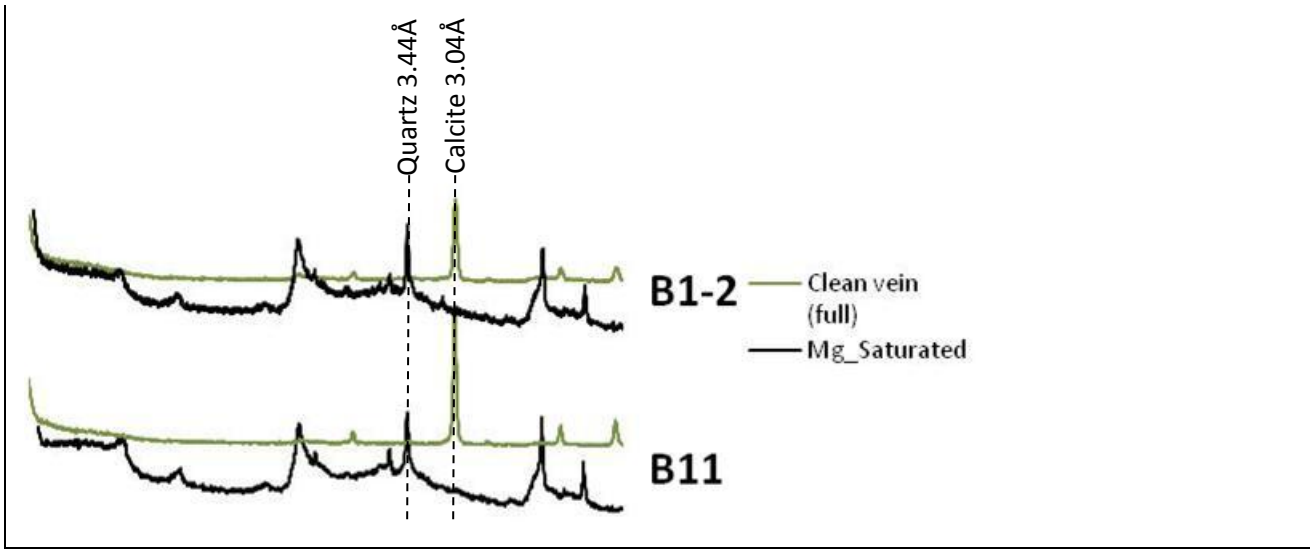

Figure 9: XRD patterns generated from bulk sample B11 and B1-2 (clean vein) materials are compared to those of clay extracts

3.3.3. Phreeqc data modelling

Phreeqc modelling was used to determine possible neoformed phases from Vaalputs soils (Figure 9). The modelling was carried out on all samples. Mineral aragonite, $Ca(CO_3)$, is undersaturated with respect to A, B1, B1-2 and C1 meanwhile it is almost in equilibrium with respect to B2, C1-2, C2 and B11 horizons. Calcite was found to be undersaturated in A, B1, B1-2 and C1 whereas it was slightly supersaturated with respect to B2, C1, C1-2, C2 and B11 horizons. Barite on the other hand is only and slightly undersaturated with respect to the A horizon but almost in equilibrium with respect to C1, C1-2 and C2. With respect to B1, B1-2, B2 and B11, mineral barite shows relatively high saturation indices. The highest SI values for barite were in B11 and B1 horizons.. Due to large negative SI, mineral celestite ($SrSO_4$) could not be modelled for the B1 horizon but the rest of other models, indicated that celestite was not too far from equilibrium, with the most negative SI value of 3.7. Fluorite (CaF_2) is slightly supersaturated with respect to B1-2, B2, and C1-2. Model of sample C2 indicated the highest SI value for fluorite whereas the rest of the samples indicated undersaturation indices for mineral fluorite. Witherite, gypsum, amorphous silica, sepiolite and palygorskite minerals were always undersaturated with respect to all horizons whereas hydroxyapatite was supersaturated with respect to C1, C1-2 and C2 horizons.

a

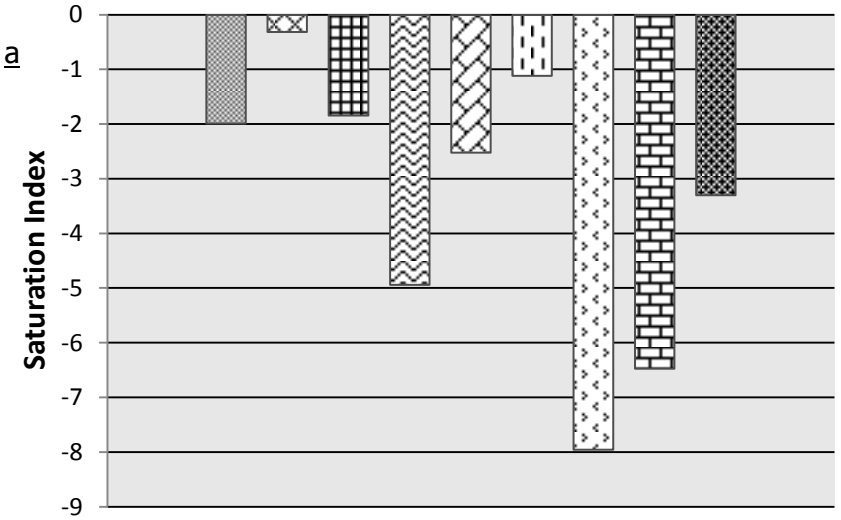

b

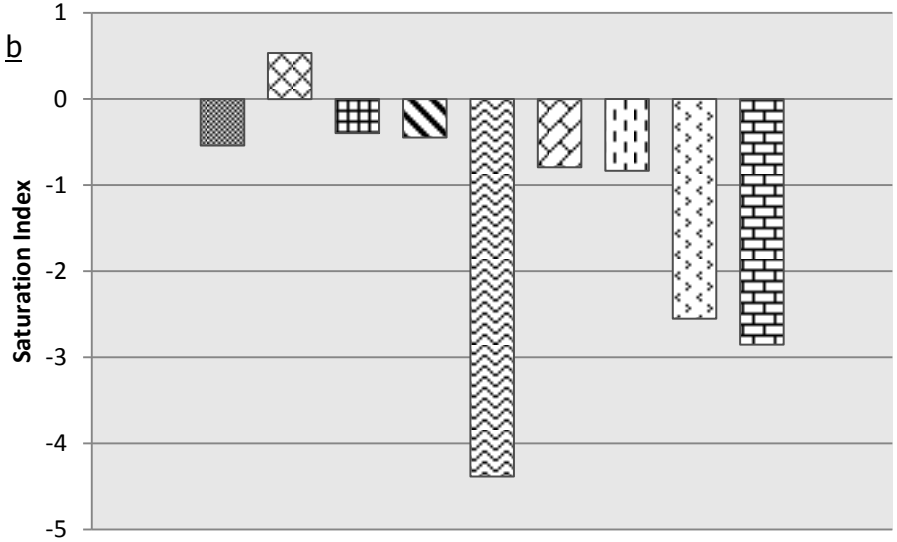

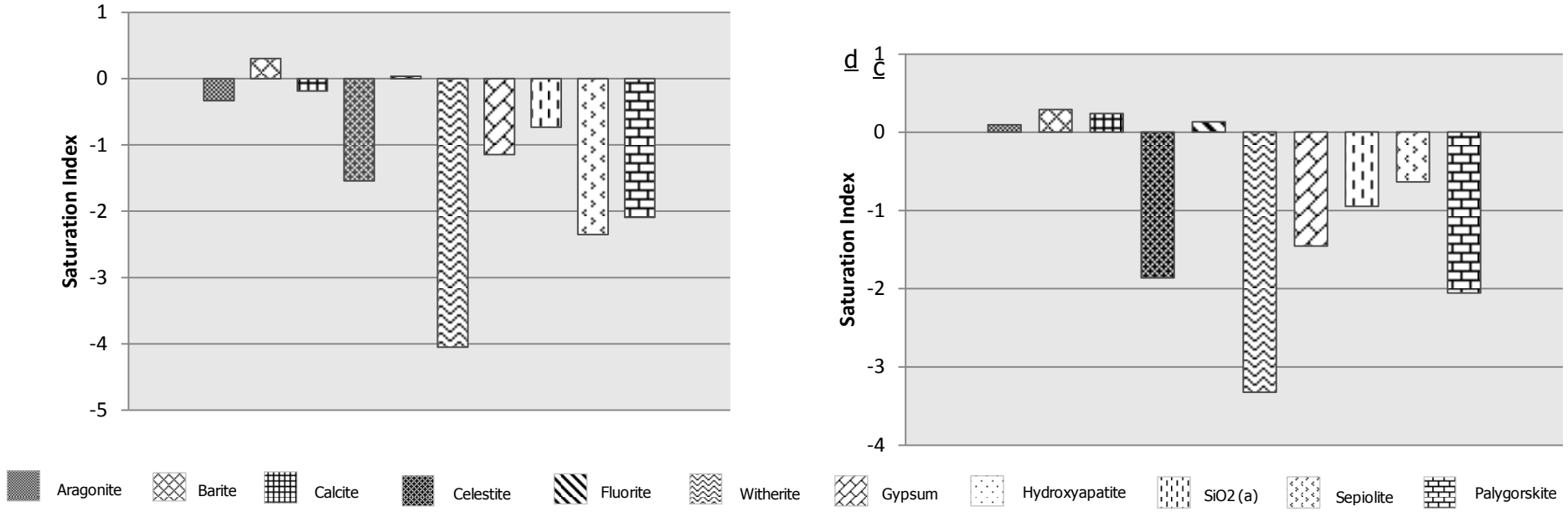

Figure 45: possible neoformed minerals expected that may be expected to precipitate from Vaalputs soils: a) A, b) B1, c) B1-2, d) B2, e) C1, f) C1-2, g) C2 and h) B11 horizons

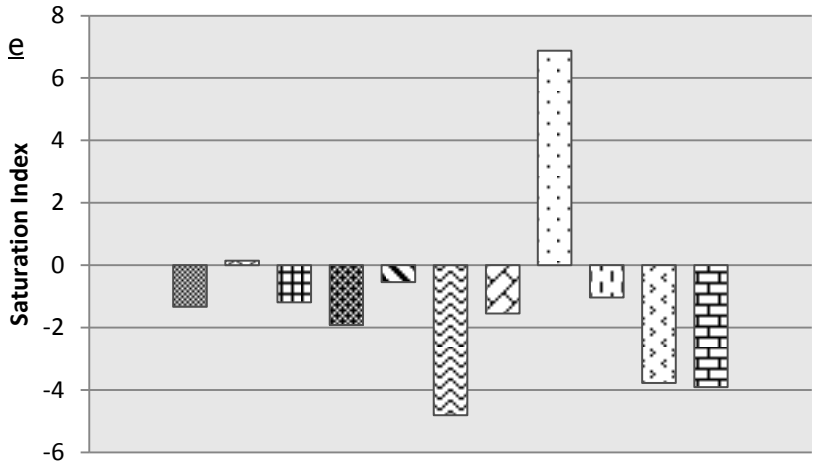

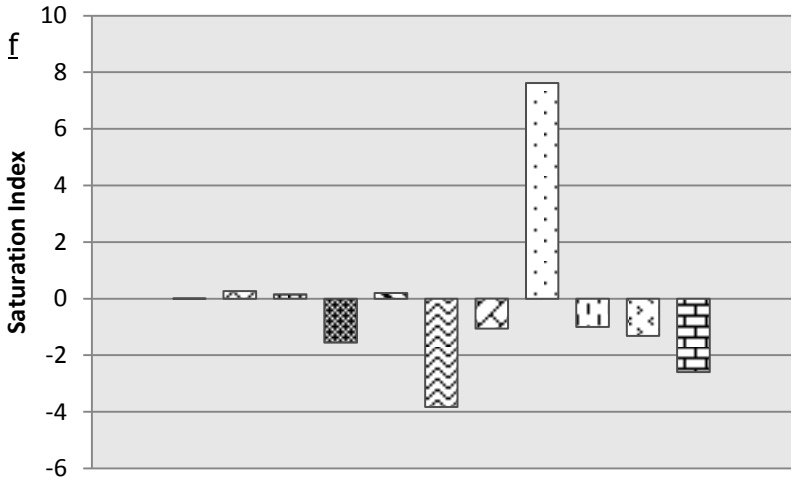

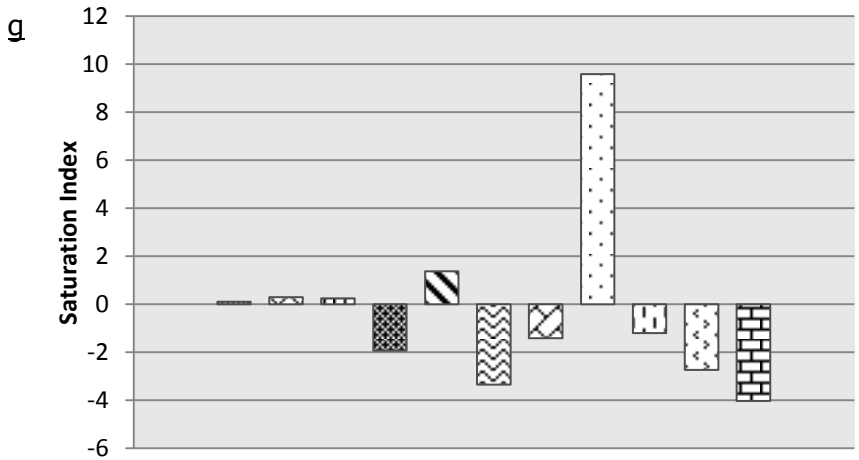

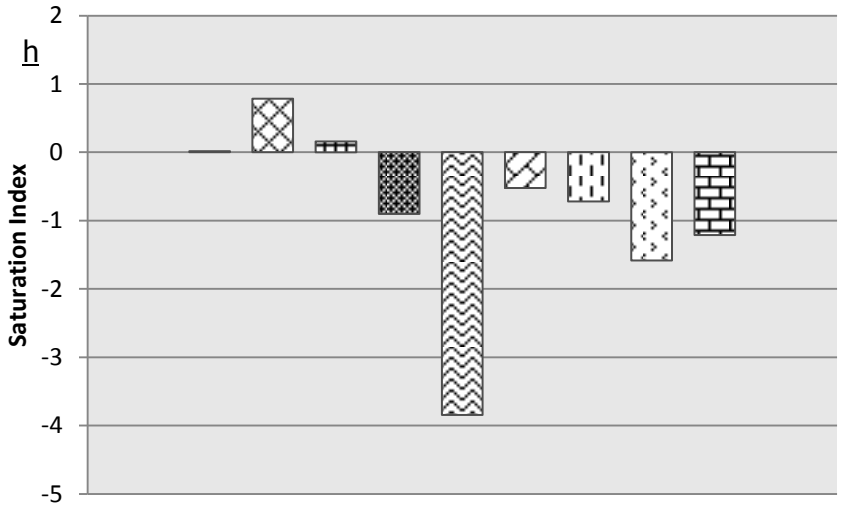

Figure 9: continued

4. DISCUSSION

Although some authors (including Logue, 2010, Francis, 2008; Francis *et.*al, 2007; Singer, 1955 and authors therein) have conducted intense studies in the soils of Namaqualand region, large gaps of knowledge in regional soils still exists. This introduced a problem of limited information about the Namaqua soils over the duration of the research.

The Vaalputs region has been characterized by a wet and humid period transitioning to a cooler and more arid climate since the Late Mesozoic to Early Cenozoic (80-60 Ma) period, (De Wit, 2000 and Logue, 2010).

4.1. Profile Soil Characteristics

The top soil, A horizon, of Gordonia formation is largely unconsolidated sediments of aeolian origin that forms a dune field which trends NNE-SSW in Vaalputs and the surrounding areas (Figure 10 on the appendix B) (Logue, 2010 and Brandt, 1998). Although Fe does not form the major chemical constituent of the A horizon, the red colour of this sample is donated to the Fe-minerals (most likely haematite, Fe_2O_3 and magnetite, Fe_3O_4) that may be present in the soil. This red colour is weakly developed on the underlying brittle dorbank; this is interpreted as the chemical leaching of the overlying iron-rich Gordonia sand (Logue, 2010).

The underlying dorbank horizon (Figure 2band 6) is extremely hard and brittle due to secondary silica cementation (SiO2, presumably amorphous and microcrystalline silica); calcite and sepiolite may form secondary cementing agents (Logue, 2010). Such cemented soils of Namaqualand may be widely classified into three petrological groups based on their cementing agents: soils that are largely cemented by amorphous silica (dorbank), calcrete (calcite cemented) and sepiocrete, cemented by secondary mineral sepiolite (Fey, 2010; Francis, 2008 and Francis et *al,* 2007).

At depth of about 90 cm, the dorbank horizon begins to grade into the underlying less consolidated and less compacted sediments of C1 and C2 which are generally referred to as greywacke in Vaalputs (Logue, 2010).

The red colour decreases from deep red on the top horizon to slightly red on the lower B1 and B2 to greenish C1 and C2 horizons. The systematic decrease in red colour of the profile may be an indication that these soils were at some stage waterlogged and reducing which could have lead to much removal of pigmenting Fe-oxides on the lower parts of the profile.

4.2. Profile Chemical Characteristics

The x-ray fluorescence data of analysed major cations (Table 4) shows relatively high concentrations of Al_2O_3 for all the horizons. The CaO ion is significantly enriched in B1-2 and C1-2 vein materials compare to the matrix samples. Furthermore, the sample B1-2 is depleted in SiO_2 whereas C1-2 shows relatively comparable concentrations in relation to the matrix samples. This is an indication that the B1-2 vein material may consists of high calcite concentrations that which be acting as a secondary cementing agent on the vein.

The x-ray fluorescence data of trace element analysis produced from vein B1-2 and B11 indicated metal concentrations (especially for Ba analysis) are generally higher in the B1-2 vein material than found to be in the B11 vein. The metal concentration variations may be related to the level of compaction of each vein. The vein of B11 veins are to a large degree very compacted compared to that of B1-2 veins. The less compacted vein structures seem to have been able to host and accumulate more dissolved solutes (during flooding) which have resulted to higher concentrations as evaporation proceeds. This may be the reason that has lead to trace metal depletion along the more compacted B11 relative to B1-2.

Enrichment ratios were calculated from the XRF data of trace metals for vein sample B1-2 relative to the dorbank matrix (B1 and B2) (Table 2 and 3). The B1-2 relative to B1 and B2 indicated high enrichment ratios for Cu, Sr and Ba. Generally, the B1-2/B1 has higher enrichment ratios compared to B1-2/B2. This means that the top unit, B1, is relatively enriched in trace metals compared to the lower B2 horizon. This may indicate that the trace metal input is external to the soils; therefore metals are deposited from metal enriched surface waters that may percolate downward but much of it may also be trapped on the above soil unit. This seems to be true for Ba where B1-2/B1 has an enrichment ration of 10.4 whereas B1-2/B2 is enriched by a factor of 23.5.

4.3. Profile Mineralogy

4.3.1. Slaking tests

The slaking tests were to determine the secondary matrix mineral which may be the cementing mineral. As the tests were carried out in 5M HCl and 6M NaOH, the first and most intense effervescence was observed from C1-2 sample placed in 5M HCl solution. This meant that high carbonate concentrations were present in the sample (probably calcite since the XRF analysis indicated high CaO concentrations) (Table 8 in text and Table 9-11 in the appendix B section). At the end of the first test, sample C1-2 had slightly slaked. The B1-2 and B11 vein samples also slaked along the veins, although the B11 vein had slaked slightly more than the B1-2 vein in NaOH solution. This was an indication of silica cemented

horizons. At the end of the first test, the second test was executed by alternating samples that were initially placed in HCl acid solution and moved to NaOH base solution and those initially placed in base were moved to acid. The samples that were previously exposed to NaOH (B1-2, C1-2 and B11) all illustrated vigorous effervescence calcite reaction with 5M HCl. Note that this was not the case when the samples of the same materials were placed for the first time on acid solution. This meant that the enveloping silica layer had to be dissolved before this reaction could be observed from the B11 and B1-2 veins materials. Further acid and base solution alternations were carried out on sample B11, as the B1-2 sample had slaked to a large degree. Each time the sample B11 would be exposed to an acid solution after being removed from a base solution, an effervescence reaction was observed. The observed sample effervescence in HCl solution after the being removed from the base solution was interpreted as the repetitive cementation of sample by amorphous silica, followed by secondary calcite. This seemingly "cyclical", deposition of silica followed by calcite in the vein may have been largely controlled by soil pH changes. At high pH levels, dissolution of silica would occur meanwhile calcite would precipitate. Conversely, at low pH conditions, calcite would dissolve and that of silica would precipitate.

Since both the silica and calcite were found as cementing agents in the Ba-rich veins, a possible scenario that may have lead to the preservation of one cementing agent when the pH conditions favoured the formation of the other one is as follows:

> The formation of one cementing agent (example: calcite) should occur at pH levels that are not too high (>9) to prevent accelerated dissolution of silica as the calcite precipitates while buffering the pH to less than 9 to preserve the amorphous silica.

The slaking tests also pointed out that the mineral barite does not form the major mineral constituent of the dorbank hosted veins as it was originally thought by Logue, 2010. In fact, the major mineral constituents seem to be amorphous silica and calcite; barite seems to be an abnormally high concentration accessory mineral.

4.3.2. X-ray Diffraction

The X-ray diffraction patterns indicated the presence of mineral smectite to only exist in from the B1 and B2 samples. Only the B1 and B2 samples indicated the presence of mineral smectite after they were treated with Mg-Glycerol, which resulted to the shift of the 14Å peak to 18Å. The C1 horizon was the only sample that indicated the presence of vermiculite (collapse of the 14Å to 10Å). All of the samples had prominent peaks for mineral illite, kaolinite and quartz whereas palygorskite was also measured in all samples apart from the unconsolidated A horizon (Figure 7). This mineral was indicated by small peaks, where the intensity of the peaks is directly proportional to the relative abundance of that mineral on a sample. Just like mineral smectite, vermiculite was also found to exist in very small concentrations but only one horizon, C1. Clay minerals were found to dominate the Vaalputs soils were identified as kaolinite with d-distances of 7.15 Å and 3.56 Å and illite with d-distances of 10.0 Å and 5.05 Å. The small concentrations of smectite and vermiculite as well as the presence of kaolinite and illite in high concentrations imply that these soils have very low swelling ability. The high kaolinite and illite concentrations may have respectively resulted from feldspar and muscovite weathering in the surrounding granite-gneiss.

The mineral quartz was in very high concentrations from all the horizons.

The barite peak was observed from all samples, except for those of A and B1 horizon, at a d-distance of 3.44Å. Its most intense peaks were observed from B11 and B1-2 samples. These results are analogous with the high Ba concentrations measured from XRF analyses.

The palygorskite may have formed as described by Francis, 2008 and Singer 1995. The high Mg and Al concentrations would lead to the formation palygorskite, under the right conditions

The calcite peak observed at d-distance 3.04Å from samples B1-2, B2, C1, C2 and its most intense peak was observed from sample C1-2. The XRD analyses conducted on the B11 and B1-2 vein materials indicated intense calcite peaks when the milled bulk (clean vein) samples of both veins were analysed. However, calcite peaks were not observed in the clay phase of B1-2 veins and the B11 veins. The method using acid to extract the clay minerals from the bulk sample could have reacted the carbonates out of the bulk sample (figure 8 and figure 7).

4.3.3. Phreeqc data modelling

Phreeqc data modelling produced SI graphs of selected minerals of each horizon (Figure 9). Mineral aragonite and calcite were supersaturated with respect to B2, C1-2, C2 and B11 but undersaturated with respect to A, B1, B1-2 and C1 horizons. This indicates that the carbonates in some parts of today's Vaalputs soils, are in continuous precipitation and dissolution in others. Amorphous silica seems to be always undersaturated in Vaalputs soils, this indicates that the dorbank formation may have ceased and the dissolution of silica may be occurring today. Witherite, BaCO3, is also found to be undersaturated. This may mean that the high concentrations of Ba measured from XRF analyses present in Vaalputs soils in the form of mineral barite. Mineral palygorskite remains undersaturated when modelled with phreeqc but it is indicated in XRD patterns. According to Singer et.al (1995), there are two reasons for this

1. the time to it takes to equilibrate mineral palygorskite in soils with water may be too long, or
2. the saturated past extracts are no longer in equilibrium with palygorskite therefore mineral palygorskite is unstable.

To qualify this, further studies would be required.

4.4. Pedogenesis of Dorbank

Pedogenic processes of duric soils from Batswana and Namibia have also been discussed by Nash and Shaw (1998) and Kampunzu et al (2006).

The main factor controlling paedogenesis of dorbank is the pH of soils which in turn controls dissolution and precipitation of silica and calcite. At low pH levels (<9), silica may be expected to precipitates and calcite is unstable at such pH condition, it dissolves which leads to siliceous dorbank formation whereas at high pH levels (>9), calcareous duripans may be expected to form due to the dissolution of silica and the precipitation of calcite. This suggests that at low pH, during genesis of siliceous duripan, silica will act as a cementing agent that is independent of calcite and same applies to the genesis of calcareous duric soils, calcite acts as a cementing agent that is independent of silica at high pH levels. The effervescence of siliceous duric soils in 5M HCl which only slaked in 6M NaOH solution during slaking tests (table 8; table 9-11 in the appendix A section) also confirmed the existence of calcite in silica dominant soils. This phenomenon has been noted by several workers (Francis, 2008; Francis et al, 2007; Kampunzu, 2007 and Nash and Shaw, 1998). Such soils in Kalahari have been largely studied and referred to as calc-silcrete integrates (Kampunzu, 2007 and Nash and Shaw, 1998).

4.5. Vein Genesis Mechanism

The B1-2 and B11 veins are prominent features exposed in Vaalputs by trench excavation processes. These veins may be the result of chemicals from the dorbank and the lower units accumulating along the weakest soil cracks and finally propagating in the direction of lower pressure (upward). The upward movement of water may be due to high degree of evaporation and the nocturnal chilling that may results to the upward movement of the water vapour carrying salts was described by Francis 2008, 2007 and Prinsloo, 2005. The veins may also be the result of external input of chemically enriched waters to the dorbank. As the porosity of the dorbank is expected to be reduced by the silica on its matrix as a cementing agent, the percolation of waters will also decrease. The downward movement of chemically enriched surface waters would preferably occur along fissure zones of low pressures. A repeatedly continuous flooding of the area would result to the precipitation evaporative minerals and vein formations along the cracked zones. Assuming that the chemical elements enriched in the dorbank hosted veins originated from different sediment sources, both the downward (external input trough precipitation during wet seasons) and the upward (evaporation and nocturnal chilling during dry season) movement of water would contribute to the formation of the veins. During wet seasons, the chemically enriched waters from weathered rocks and sediments would provide infill for the surface fissure zones to depth and this could have resulted to mobilising of more elements with increasing depth of penetration. During the dry seasons, the evaporation would begin to dry out water from the upper most unit (which was at the time, today's dorbank) and then gradually pulling much of the deeper waters which may be even enriched in dissolved solutes. Closer to surface where liquid water begins to gasify, solutes would also begin to precipitate at the base of the veins and gradually propagate in the upward direction with increasing evaporation. Given correct conditions, saturation indices of evaporative minerals would be reached and mineral precipitations would follow. The "cyclical" wet and dry seasons (De Wit, 2000, 2007; Logue, 2010) may produce repetitive silica-calcite (and maybe minor barite) layers, confirmed by slaking tests (Table 8 in text and 9-12 in appendix A). The high density of the B1-2 sample suggests very old soil formations. The C1-2 veins may be the result of the leached B1-2 veins during the wet seasons when the highly mobile elements go into solution and percolate down the profile.

5. CONCLUSION

- Soils of Namaqualand have complex features such as the vein systems discussed in this thesis. These soils are colluvial sediments which have been pedologically altered since the late Cretaceous, over a period of ca. 67 million years.
- According to the XRD patterns a variety of mineral phases is present in these soils. Of the clay minerals non-swelling kaolinite, illite and palygorskite seem dominant in Vaalputs.
- The Ba-rich veins may be the result of chemical migration from the dorbank and the lower units accumulating along the weakest soil cracks and finally propagating in the direction of lower pressure (upward). The upward movement of water may be due to high degree of evaporation which leads to the deposition of metals near surface.
- The XRD patterns and phreeqc models, mineral barite is present in all soul horizons except for the A horizon.
- The deposition and precipitation of silica and calcite along the veins seems to be alternating and "cyclical". It is thought to be controlled by pH; where high pH levels lead to the dissolution of silica while calcite precipitates out of solution and at low pH conditions, calcite dissolves and silica precipitates.
- Slaking tests indicated the major mineral constituents of the veins were silica and calcite, not barite as it was initially thought.
- Phreeqc data indicates the amorphous silica is undersaturated for all horizons and calcite is saturated in the B2, C1-2, C2 and B11 horizons and undersaturated in the A, B1, B1-2 and C1 horizons.
- The pebbles and rock fragments found on the lower most horizons may be related to a high energy depositional sedimentary environment and the colour variation may be related to the horizon being waterlogged and reducing.

6. REFERENCES

1. Andreoli, M.A.G., Hart, R.J., Ashwal, L.D. and Coetzee, H. (2006b). Correlations between U, Th Content and Metamorphic Grade in the Western Namaqualand Belt, South Africa, with Implications for Radioactive Heating of the Crust. *Journal of Petrology, 47 (6), 1095-1118*

2. Brandt, D., Andreoli, M.A.G., and McCarthy, T.S. (2005). The late Mesozoic palaeosoils and Cenozoic fluvial deposits at Vaalputs, Namaqualand, South Africa: possible depositional mechanisms and their bearing on the evolution of the continental margin. *South African Journal of Geology (2005), 108, 271-284*

3. Brandt, D. (1998). The Recent Morpho-Tectonic History of the Vaalputs Radioactive Waste Depository and Environs. Ph. D. thesis, University of the Witwatersrand, Johannesburg

4. Francis, M.L. (2008). Soil Formation on the Namaqualand Coastal Plain. Ph. D. thesis, University of Stellenbosch

5. Francis, M.L., Fey, M.V., Prinsloo, H.P., Ellis, F., Mills, A.J., and Medinski, T.V., (2007). Soils of Namaqualand: Compensations for aridity, *Journal of Arid Environments* 70 (4): 588-603

6. De Wit, M.C.J., Marshall, T.R. and Partridge, T.C. (2000). Fluvial deposits and drainage evolution. In: Partridge, T.C. and Maud, R.R. (Eds.), The cenozoic of southern Africa. Oxford University Press, London, Special Publication

7. Eglington, B.M. (2006). Evolution of the Namaqua-Natal Belt, southern Africa – A geochronological and isotope geochemical review. *Journal of African Earth Sciences*, 46, 93-111

8. Fey, M. (2010). Soils of South Africa. *Silicic Soils.* pp53-61

9. Kabata-Pendias, A. (2001). Trace elements in Soils and Plants. *Elements of Group IV.* Pp129-130

10. Land Type Survey Staff, (1987). Land Types of the Maps 2816 Alexandra Bay; 2818 Warmbad; 2916 Springbok; 2918 Paffader; 3017 Garies; 3018 Loerisfontein. Memoirs on the Agricultural Natural Resources of South Africa No. 9

11. Logue, A., (2010). A borehole-based investigation of the Post Karoo Sedimentary deposits at Vaalputs

12. McCarthy, T.S., Moon, B.P. and Levin, M. (1985). Geomorphology of the Western Bushmanland Plateau, Namaqualand, South Africa. *South African Geographical Journal* (1985), 67 (2), 160-178

13. Singer, A., Kirsten, W., Biihmann, C. (1995). Fibrous clay minerals in the soils of Namaqualand, South Africa: characteristics and formation

14. RSA Soil Classification Working Group, 1991

15. Kampunzu, A.B., Ringrose, S.,Huntsman-Mapila, P., Harris, C., Vink, B.W., Matheson, W. Origins and palaeo-environments of Kalahari duricrusts in the Moshaweng dry valleys (Botswana) as detected by major and trace element composition

16. Nash, D.J., and Shaw, P.A. (1998).Silica and carbonate relationships in silcrete-calcrete intergrade duricrusts from the Kalahari of Botswana and Namibia

17. Prinsloo, H. (2005). Alteration of the Soil Mantle by Strip Mining in the Namaqualand Strandveld. Master's Thesis, University of Stellenbosch

7. APPENDIX A:

Detailed clay extraction procedure that was used in the study

In this investigation, XRD was designed to quantify the process of clay and clay-sized mineralogical phase identification that may be present in each horizon. 30 grams of the bulk sample and 300ml of deionised water ware mixed together into a 500ml glass beaker. While stirring with a magnetic stirrer bar, the pH of mixture was brought up to 9.5 with $NaCO_3$ solution. Thereafter, the mixture was placed on an ultrasonic bath for a period of 5 minutes. From the ultrasonic bath, a 5 centimetre mark line was drawn from the top of the mixture to the down direction. The mixture was left to settle over 30 minute. At the end of the 30 minutes, using an automatic pipette, 80ml of the mixture are extracted above the 5 centimetre mark line into two 50 ml centrifuge tubes (40ml in each). The first centrifuge tube was labelled "KCl" and the second one was labelled "$MgCl_2$". While shaking by hand, the pH of water-soil mixture in the $MgCl_2$ labelled tube was brought down to 5 by the addition of 0.01M HCl (to prevent brucite formation). 10ml of KCl solution was added to mixture in the KCl-labelled tube and $MgCl_2$ solution was added to the mixture in the $MgCl_2$-labelled tube. The fine clay extracts were completely suspended using vortex and then centrifuged at 1500 rpm for 4 minutes. The supernatant was discarded and another 25ml solution of KCl/$MgCl_2$ was added. Further shaking of the mixture was done on the vortex until the clay was suspended, the mixture was centrifuged at 1500 rpm for 4 minutes and then the supernatant was discarded. This previous step was repeated twice more. 25 ml of deionised water and 25ml of methanol were added to the clay concentrate. Some more shaking on the vortex was done to suspend the clay and then centrifuged at 1500 rpm for 4 minutes. The washing was repeated using 10ml of 95% acetone. The supernatant was decanted into a smaller beaker; few drops of $AgNO_3$ were added to test for zero precipitate formation. Few drops of deionised water were added to the clay concentrate to create very mobile slurry. Using a plastic dropper, the suspended clay was added to a clean ceramic disc and the excess water was sucked off using to suction pump. The extract was left to dry at room temperatures.

APPENDIX B:

Detailed Slaking test notes

The only observed reactivities at the beginning of the first slaking tests were those of B1-2 sample when placed in a 5M HCl solution. This sample illustrated vigorous effervescence in the HCl solution. The rest of the samples were non reactive in both HCl and NaOH solutions.

Table 21: results of the first tests 14 days later

Sample name	**in 5M HCl**	**in 6M NaOH**
B1	Did not slake at all.	Did not slake at all; only few and small sediment fragments settled at the bottom of the beaker.
B1-2	Did not slake at all.	Strongly slaking on both sides of the vein but the white part of the vein is still intact.
B2	Did not slake at all.	Did not slake at all, only a few and small sediments settled at the bottom of the beaker.
C1-2	Very fine sediment material settled at the bottom of the beaker.	Did not slake at all.
B11	Did not slake, only fine sediment material settled at the bottom of the beaker along the beaker rims.	Partially slaking but the sample was still in one piece although more than 2mm cracks had developed between the vein and the surrounding dorbank matrix on either side of the veins.

At the end of the first slaking test, all the samples in the acid solution, apart from B11, had been strongly bleached to grey colour and the acid colour had turned from colourless to bright yellow.

The Samples initially exposed to acid were swapped to NaOH base solution and those in base were placed in HCl acid solution and the following observations were made.

Table 22: observations when the samples were swapped from acid to base and form base to acid solution

Sample name	**in 5M HCl**	**in 6M NaOH**
B1	No reaction	No reaction

B1-2	Effervescenced vigorously along the veins and the surrounding dorbank.	No reaction
B2	No reaction	No reaction
C1-2	Vigorous effervescence reaction.	No reaction
B11	Also displayed vigorous effervescence reaction which triggered a fast and intense slaking along the vein and the surrounding dorbank.	No reaction

Table 23: results after acid and base solution swapping of samples

Sample name	**in 5M HCl**	**in 6M NaOH**
B1	Only slaked to a small degree, with few sediment fragments settling at the bottom of the beaker.	Did not at all slaked, the sample still looks the same as it did when it was swapped from the acid solution.
B1-2	The vein has slaked to a very large degree, but most of the white part was still intact.	Has broken down to a very large extent. More than halve of the sample has settled down as fine sediments. The vein material has slaked down completely and there is no evidence of its existence.
B2	Sample is still intact, few and small fragments have settled at the bottom of the beaker.	Same results apply as in HCl equivalent.
C1-2	Very intact, no slaking has occurred.	Very intact, no slaking has occurred.
B11	A jelly-like material formed on encompassing the entire sample. About 40% of the sample has settle at the bottom of the beaker as fine sediments.	The block of dense sample has not slaked but it has broken into two pieces along the vein.

Observation when the B11 samples were swapped again from acid to base and from base to acid solution.

Sample name		**in 5M HCl**	**in 6M NaOH**
B11	**Observations**	Vigorously effervesce	No reaction
B11	**Results**	Strong Slaking along the vein	Weakly slaking along the vein and dorbank

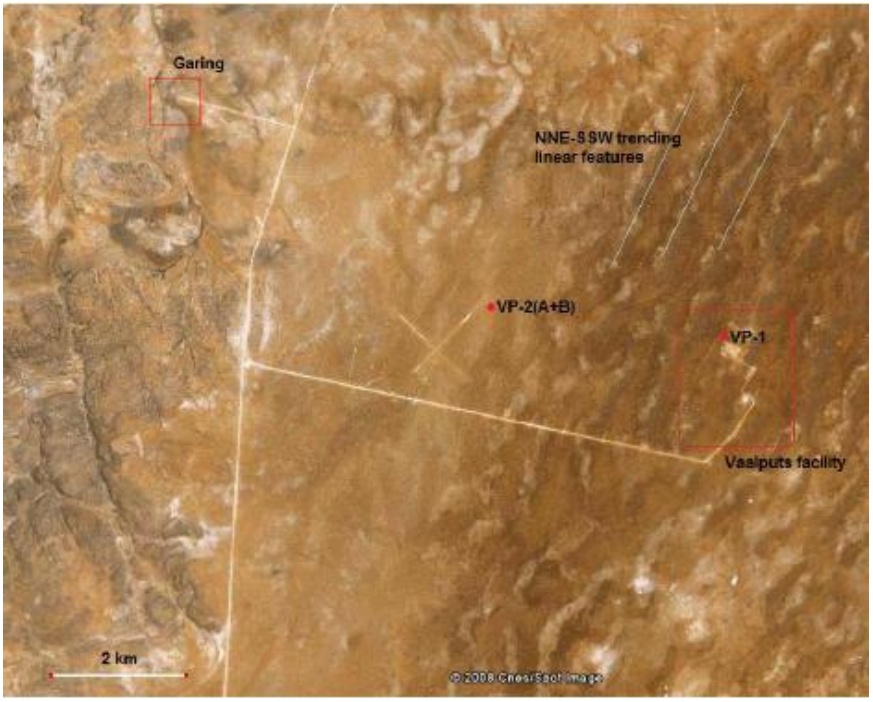

Figure 11: Google earth image showing the NNE-SSW trending dune field, taken from Logue, 2010

8. APPENDIX A:

Table 24: ICP-MS (and ICP-AES) and ion chromatography data in mg/L; pH from 1:2.5 soil-water ratio; alkalinity from potentiometric titration

Sample	C02 A	CO2 B1	CO2 B1-2	CO2 B2	CO2 C1	CO2 C1-2
pH	6.70	7.08	7.87	7.40	7.66	7.45
F	0.000	2.000	3.000	4.000	3.000	18.000
Cl	50.000	3063.000	1042.000	456.000	1764.000	1332.000
NO_3-	5.000	25.000	0.000	0.000	0.000	0.000
P	0.000	0.000	0.000	15.329	76.318	201.232
SO_4^{-2}	52.000	709.000	238.000	173.000	367.000	136.000
Si	8.988	16.515	21.008	13.144	10.560	11.403
Alkalinity	64.050	73.200	94.550	118.950	149.450	103.700
Ca	12.286	341.362	409.268	130.791	54.461	226.060
Mg	6.070	413.820	370.310	109.584	47.221	188.625
Na	34.428	939.976	1350.390	628.393	371.643	810.139
Sr	0.036	2.642	3.174	0.960	0.383	1.375
B	0.079	0.222	0.245	0.193	0.343	0.431
Al	0.025	0.006	0.022	0.004	0.013	0.004
K	44.229	93.478	111.391	58.922	49.207	89.881
Ti	0.005	0.000	0.001	0.000	0.000	0.000
V	0.002	0.013	0.018	0.025	0.037	0.023
Cr	0.000	0.000	0.004	0.000	0.001	0.001
Mn	0.255	0.094	0.031	0.009	0.008	0.012
Fe	0.024	0.002	0.009	0.001	0.002	0.001
Co	0.548	0.133	0.013	0.014	0.007	0.021
Ni	0.005	0.012	0.012	0.002	0.001	0.003
Cu	0.125	0.040	0.272	0.014	0.011	0.026
Zn	9.831	0.009	0.043	0.004	0.005	0.004
As	0.001	0.008	0.006	0.007	0.011	0.005
Se	0.005	0.017	0.021	0.006	0.005	0.011
Mo	0.014	0.129	0.029	0.032	0.026	0.021
Cd	0.001	0.001	0.002	0.000	0.000	0.000
Sb	0.000	0.000	0.001	0.000	0.000	0.000
Ba	0.030	0.119	0.173	0.108	0.039	0.076
Pb	0.002	0.001	0.002	0.000	0.000	0.000